Model test investigation of level & multi-year ridge ice forces on downward breaking conical structures. Volume I: Main Report, Volume II: Appendices

Lau, M.

Contractor Report (National Research Council of Canada. Institute for Marine Dynamics); no. CR-1990-08, 1990

National Research Council Canada
Conseil national de recherches Canada
Institute for Ocean Technology
Institut des technologies océaniques

CR-1990-08

Contractor Report

Model Test Investigation of Level and Multi-year Ridge Ice Forces on Downward Breaking Conical Structures.

Volume 1 - Main Report

Michael Lau

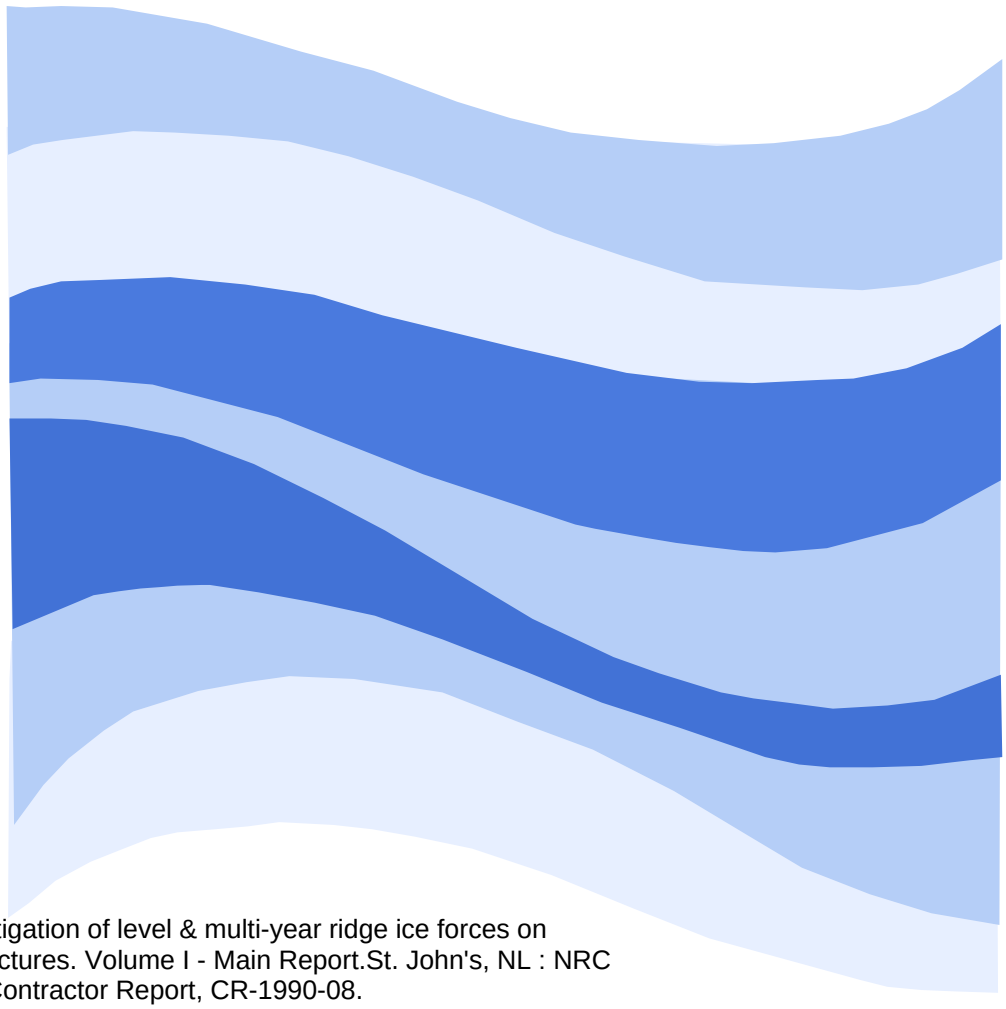

Lau, M., 1990. Model test investigation of level & multi-year ridge ice forces on downward breaking conical structures. Volume I - Main Report.St. John's, NL : NRC Institute for Marine Dynamics. Contractor Report, CR-1990-08.

Canada

MODEL TEST INVESTIGATION OF LEVEL AND MULTI-YEAR RIDGE ICE FORCES ON DOWNWARD BREAKING CONICAL STRUCTURES

VOLUME I - MAIN REPORT

DOCUMENTATION PAGE

REPORT NUMBER CR-1990-08 (Volume 1 of 2)	DATE March 1990
REPORT SECUR TY CLASSIFICATION Unclassified	DISTRIBUTION Unlimited

TITLE: MODEL TEST INVESTIGATION OF LEVEL AND MULTI-YEAR RIDGE ICE FORCES ON DOWNWARD BREAKING CONICAL STRUCTURES VOLUME 1 MAIN REPORT

AUTHOR(S)
Michael Lau

CORPORATE AUTHOR(S)/PERFORMING AGENCY(S)

NORDCO Limited

PUBLICATION
-

SPONSORING AGENCY(S)
Institute for Marine Dynamics
National Research Council Canada

IMD PROJECT NUMBER 087	NRC FILE NUMBER 7816

KEY WORDS:	PAGES	FIGS.	PLATES	TABLES
structures, ice, ridges, model test	31	53	18	14

SUMMARY: This report presents the results of model tests in both level ice and multi-year ridges with a fixed 45 degree downward breaking cone carried out at the Institute for Marine Dynamics in January 1989. The objectives were to examine the mode of failure and the resulting failure load during the ridge/cone interaction, and to conduct further tests in thick level ice to verify the velocity and thickness effects observed in a previous test program. Results from the ridge tests provide the first set of test data on downward breaking cone/ridge interaction in open literature. A theoretical model which takes into account the difference in mechanical properties between the sheet ice and the ridge is proposed. Good agreement is found between the model predictions and the measurements.

ADDRESS: National Research Council
Institute for Marine Dynamics
P.O. Box 12093, Station 'A'
St. John's, NF
A1B 3T5

ABSTRACT

This report presents the results of model tests in both level ice and multi-year ridges with a fixed 45 degree downward breaking cone carried out at the Institute for Marine Dynamics in January 1989. The objectives were to examine the mode of failure and the resulting failure load during the ridge/cone interaction, and to conduct further tests in thick level ice to verify the velocity and thickness effects observed in a previous test program (References 1 and 2).

The test program consisted of 5 tests, of which 3 were in level ice yielding a total of 33 data points, two were with multi-year ridges embedded in level ice sheet yielding a total of 29 data points.

Effects of the velocity and the ice thickness were examined and compared with data from the previous model tests. A detailed explanation of the trends observed was provided from available theories and model tests. A good correlation exists between data from the present and the previous test series.

Results from the ridge tests provide the first set of test data on downward breaking cone/ridge interaction available in the open literature. Three failure scenarios are described with significant ice breaking events identified. A theoretical model which takes into account the difference in mechanical properties between the sheet ice and the ridge ice is proposed. A method to calculate the non-dimensional forces and the non-dimensional width based on the model is also developed. Good agreement is found between the model predictions and the measurements.

ACKNOWLEDGMENTS

This project was funded by the National Research Council of Canada through the Institute for Marine Dynamics (IMD). The author sincerely thanks Dr. F.M. Williams of the institute for her valuable input through several discussions regarding some of the findings in this study.

The technical assistance of all the IMD staff working in the ice tank during the model test is gratefully acknowledged. Thanks are also due to Dr. D.B. Muggeridge who kindly loaned out the 45 degree cone model for testing during this project.

TABLE OF CONTENTS

TABLE OF CONTENTS (CONT'D)

MODEL TEST INVESTIGATION OF LEVEL AND MULTI-YEAR RIDGE ICE FORCES ON DOWNWARD BREAKING CONICAL STRUCTURES

1.0 INTRODUCTION

The discovery of large oil and gas resources in Arctic regions has stimulated significant activity in the development of novel offshore structures. A downward breaking conical structure is considered to be one of the most promising designs. For design purposes and for safety considerations, information about the magnitude and the nature of the ice loads is required.

This report presents the results of model tests in both level ice and multi-year ridges with a 45 degree downward breaking conical structure. The tests were carried out using the ice tank at the Institute for Marine Dynamics (IMD), in January 1989.

Similar models were previously tested in level ice at IMD, in April 1987. (References 1 and 2) A total of 142 test runs were conducted. Ice thickness, flexural strength, cone angle, waterline diameter, ice-cone friction coefficient, advancing speed, and model set-up were systematically varied and their effects examined. A number of trends were identified but not fully explained indicating the need for further investigation.

The present test program was launched to further examine the adequacy of conical structures in ice defence. The objectives are:

i) to study the interaction between a fixed 45 degree conical structure and multi-year pressure ridges frozen into a level ice field as they may represent the worst load case, and

ii) to conduct further tests in thick level ice to verify the velocity and thickness effects observed in the previous test program.

The experiment is described in Section 2. Results of the tests in level ice and in multi-year ridges are given in Section 3. Conclusions are contained in Section 4.

2.0 THE EXPERIMENTS

2.1 Test Facility

The ice tank is 96 m long, 12 m wide and 3 m deep with a usable ice sheet length of 76 m. (See Plate 1)

The main towing carriage, weighing 80,000 kg, has a speed range of 0.001 m/s to 4.000 m/s with an accuracy of 0.1%. Carriage speed, acceleration and constant speed run distance are

automatically controlled by a preset control program.

The test frame, which is located at the center of the carriage, can be raised from the water level to over a meter above the water level, thus allowing for adjustment of the model cone's waterline. The computer for the drive control and the data acquisition system are housed in the thermally insulated control room on the carriage.

The refrigeration system provides a cold air supply over the upper part of the basin with heat transfer near the ice sheet/air interface by natural convection; thus a uniform temperature distribution near the water surface is maintained. Air temperature at the water surface and the water temperature are monitored by a series of thermocouples and are computer logged.

2.2 Model Ice

2.2.1 Homogeneous Level Ice

The IMD tank uses the EG/AD/S model ice invented by Timco (Reference 3). The ice was grown through carefully controlled seeding, freezing and tempering procedure as described by Jones et al (Reference 4). The percentage concentrations of EG/AD/S for the present test series were 0.39/0.27/0.0.

For each ice sheet flexural strength, effective elastic modulus, ice thickness, ice density, compressive and shear strengths were measured according to the standard procedures outlined by Jones et al (Reference 4). The properties are summarized in Table 1. A brief description of the standard procedure used for each characterization test is given below.

2.2.1.1 Flexural Strength

The flexural strength, σ_f, was monitored every hour as the ice was tempered, and immediately prior to and after tests to establish the ice tempering curve. The flexural strength corresponding to each individual test can then be directly interpolated from the curve.

The flexural strength was measured using in-situ cantilever beam tests at locations on both sides of the model track in the middle area of the tank as shown in Plate 2. A set of six beams with the proportion of thickness(h):width(w):length(L) of 1:2:6 was prepared at one location. A hand held spring gauge was used to fail the beams, five were downward loading and one was upwardly loaded. The load P on the beam was applied manually with a hand held push-pull gauge and failure occurred in about 0.8 sec. The mean of the five downward loading points and the standard deviation were calculated.

The flexural strength was calculated from the linear elastic theory as:

$$\sigma = \frac{6PL}{wh^2} \qquad (1)$$

where P is the load applied at the free end to break the beam.

2.2.1.2 Elastic Modulus

Shortly prior to the tests, the effective modulus of elasticity was measured using the plate deflection test procedure outlined by Sodhi et al (Reference 5 and Plate 3). The incremental load, ΔP, was applied near the center of the ice sheet and the resulting deflection, $\Delta\delta$, at the point of loading was measured using a deflectometer (LVDT) and recorded on a strip chart recorder. The elastic component of the deflection was then distinguished for analysis.

The characteristic length, l_s, was calculated according to the theory of an infinite plate on an elastic foundation (Reference 5):

$$l_s = \left\{ \frac{\Delta P}{8\tau_w \Delta\delta} \left[1 + \frac{\alpha_p^2}{2\Pi} \left(\ln \frac{\tau_w \alpha_p}{2} - \frac{5}{4} \right) \right] \right\}^{1/2} \qquad (2)$$

where ΔP = incremental load placed suddenly on the ice sheet
$\Delta\delta$ = elastic deflection increment of the ice sheet
τ_w = specific weight of water
$\ln\tau_w$ = 0.55772157 (Euler constant)
α_p = r_p/l_s
r_p = radius of the applied load.

From this value for the characteristic length, the effective elastic modulus, E, can be calculated using the following relationship:

$$E = \frac{12(1 - v^2)\tau_w l_s^4}{h^3} \qquad (3)$$

where v is the Poisson's ratio which was taken as 1/3.

This test was done just prior to (or subsequent to) the flexural strength tests and was used to establish the E/σ_f ratio of the ice sheet.

2.2.1.3 Ice Thickness

Immediately after each test the ice thickness was measured

at 2 m intervals on both sides along the test track. Precision calipers accurate to 0.01 mm were used.

More than 30 data points were obtained on each side, and the mean and standard deviation calculated. Variation of thickness within an ice sheet was negligible with a standard deviation of less than 3%.

2.2.1.4 Ice Density

The Ice density was estimated by measuring the force required to submerge a certain volume of ice. The force, F, was determined by placing a beaker of doped water with a piece of 10 cm x 10 cm x thickness model ice floating in it on a scale as the ice was submerged. The volume, V_i, of the ice piece was determined by measuring it's dimensions using a precision caliper. The density was calculated using the following relationship:

$$p_i = p_w - F/V_i \qquad (4)$$

where p_w is the density of the doped water.

2.2.1.5 Compressive and Shear Strength

During the warm-up period the compressive and shear strength of the broken beam from a beam test was measured using a hand-operated level apparatus at the IMD. (See Plate 4) Only a limited number of these tests were performed as they were done to provide index values for comparison with the measured flexural strengths.

2.2.2 Multi-Year Pressure Ridges

This program represents the first time an attempt was made to model a multi-year ridge in IMD's ice tank. A two stage ridge formation technique was adopted.

A parental ice sheet with a thickness of 21 mm lower than the target thickness of the ridges was created by growing a level ice sheet using IMD's standard procedure. Half of the ice sheet was used in the level ice test. After the test in level ice was completed, the broken ice was cleared out of the ice tank and the remaining unbroken portion was cut (across the tank width) into 14 to 15 rectangular ridges with specific widths (Plate 5). The ridges were then towed to locations 4 m apart along the tank (Plate 6), and a level ice sheet with a thickness of 36 mm and a flexural strength of 40 kPa was grown in the residual open water area of the tank by a second freeze (Plate 7).

This approach offers many advantages, including:

i) high cost efficiency. Half of the parental ice sheet is available for level ice test, and more than 14 ridges can be built by simple cutting and towing operation. Moreover, the process requires minimal manpower, experience, and ridge building time.

ii) high uniformity of the ridges' mechanical properties.

2.2.2.1 Ridge Ice Properties

Due to the tempering and refreezing process, the brine content or salinity of the ridge ice was less then the surrounding sheet ice due to brine drainage. Consequently, the ridge ice was stronger and exhibited different material properties from the surrounding sheet ice.

Typical vertical cross-section of the model ridges is shown in Figure 1 and Plate 8. The structure consists of two distinct materials. A strong rectangular cross-sectional area, made of the parental ice sheet, surrounded by a layer of weaker sheet ice grown from the second freeze resulting in a trapezoidal shape.

The properties of the ridge ice and the surrounding ice sheet were measured following the procedure described in Section 2.2.1. Table 2 summarizes the measured values.

It is impossible to conduct sufficient ice property tests utilizing unbroken portions of ridges. Therefore, flexural strength, effective elastic modulus[1], and compressive strength tests were performed either on a two-meter or a four-meter wide ridge plate located at the center of the tank. Since all ridges were formed using the same procedure, the measured values were regarded as representative of the ice properties of the test ridges.

Immediately prior to a test, the width W_T of each ridge, defined as the width of the parental ridge beam, was measured using a meter stick. The width of the ridge at water level, W_R, is estimated assuming the angle, α_R, of the ridge is equal to 45 degrees. (See Figure 1)

Immediately after each test, thickness of each ridge was

---

[1]The in-situ cantilever beam method proposed by Tatinclaux and Hirayama (Reference 6) is preferred over the plate deflection method due to the limited widths of the ridge plate and the adjacent ice sheet; however, the standard equipment for the test was not available at the time of testing, and the plate deflection method was adopted instead.

measured using a precision caliper accurate to 0.01 mm. Variation of ridge thickness in each test was negligible with a standard deviation of less than 3%.

2.3 Model Description

Tests were conducted using a 45 degree cone from the previous test program as shown in Plate 9. The model dimensions are shown in Figure 2. The model was constructed of 1/8 inch thick steel sheet over a rigid, welded frame. The exterior surface was finished to yield a friction coefficient of 0.15.

The model was rigidly connected to the test frame by a 6-component load cell.

2.4 Test Program

The test program consisted of 5 tests, of which 3 were in level ice, and 2 were with multi-year ridges. Table 3 summarizes the tests that were conducted.

Tests for the level ice sheet were planned to study the effects of velocity and ice thickness on structure load. Three level ice sheets with the thickness of 35.6 mm, 54.6 mm, and 85.1 mm were used. For each ice sheet, the model was tested at 3 waterlines with a towing speed range from 0.01 m/s to 0.1 m/s. For the 35.6 mm thick ice, test runs at velocities of 0.25 and 0.5 were also performed.

Each of these tests were run a sufficient distance to achieve a steady state condition.

A number of open water test runs were also carried out as summarized in Table 4.

Tests for the multi-year ridges were planned to study the effects of ridge width on the interaction and the structural load. Two ice sheets embedded with ice ridges were used. The thickness and flexural strength of the ice sheets were kept constant throughout the tests at approximately 36 mm and 35 kPa.

The first test, test CONE10, was performed at waterlines of 1.28 m and 1.48 m and a ridge thickness of 75.8 mm. The second test, test CONE12, was performed at waterlines of 1.08, 1.28, and 1.48 m and ridge thickness of 106.5 mm. Ridge beams with widths ranging from 0.17 to 1 m were tested in each series with a velocity of 0.05 m/s. Test runs were also performed in the wide ridge plates. A total of 29 multi-year ridges with two ridge thickness were tested. All ridges were tested with the long axis perpendicular to the direction of the cone's motion.

2.5 Instrumentation and Data Acquisition System

A schematic arrangement of the transducers is given in Figure 2. Measured data included 10 channels of forces and cone motion parameters as follows:

CHANNELS	PARAMETERS[2]	CHANNELS	PARAMETERS
8	force in x-axis	22	moment about z-axis
9	force in y-axis	26	acceleration in z-axis
10	force in z-axis	29	acceleration in z-axis
20	moment about x-axis	47	model speed (low)
21	moment about y-axis	46	model speed (high)

An AMTI's SRMC8-X 10000 lb. six-component load cell was used to measured forces and moments in three principle directions. The horizontal and vertical accelerations of the model were measured by two Systron Donner accelerometers.

A schematic arrangement of the data acquisition system is given in Figure 3. Excitation for the transducers was provided by a NEFF System 620 Series 300 signal conditioner. The transducer outputs were filtered by a 100 Hz low pass filter and digitized at a rate of 20 Hz by a NEFF System 620 Series 100 amplifier/multi-plexer and stored on a Vax 11/750 computer for analysis. The Analog outputs of the transducer were recorded by a KYOWA RTP-600B 14 channel tape recorder as backup.

A considerable amount of effort was devoted to obtaining good visual records of each test. An underwater video camera was used to record the clearing of broken ice around the cone and another video camera was located behind the model to record the broken channel width and ice pieces size. A still camera was located in front of the cone to record the initial ice breaking pattern and the size of the ice pieces. In the ridge tests, an additional video camera and high speed sequential camera were located in front of the model to record the ridge failure sequence.

3.0 RESULTS AND DISCUSSION

The results of this study are presented in two sub-sections. In Sub-section 3.1 results of the level ice tests are presented, followed by a discussion of the results of ridge tests in Sub-section 3.2.

---

[2] X- in the direction of model's motion; Y - perpendicular to model's motion; Z - vertical direction

3.1 Level Ice

The test results are summarized in Table 5. In this section, the effects of model speed and ice thickness on mean peak ice forces[3] as well as average ice forces[4] are examined. The results are compared with model test data from previous tests. (Reference 7)

3.1.1 Method of Data Comparison

Due to the decrease of ice strength with testing time, the exact target strength was not achieved and hence it was necessary to correct the raw data to a reference strength value. An expression developed in the previous test program is used.

$$F_{sc} = F_m \left[1 + \frac{r}{\sigma_m} (\sigma_{sc} - \sigma_m) \right] \qquad (5)$$

where
- F_{sc} = force at standard strength condition for comparison
- F_m = measured force
- σ_{sc} = standard strength for comparison (average value of measured strengths)
- σ_m = measured strength
- r = ice breaking force/total force ratio

This expression is derived based on the fact that the horizontal and vertical forces vary linearly with flexural strength, over the range concerned. In the present tests when the presawn ice test data were absent, the measured values for r could not be obtained, and the theoretical values of r from Ralston's analysis were used instead. (Reference 7)

The F_{sc} values are used in Figures 17 to 29. The values of σ_{sc} and F_{sc} for each figure are given in Table 6.

Variation of ice thickness from the reference condition was negligible and no adjustment was made.

3.1.2 Velocity Effect

The effect of velocity on non-adjusted ice forces is presented in Figures 4 to 12 for three waterline diameters at three thicknesses. At low velocity ($v \leq 0.1$ m/s) both horizontal

---

[3]The mean peak ice force is the arithmetic mean of a number of peak forces over a time interval of steady state interaction.

[4]The average ice force is the arithmetic mean of the digital data over a time interval of steady state interaction.

and vertical forces increase with velocity by a comparable amount. At higher velocities (V > 0.1 m/s) the vertical force starts to drop off rapidly while the horizontal force continues to increase (Figures 10 to 12).

These trends were reported in the previous study (Reference 7) and are verified by the present data.

3.1.2.1 Effect of Velocity on Different Force Components

These trends can be explained by considering the effect of velocity on the individual force components the model experiences during the interaction.

The ice breaking, ice clearing and open water components of the total forces on the cone tested at 1.28 m waterline in ice thickness of 33.5 mm and flexural strength of 40 kPa are plotted against model speed in Figure 13.

The components are calculated using the following relationship:

$$F_t = F_w + F_b + F_c \qquad (6)$$

where F_t = total resistance in level ice
F_w = total resistance in open water
F_p = total resistance in presawn ice
F_b = ice breaking component, $F_t - F_p$
F_c = ice clearing component, $F_p - F_w$

The ice breaking component is contributed mainly by the fracturing of the solid ice sheet and can be defined as the total ice resistance minus the presawn ice resistance. The ice clearing component mainly arises from the clearing of broken ice pieces around the cone and is defined as the presawn ice resistance minus the open water resistance.

The resistance in level ice is estimated from the strength curves obtained in the previous test by assuming a flexural strength of 40 kPa. (Reference 7) These curves were found to be satisfactory in estimating total ice resistance in 33.5 mm thick ice under the present test conditions. Equations for these curves are given in Table 7. The corresponding presawn resistance values are taken from test data obtained in the previous test program[5]. The open water resistance values were measured in the present test series. These values and the corresponding force components are given in Table 8.

---

[5] Test data associated with test condition No. 18. (Reference 7)

In Figure 13, an increase in the ice clearing force component with the increase of velocity is noticed, while the ice breaking force component increases with velocity at a more rapid rate at low velocity ($V \leq 0.1$) m/s and levels off at higher velocities ($V > 0.1$ m/s). The open water resistance at low velocity is negligible, but it is evident that at higher velocities it substantially increases the horizontal component and decreases the vertical component.

The ice breaking force component is sensitive to the mechanical properties of ice. Its increase with velocity may be due to the dynamic breaking of ice, and the strain rate dependence of flexural strength and crushing strength. The fact that there is no further increase of ice breaking force at higher speeds was observed indicates a limiting factor for the dynamic ice breaking load.

The ice clearing force component is sensitive to the volumetric properties of ice. It tends to increase linearly with velocity due to the inertial force of the ice pieces exerted on the cone.

The open water resistance is sensitive to the flow condition around the cone. Since the resistance is expected to be proportional to V^2, the effect is prominent at high speed.

3.1.2.2 Contribution of Force Components at Different Velocities

At low velocities ($V \leq 0.1$ m/s), the increases in both the open water and the presawn ice resistances are negligible, while the level ice resistance increases by a substantial amount. The increase is mainly due to the ice breaking component of the force.

At velocities greater than 0.1 m/s the effect of open water overshadows the other two effects.

In the previous study a hypothesis was proposed to explain the trends encountered at velocities higher than 0.10 m/s. It was hypothesized that a suctional force, which acted perpendicular to the rear surface of the cone wall, induced a downward pull on the cone. It was also suggested that this hydrodynamic phenomenon could be accentuated by the effect of the restricted channel the model created. (The channel created by the cone was typically a few centimeters wider than its waterline.) The hypothesis is verified by the present test data.

The open water resistance at waterline diameters of 1.08, 1.28 and 1.48 m is given in Table 9 and shown in Figures 14 to 16 respectively. For the cone with a waterline diameter of 1.28 m,

the resistance in a restricted channel[6] at velocities of 0.25 and 0.5 m/s is also given (Figure 15).

At a velocity greater than 0.1 m/s, the open water resistance shows the same trend exhibited by the level and the presawn ice resistances. Underwater video shows a clear ventilation at the rear of the cone wall near the water surface indicating the existence of a suctional force. A hydrodynamic effect due to the flow of water around the cone is definitely present. Furthermore, Figure 15 shows the same level of horizontal force for both the open water and the restricted channel conditions, while a greater downward pull (~ 30 N) is evident for the restricted channel condition.

The ice breaking and the ice clearing force components in Figure 13 are deduced from the open water resistance as opposed to the restricted channel resistance. The fact that both the horizontal and the vertical forces are of similar magnitude (as expected) suggests that the restricted channel did not influence the water resistance component during the level ice as well as the presawn ice tests.

The set-up of the present experiment unrealistically modelled the velocity of the water current by using a moving model. The flow speed is equal to the model's advancing speed. In the field, a current of such a high velocity is rare (a full scale velocity around 2 m/s), and the trend at high velocity may not be observed in the field. Thus for a fixed structure, the trend for lower velocities is more realistic and of much more interest.

3.1.3. Thickness Effect

The effects of ice thickness on adjusted ice forces at waterline diameters of 1.08, 1.28,and 1.48 m, and at three velocities are shown in Figures 17 to 25. Results show an increase of both the horizontal and the vertical forces with the increase of ice thickness.

Selected data from the previous and the present test series are plotted against the square of thickness in Figures 26 to 29, as the ice forces are expected to depend on ice thickness with a power of two.

There is good correlation between both sets of data with thicknesses less than 54 mm. Within this range, the data show a quadratic dependence between forces and ice thickness; however,

---

[6]Restricted channel resistance is the resistance of the model when it advanced in a clear channel with the width only a few centimeters wider than the waterline diameter of the model.

both the horizontal and the vertical forces in the 68 mm thick ice are substantially higher than expected which indicates a higher order relationship between forces and thickness as discussed in the previous reports. (References 1 and 2)

At an even higher thickness of 85 mm, both forces are substantially lower than expected. There is no further increase of horizontal force, and the vertical force decreases substantially when the thickness increases from 68 mm to 85 mm.

By re-examining the test records, no flaw could be found to account for the for-mentioned anomalies.

The apparently higher order relationship of forces to ice thickness can be explained partially by the effect of inplane force and the corresponding edge moment, while the lower than expected force level at thickness of 85 mm is believed to be a direct consequent of the abrupt change of failure process from bending to shear the ice experienced as discussed in the following two sections.

3.1.3.1 The Effect of Inplane Force and Edge Moment

The effect of inplane force on the ultimate failure loads depends on the magnitude as well as the eccentricity, e, of the applied force relative to sheet's mid-surface. An expression for the ultimate moment can be derived by taking moments about the intersection of the mid-surface and the plane at x_u at which the maximum moment M_u is generated,

$$M_u = P_u' x_u - \beta P_u' e - M_B \qquad (7)$$

where P_u' = vertical failure load
β = resolution factor
= $\tan(\alpha + \tan^{-1}(\mu))$
α = cone inclination
μ = dynamic friction coefficient
$\beta P_u'$ = horizontal failure load
M_B = buoyant force moment.
e = eccentricity

Neglecting M_B and substituting $M_u = P_u x_u$, where P_u is the estimated ultimate load when the moment resulting from the inplane force is neglected, gives

$$P_u' = \left(1 + \frac{\beta e}{x_u - \beta e}\right) P_u \qquad (8)$$

or

$$P_u' = M_{aj} P_u \qquad (9)$$

where the adjustment factor, M_{aj}, is dependent on the eccentricity of the inplane force and the length of the wedge beam, x_u. Since the inplane force is transferred to the upper edge of the ice sheet where compressive failure occurs, and with comparable compressive strength and inplane force for each ice sheet, it is expected that the location for its point of action near the top surface will be essentially the same. Thus, the eccentricity of the inplane force, and subsequently the adjustment factor, will increase with thickness, e.g.

$$M_{aj} \propto h^c \tag{10}$$

or

$$P_u' \propto h^c P_u \tag{11}$$

where c is a positive number.

By assuming $P_u \propto h^2$, the relation 11 becomes

$$P_u' \propto h^{2+c} \tag{12}$$

Thus the ultimate load has a higher order dependency on ice thickness.

3.1.3.2 Shear Failure

It has been suggested that under conditions such as low velocity, low friction coefficient, small cone inclination and small ice thickness that flexural failure predominates. However, the influence of shear stresses becomes more important with increasing thickness and is finally predominant. (Reference 8)

Schwarz et al (Reference 9) suggested that by observing the actual fracture patterns in ice, one may find pure bending, when circumferential cracks form at distances slightly higher than the characteristic lengths; with increasing thickness the average length of a broken piece does not increase as does the characteristic length, instead it decreases which may be regarded as an indication of a combination of bending and shear failure.

This phenomenon was initially reported by Wessels (Reference 10) in test conditions similar to those in the present test series. (Figure 30) At V = 0.2 m/s, shear failure was observed in 70 mm thick ice with a decrease of ice piece size and ice forces.

In the present tests, the some evidence for shear failure was observed. Figures 31 to 33 show the variations of piece size with thickness at the three test speeds. In all cases the piece size increased with thickness up to the 54 mm thick ice

indicating flexural failure, while at the higher thickness of 85 mm, the piece size decreased indicating shear failure. This abrupt change from bending to shear explains the lower resistance observed.

3.1.4 Comparison with Data from Previous Tests

Predictions from Ralston's plastic model (Reference 11) are plotted against the measured average peak forces from the present as well as the previous test programs for V = 0.01 m/s in Figure 34 to assess the consistency of both sets of test data. Only data with an ice thickness equal to or less than 54 mm are used in the comparison because the analytical model does not take account for the trends mentioned in Section 3.1.3. A good correlation exists between both sets of data.

3.2 Ridge Test

Various failure processes observed during the ridge/cone interaction are described in Section 3.2.1, and the test results are given in Section 3.2.2. In Section 3.2.3 an analytical model is presented to explain the failure sequences observed and its predictions are compared to the measured values. In Section 3.2.4 non-dimensional analysis is preformed to examine the effect of ridge width on ridge forces.

3.2.1 Description of the Interaction Process

Three distinct failure processes were observed during the ridge/cone interaction:

1. Ridge failure at the center followed by hinge cracks. No apparent ridge ice sheet separation was observed.

2. Similar to scenario 1. However, separation of ice sheet at both the forward and the trailing side of the ridge took place before the hinge cracks fully developed.

3. Local bending failure or circumferential cracks emerged in the middle of the ridge.

Typical broken ridge fragments associated with the above failure processes are shown in Plates 10 and 11.

The variation of failure scenarios is given in terms of ridge width and the ridge thickness in Figure 35. For the 106.5 mm thick ridges the failure process denoted as Scenario 2 was predominant. For the 75.8 mm thick ridges Scenario 3 was predominant for the ridges whose widths were greater than 0.7 m, while both Scenario 1 and Scenario 2 were observed with the

narrower ridges.

Efforts were given to correlate the failure sequence observed from the visual record to the measured forces. The failure scenarios are described in detail in the following sections.

a) Scenario 1: Beam Failure without Separation

Ridge Nos. 1, 2, 5, and 12 of test CONE10 failed without separation. A typical force time history (CONE10, ridge No. 2) is given in Figure 36. Six significant events were identified. A typical failure process of the ridges is depicted in Figure 37.

Event 1: Sheet Failure

As the cone approaches the pressure ridge, the ice sheet in front of the cone broke in the usual characteristic manner. A circumferential crack formed at the sheet ridge interface as shown in Figure 37a and Plate 10.

Event 2: Center Crack Formation

When the ridge encountered the cone, it was deflected downward slightly, causing a center crack in the ridge at the point of contact perpendicular to the ridge beam. The crack did not progress into the surrounding ice sheet. The formation of the center crack resulted in a noticeable change in stiffness of the ridge-sheet system which manifested itself by a change of slope in the force time history (Figure 36). It occurred at an early stage of the interaction process when the cone contacted the upper edge of the ridge as shown in Figure 37b and Plate 11.

Event 3: Appearance of the Hinge crack

Shortly after the formation of the center crack, the first hinge crack was observed within 0.5 sec at some distance away from the cone. (Figure 37c and Plates 12) In the present tests the failure strain of the sheet ice, defined as σ_f/E_S, was typically 3 times greater than the failure strain, σ_F/E_R, of the ridge beam; therefore, the crack was confined to the top surface of the ridge beam without penetrating into the ice sheet. As the loading increased the crack penetrated downward with the redistribution of tensile stress to the ice sheet. At this point, the ice sheet acted as a tensile reinforcement to the ridge beam. It tended to slow down the crack development, thus allowing a number of hinge cracks to develop adjacent to the first hinge crack as shown in Figure 37c and Plate 13.

Event 4: Shear Failure at Front Edge of Ridge

As the ridge continued to be deflected downward, shear

failure occurred at the cone-ridge interface as the shear strength of the ice at the triangular portion of the ridge was exceeded.[7] A sudden drop of resistance occurred as the ridge was momentarily dislodged from the cone. (See Figure 37d)

Event 5: Rebound of the Ridge

The ridge immediately rebounded and hit the cone causing a dynamic impact load on the cone as shown in Figure 37e. Due to the dynamic nature of the impact, A number of peaks with frequencies at around 8 to 10 Hz were observed. (See Figure 36)

Event 6: Failure by Hinge crack Extension into Ice Sheet

The final failure associated with the maximum load occurred when one of the hinge cracks extended into the ice sheet forming a circumferential crack. (Figure 37f and Plate 14) The time from the appearance of the first hinge crack to the final failure is typically more than 2 seconds, thus the ridges were deflected at least .1 m at failure.

a) Scenario 2: Beam Failure with Separation

For ridges Nos. 9, 10 and 11 of test CONE10 and all ridges of test CONE12, failure was associated with the separation of the ice sheet from the ridge beam. A typical force time history (CONE12, ridge No. 7) is given in Figure 38. The profile is remarkably similar to the one described previously.

Events 1 to 5

Failure sequence proceeds from Events 1 to Event 5 as described previously.

Event 6

The final failure associated with the maximum load occurred when the forward and the trailing ice sheet separated from the ridge before the hinge cracks fully developed. The onset of the separation began at the center crack location and propagated quickly to one of the hinge cracks. (See Plate 17) Without the strengthening effect of the ice sheet, the hinge crack failed immediately with a much lower load.

c) Scenario 3: Beam Failure with Circumferential Cracks

Ridge Nos. 3, 6, 7, 13, 14 of test CONE10 failed in this mode. With a low ridge/sheet thickness as well as a low

---

[7]This portion of the ridge beam is made up of ice material grown from the second freeze with low shear strength.

ridge/sheet strength ratios associated with these tests, the failure process tends to become complex. Due to the high confinement of the surrounding ice sheet, local bending failure resulting in a number of circumferential cracks in the middle of the ridge was observed. A typical force time history (CONE10, ridge No. 6) is given in Figure 39. The cracking sequence was not clear; however, cracks similar to hinge crack were always observed a distance from the cone. (Plate 16)

The formation of circumferential cracks resulted in a cyclical loading pattern; however, a major peak load could always be identified as the failure load.

3.2.2 Test Results

The test results are summarized in Table 10. In this table the loads corresponding to events 4, 5 and 6 as defined in Section 3.2.1 are listed together with the dimensions of the broken ridge fragments. The mean peak forces measured in the ridge plate tests are given in Table 11.

The measured total ridge loads are plotted against the ridge width in Figures 40 and 44 for each ridge thickness and cone waterline. Data with the same thickness are also re-plotted in Figures 45 and 46. Mean peak forces measured from the ridge plates are also included to compare with the ridge forces. The variation of the flexural strength is typically less than $\pm 5\%$ from the mean; thus, no attempt was made to adjust the data to a standard strength.

The following trends are observed:

a. Relationship between horizontal and vertical force

Theoretically, the horizontal force is related to the vertical force by a resolution factor, β:

$$F_H = F_V \beta = F_V \tan(\alpha + \tan^{-1}(\mu)) \qquad (13)$$

where α is the cone angle, and μ is the dynamic friction coefficient. The resolution factor for the present tests is equal to 1.35 or the horizontal force is expected to be 35 % higher than the vertical force. However, the data do not show such dependency. In most cases the horizontal force is lower than the vertical force indicating a negative friction factor. The reason is not clear.

b. Waterline diameter effect

Despite a variation in the waterline diameter, all data points follow the same relationship with ridge width with only a slight scattering of data. (Figures 45 and 46) Thus, the data do

not show any significant effect of waterline diameter.

c. Effect of failure process on failure load

The results of CONE10, in which all three failure processes occurred, are plotted again in Figure 47 showing different failure processes. Again, data points associated with failure modes 1 and 2 follow the same linear relationship with ridge width, while failure load associated with failure mode 3 deviated slightly from the linear relationship. Thus, the data from CONE10 does not show significant effect of failure process.

3.2.3 Analytical Model

An analytical model was developed to explain the failure sequence observed during the hinge crack formation.

The procedure adopted in this study to calculate the force for hinge crack formation is based on Hetenyi's theory of an elastic beam on an elastic foundation. (Reference 12) The algorithm is shown in Figure 48. A detailed discussion of each step is given in the following section.

3.2.3.1 Effect of Ice sheet Spring Stiffness

As the ridge slides down the cone surface the level ice sheet connected to the ridge is forced to follow the deflection of the ridge beam, which has the effect of making the foundation "appear" to be stiffer than if the ridge were considered by itself. Thus, the effects of the spring stiffness and the effective flange of the level ice sheet during deflection of the ridge beam are considered.

The effect of the surrounding ice sheet on ridge deflection is accounted for by replacing the foundation modulus, k, by an adjusted foundation modulus

$$k^* = p_w g \, (W_R + 2 \, (2)^{0.5} \, l_s) \qquad (14)$$

where W_R = width of ridge at waterline
l_s = characteristic length of ice sheet as given by

$$l_s = \left(\frac{E_s h^3}{12 \, (1 - v^2) \, p_w g} \right)^{1/4} \qquad (15)$$

E_s = elastic modulus of ice sheet
v = Poisson's ratio for ice
h = ice sheet thickness

With the above adjustment, simple beam formulae related to deflection and stresses may be used.

3.2.3.2 Effective Flange

For practical purposes, the concept of an effective flange width, b_{eff}, is used to simplify the more complex lateral distribution effect for an infinitely wide ice sheet. The effective width of each flange is

$$b_{eff} = \frac{(2)^{0.5}\, l_s}{(1 - \nu^2)} \qquad (16)$$

In deriving this effective width, the objective is to select an equivalent uniform stress, which is assumed to act over a reduced width, b_{eff}, which produces the same resultant force in the ice sheet as the actual stress, which varies over the full width of the ice sheet.

3.2.3.3 Simple Beam Equation for Infinitely Long Homogeneous Beam

For a homogeneous ridge beam, the vertical force on the cone for the hinge crack formation is estimated by the following ridge beam formula:

$$P_V = 6.2 \frac{\sigma_{gov}\, I_R}{y\, l_R} \qquad (17)$$

where

I_R = moment of inertia of pressure ridge with or without ice sheet attached
y = distance to outer fiber where failure occurs from neutral axis
l_R = characteristic length of the ridge

$$l_R = \left(\frac{4\, E_R\, I_R}{k^*} \right)^{1/4} \qquad (18)$$

E_R = elastic modulus of ridge
σ_{gov} = flexural strength or compressive strength of the ridge depended on the stress distribution at failure

The horizontal force is related to the vertical force by the resolution factor, β, as given in equation 13.

3.2.3.4 Failure Model for Infinitely Long Composite Beam

The simple beam formula (Equation 17) given in the previous section only holds for a homogeneous material when a constant value of elastic modulus applies across a section. It cannot be

used directly to solve the composite beam problem as in the present case the elastic modulus, E_s, of the ice sheet is significantly different from the elastic modulus, E_R, of the ridge.

To complicate the problem, the stress distribution (thus the failure load) associated with failure depends on the failure strength of both the ice sheet and the ridge.

3.2.3.5 Transformed Section Method

To analyze this type of beam the composite section is transformed into a single material. This transformed area concept makes it possible to replace a composite member with an equivalent member of homogeneous elastic material to which the basic strength of materials relationships apply.

In the present analysis the effective flanges of ice sheet are transformed into an equivalent area, nA_s, of ridge ice in which n, the modular ratio, is given by

$$n = \frac{E_s}{E_R} \qquad (19)$$

where E_s and E_R are the elastic modulus for the sheet and ridge ice respectively. The original and the transformed sections are shown in Figure 49a. The equivalent flexural strength of the ice sheet in the transformed section is equal to σ_f/n.

Once the transformed section is obtained, the analysis of bending proceeds as though the beam were composed of homogeneous ridge ice and the simple beam equation 17 can then be applied to the transformed section.

3.2.3.6 Stress Distribution at Failure

Figure 49b shows the cross-section and stress distribution at failure. At the time of failure, the top of the ridge has already failed due to tension. The final failure will then be determined by either the equivalent sheet ice strength, σ_f/n, or the compressive ridge ice strength, σ_C, whichever is exceeded first.

After the stress distribution at failure is known, the corresponding moment of inertia, I_R, and distance y associated with the failure of the transformed section can be calculated and equation 17 can then be applied directly.

A summary of the calculation using the above model is given in Table 12.

3.2.3.7 Comparison of the Predicted Values and the Measured Values

Predictions from the proposed model are compared with the experimental data associated with failure modes 1 and 2 in test CONE10 in which hinge cracks were believed to be almost fully developed at final failure as discussed in Section 3.2.1.

The results are given in Table 13. For the test data, the forces due to ridge failure alone were obtained by subtracting the ice clearing force from the total force, because by the time the ridge failed against the cone, the broken ice of the preceding ice sheet still covered a significant portion of the front half of the cone surface. The clearing force has been determined by use of the elastic model of Kim and Kotras (Reference 13)

The predicted forces are plotted against the measured values in Figures 50 and 51. The agreement between the theory and the experiment is very good.

The model slightly under-estimates the vertical forces while it over-estimates the horizontal forces.

The present model requires an accurate measurement of the elastic modulus of the sheet ice as well as the ridge ice. However, the plate deflection method adopted in the present test is not adequate in measuring elastic modulus of the ice due to the limited size of the ridge plates and the surrounding ice sheet[8]. This may affect the model predictions.

The present test data show a resolution factor of around 1 whereas the horizontal force predictions are calculated using a resolution factor of 1.35; thus, the model prediction tends to over-estimate the test data.

3.2.4 Non-Dimensional Analysis

A non-dimensional ridge breaking force and width were derived from equation 17.

To simplify the derivation, the ridge beam combination is transformed to an equivalent rectangular beam with the same moment of inertia I_R and width W_T, thus

---

[8]The distance from the point of measurement to the sheet ridge interface is typically around one characteristic length whereas the plate deflection method requires at least a distance of three characteristic lengths.

$$I_R = \frac{1}{12} W_T H_e^3 \qquad (21)$$

and

$$y_e = \frac{1}{2} H_e \qquad (22)$$

where H_e = the equivalent thickness of the transformed rectangular beam
y_e = distance from the outer fibre to the neutral axis of the transformed section

Substituting equations 21 and 22 to equation 17, a simple relationship of the force and width in non-dimensional form can be deduced:

$$0.97 \frac{P_V}{\sigma_{gov} H_e^2} = \frac{W_R}{l_R} \qquad (23)$$

The factor, $0.97/(\sigma_{gov} H_e^2)$, is used to non-dimensionalize the horizontal and the vertical forces, and the factor, $1/l_R$, is used to non-dimensionalize the ridge width. A summary of the non-dimensional analysis with the data from CONE10 is given in Table 14.

Figures 52 and 53 show the non-dimensional forces versus non-dimensional width for test data associated with failure modes 1 and 2 in test CONE10. The non-dimensional force depends on the non-dimensional width with a slope of 1.36 for the horizontal and 1.33 for the vertical direction.

Only one set of data with similar test conditions are used for this non-dimensional analysis. Caution should be used in extrapolating the finding to other test conditions. Nevertheless, the non-dimensional factors derived in this section allow a comparison with data from other tests.

4.0 CONCLUSION

Model tests were carried out in level ice and ridges on a downward breaking conical structure. The tests have provided a valuable data set for examining ice forces on downward breaking cones.

The effects of the model speed and the ice thickness have been examined in the level ice tests. Trends observed in the previous model study have been verified, and a detailed explanation was provided from available theories and model tests.

In general, a high consistency exists between data from the present and the previous test series.

The results from the ridge tests provide the first set of test data on downward breaking cone/ridge interaction available in the literature. Due to the exploratory nature of the present tests, emphasis has been given to obtaining an accurate description of the failure sequence during the interaction. Three failure scenarios have been observed with significant ice breaking events identified.

A theoretical model based on Hetenyi's theory of an elastic beam on an elastic foundation was proposed. The difference in mechanical properties of the ridges and the surrounding ice sheet was accounted for by treating the ridge/ice system as a composite beam. Predictions from the model were compared with the test data and found satisfactory.

A method to calculate the non-dimensional forces and the non-dimensional width was also developed. The non-dimensional force was found to be linearly proportional to the non-dimensional width.

The analytical model developed in this test program only examines the development of a hinge crack, whereas to predict the relevant breaking load of ridges all possible ways of causing failure of the ice feature, i.e. crushing, bending, shear and buckling or combination of these should be considered.

5.0 REFERENCES

1. LAU, M., et al "Model Test of Downward Breaking Conical Structures in Ice," In Proceedings of the 7th OMAE Conference, v. 4, pp. 239-247,Houston, Texas, 1988.

2. LAU, M. "Analysis of Cone-Ice Interaction Test Data," IMD/NRC Report LM-AVR-27, March 1988

3. TIMCO, G.W. "EG/AD/S: A New Type of Model Ice for Refrigerated Towing Tanks" In Cold Region Science and Technology, v. 12, no. 2, pp. 175-195, 1982.

4. JONES, S.J., et al. "Ice Tank Model Test Procedures at the Institute for Marine Dynamics", IMD/NRC Report LM-AVR-20, November 1987.

5. SODHI, D.S., et al. "Determining the Characteristic Length of Model Ice Sheets", In Cold Region Science and Technology, v. 6, no. 2, pp. 99-104, 1982.

6. TATINCLAUX, J.C. and HIRAYAMA, K. " Determination of the

Flexural Strength and Elastic Modulus of Ice from In-Situ Cantilever Beam Tests", In Cold Region Science and Technology, v. 6, 1982.

7. LAU, M. "Ice Forces on Downward Breaking Cones", M. Eng. Thesis, Memorial University of Newfoundland, St. John's, April 1989.

8. LEGERER, F.J. Discussion Paper on Paper of G.P. Vance from Ice Technology 1975, The Society of Naval Architect, Montreal 1975.

9. SCHWARZ, J., WESSELS, E., and REINICKE, K.M. "Failure Modes and Failure Criteria of Level and Fragmented Ice Interacting with Conical Structures", COSMAR Final Report no. PP4-2.1, 1980.

10. WESSELS, E. "Model Test investigation of Ice Force on Fixed and Floating Conical Structures", In Proceedings of the 7th Ice Symposium, v. 3, pp. 203-220, IAHR, Hamburg, 1984.

11. RALSTON, T.D. "Plastic Limit Analysis of Sheet Ice Loads on Conical Structures:' In Proceedings of IUTAM Symposium on Physics and Mechanics of Ice, pp. 289-308, Copenhagen, Ed. Tryde, P., Springer-Verlag, Berlin, 1979.

12. HETENYI, M. "Beam on Elastic Foundations," The University of Michigan Press, Ann Arbor, Michigan, 1946.

13. KIM, J.K., and KOTRAS, T.V. "Mathematical Model to Describe the Behaviour of a Moving Ice Field Encountering a Conical Structure", APOA Project 57, Revised Report prepared for APOA by Arctec Canada Ltd., Montreal, v. 1, 1973

LIST OF TABLES

TABLES

LIST OF PHOTOGRAPHS

PHOTOGRAPHS

LIST OF FIGURES

FIGURES

LIST OF FIGURES (CONT'D)

FIGURES

LIST OF FIGURES (CONT'D)

FIGURES

LIST OF SYMBOLS

A_s	Cross-sectional area of ice flange
E_R	Elastic modulus of ice ridge
E_s	Elastic modulus of ice sheet
F	Force
F_h	Horizontal sheet ice force
F_v	Vertical sheet ice force
F_H	Horizontal ridge ice force
F_V	Vertical ridge ice force
F_b	Ice breaking force
F_c	Ice clearing force
F_m	Measured force
F_p	Presawn ice resistance
F_{sc}	Force adjusted to standard strength condition
F_t	Level ice resistance
F_w	Open water resistance
H	Thickness of ice ridge
H_e	Equivalent thickness of transformed rectangular beam
I_R	Moment of inertia of ice ridge
L	Length of cantilever beam
M_{aj}	Adjustment factor for inplane force effect
M_B	Buoyant force moment
M_u	Ultimate moment
P	Applied load
P_u'	measured vertical failure load
P_u	Calculated vertical failure load assumed no inplane force effect
V	Velocity
V_i	Volume of ice
WLD	Waterline diameter of cone
W_B	Width of ridge at bottom
W_R	Width of ridge at top
W_T	Width of ridge at waterline
e	Eccentricity of inplane force
g	Gravitational acceleration
h	Thickness of ice sheet
k_*	Foundation modulus
k^*	Adjusted foundation modulus accounted for spring stiffness of surrounding ice sheet
l_R	Characteristic length of ice ridge
l_s	Characteristic length of ice sheet
n	Modulus ratio
p_i	Density of ice
p_H	Density of ice ridge
p_s	Density of ice sheet
p_w	Density of doped water
r	Ice breaking force/total force ratio
r_p	Radius of the applied load in plate deflection test
v	Poisson's ratio for ice

LIST OF SYMBOLS

w	Width of cantilever beam
x_u	Length of wedge beam
y	Distance from neutral axis to failure surface
y_e	Distance from neutral axis to failure surface of transformed rectangular section
σ_{gov}	Governing strength at failure
β	Resolution factor
α	Cone inclination
μ	Dynamic friction coefficient
σ_C	Compressive strength of ice ridge
σ_c	Compressive strength of ice sheet
σ_F	Flexural strength of ice ridge
σ_f	Flexural strength of ice sheet
σ_S	Shear strength of ice ridge
σ_s	Shear strength of ice sheet
σ_m	Measured strength
σ_{sc}	Standard strength
ΔP	Incremental load
$\Delta\delta$	Elastic deflection increments
τ_w	Specific weight of water
α_p	r_p/l_s
α_r	Angle of the inclined surface of ridge

Table 1

SUMMARY OF MODEL ICE PROPERTIES
(LEVEL ICE)

Test Name	h (mm)	σ_f [1] (kPa)	E_s/σ_f	l_s/h	σ_s/σ_f	σ_c/σ_f	ρ_s (kg/m^3)
CONE9	54.6	26.7-23.2	1854	9.8	1.79	3.39	0.937
CONE11	85.1	46.7-36.1	2901	11.1	1.13	3.40	0.930
CONE13	35.6	41.6-33.7	802	9.8	0.81	1.40	0.936

NOTE: 1) Downward breaking strength ranging from the first run to the last run. The estimated ice strength of each run is given in Table 5.

Table 2

SUMMARY OF MODEL ICE PROPERTIES
(RIDGE ICE SYSTEM)

A) LEVEL ICE SHEET

Test Name	h (mm)	σ_f[1] (kPa)	E_s/σ_f	l_s/h	σ_s/σ_f	σ_c/σ_f	ρ_s (kg/m^3)
CONE10	36.3	35.6-23.9	660	9.4	0.51	1.34	0.942
CONE12	36.8	40.0-32.2	890	10.1	0.77	1.67	0.938

B) RIDGE PLATE

Test Name	H (mm)	σ_F[1] (kPa)	E_R/σ_F	l_R/H	σ_S/σ_F	σ_C/σ_F	ρ_H (kg/m^3)
CONE10	75.8	88.6-77.0	1920	11.6	--	2.24	0.927
CONE12	106.5	117.3-104.6	2633	13.0	--	1.96	0.920

C) SUMMARY OF RIDGE CROSS-SECTIONAL GEOMETRY DATA

Test Name: CONE10
Ridge Thickness: 75.8 mm

Run (#)	W_T (m)	W_R (m)
1	0.170	0.237
2	0.314	0.383
3	0.480	0.555
5	0.584	0.656
6	0.771	0.841
7	0.874	0.947
8	2.000	2.062
9	0.191	0.260
10	0.361	0.434
11	0.436	0.510
12	0.647	0.719
13	0.737	0.810
14	1.000	1.071
15	2.000	2.062

Test Name: CONE12
Ridge Thickness: 106.5 mm

Run (#)	W_T (m)	W_R (m)
1	0.439	0.563
2	0.598	0.722
3	0.827	0.951
4	4.000	4.124
5	0.238	0.362
6	0.407	0.531
7	0.590	0.714
8	0.813	0.937
9	4.000	4.124
10	0.257	0.381
11	0.452	0.576
12	0.586	0.710
13	0.811	0.935
14	4.000	4.124

NOTE: 1) Downward breaking strength ranging from the first run to the last run. The estimated ice strength of each run is given in Tables 10 and 11.

TEST MATRIX
(LEVEL ICE TESTS)

Test Name	Run No. (#)	h (mm)	WLD (m)	V (m/s)
CONE9	4	54.6	1.28	0.01
CONE9	5	54.6	1.28	0.05
CONE9	6	54.6	1.28	0.10
CONE9	7	54.6	1.48	0.01
CONE9	8	54.6	1.48	0.05
CONE9	9	54.6	1.48	0.10
CONE9	10	54.6	1.08	0.01
CONE9	11	54.6	1.08	0.05
CONE9	12	54.6	1.08	0.10
CONE11	1	85.1	1.48	0.01
CONE11	2	85.1	1.48	0.05
CONE11	3	85.1	1.48	0.10
CONE11	4	85.1	1.28	0.01
CONE11	5	85.1	1.28	0.05
CONE11	6	85.1	1.28	0.10
CONE11	7	85.1	1.08	0.01
CONE11	8	85.1	1.08	0.05
CONE11	9	85.1	1.08	0.10
CONE13	1	35.6	1.48	0.01
CONE13	2	35.6	1.48	0.05
CONE13	3	35.6	1.48	0.10
CONE13	4	35.6	1.48	0.25
CONE13	5	35.6	1.48	0.50
CONE13	6	35.6	1.28	0.01
CONE13	7	35.6	1.28	0.05
CONE13	8	35.6	1.28	0.10
CONE13	9	35.6	1.28	0.25
CONE13	10	35.6	1.28	0.50
CONE13	11	35.6	1.08	0.01
CONE13	12	35.6	1.08	0.05
CONE13	13	35.6	1.08	0.10
CONE13	14	35.6	1.08	0.25
CONE13	15	35.6	1.08	0.50
CONE13	16	35.6	1.08	0.25

TEST MATRIX
(RIDGE TESTS)

Test Name	Run No. (#)	H (mm)	WLD (m)	W_T (m)
CONE10	1	75.8	1.28	0.17
CONE10	2	75.8	1.28	0.31
CONE10	3	75.8	1.28	0.48
CONE10	5	75.8	1.28	0.58
CONE10	6	75.8	1.28	0.77
CONE10	7	75.8	1.28	0.88
CONE10	8	75.8	1.28	2.00
CONE10	9	75.8	1.48	0.19
CONE10	10	75.8	1.48	0.36
CONE10	11	75.8	1.48	0.44
CONE10	12	75.8	1.48	0.65
CONE10	13	75.8	1.48	0.74
CONE10	14	75.8	1.48	1.00
CONE10	15	75.8	1.48	2.00
CONE12	1	106.5	1.48	0.44
CONE12	2	106.5	1.48	0.60
CONE12	3	106.5	1.48	0.83
CONE12	4	106.5	1.48	4.00
CONE12	5	106.5	1.28	0.24
CONE12	6	106.5	1.28	0.41
CONE12	7	106.5	1.28	0.59
CONE12	8	106.5	1.28	0.81
CONE12	9	106.5	1.28	4.00
CONE12	10	106.5	1.08	0.26
CONE12	11	106.5	1.08	0.45
CONE12	12	106.5	1.08	0.59
CONE12	13	106.5	1.08	0.81
CONE12	14	106.5	1.08	4.00

NOTE: V = 0.05 m/s for all tests

Table 4

TEST MATRIX
(OPEN WATER TESTS)

Test Name	Run No. (#)	WLD (m)	V (m/s)
CONE_OW	1	1.28	0.01
CONE_OW	2	1.28	0.05
CONE_OW	3	1.28	0.10
CONE_OW	4	1.28	0.25
CONE_OW	5	1.28	0.50
CONE_OW	6	1.48	0.01
CONE_OW	7	1.48	0.05
CONE_OW	8	1.48	0.10
CONE_OW	9	1.48	0.25
CONE_OW	10	1.48	0.50
CONE_OW	11	1.08	0.01
CONE_OW	12	1.08	0.05
CONE_OW	13	1.08	0.10
CONE_OW	14	1.08	0.25
CONE_OW	15	1.08	0.25
CONE_OW[1]	16	1.28	0.50
CONE_OW	17	1.28	0.05

NOTE: 1) Tested in restricted channel

SUMMARY OF THE LEVEL ICE RESISTANCE TEST DATA

Run No. (#)	WLD (m)	V (m/s)	σ_f (kPa)	Horizontal Force (F_x) Average Mean (N)	Horizontal Force (F_x) Average RMS (N)	Horizontal Force (F_x) Peak Mean (N)	Vertical Force (F_z) Average Mean (N)	Vertical Force (F_z) Average RMS (N)	Vertical Force (F_z) Peak Mean (N)	Pitching Moment (F_y) Average Mean (Nm)	Pitching Moment (F_y) Average RMS (Nm)	Pitching Moment (F_y) Peak Mean (Nm)	Piece Size[1] (m)
Test Name: CONE9 Ice Thickness: 54.6 mm													
4	1.28	0.01	26.7	113	16	135	145	16	166	26	7	36	0.202
5	1.28	0.05	26.0	118	34	162	140	38	186	29	14	49	0.205
6	1.28	0.10	25.6	142	44	209	162	54	252	31	18	61	0.228
7	1.48	0.01	25.1	108	22	136	144	27	165	41	13	56	0.341
8	1.48	0.05	24.6	119	37	164	148	46	201	45	22	72	0.255
9	1.48	0.10	24.4	124	31	172	141	41	212	41	21	78	0.218
10	1.08	0.01	23.8	80	19	101	84	19	103	4	5	11	0.286
11	1.08	0.05	23.3	85	28	122	79	26	111	4	6	14	0.244
12	1.08	0.10	23.2	99	28	141	86	31	134	4	7	16	0.183
Test Name: CONE11 Ice Thickness: 85.1 mm													
1	1.48	0.01	46.7	365	125	485	460	132	557	138	55	180	0.204
2	1.48	0.05	45.4	422	110	520	529	104	648	137	45	192	0.223
3	1.48	0.10	44.8	422	129	548	508	155	688	155	65	255	0.361
4	1.28	0.01	42.9	324	86	385	386	80	425	53	24	78	0.204
5	1.28	0.05	41.9	320	83	396	376	83	457	55	23	87	0.176
6	1.28	0.10	41.5	382	102	497	425	112	573	73	35	146	0.153
7	1.08	0.01	37.4	285	120	315	310	118	379	13	19	32	0.171
8	1.08	0.05	36.5	288	76	360	314	59	381	3	12	27	0.162
9	1.08	0.10	36.1	306	75	395	311	69	421	5	15	34	0.181

Table 5 (1 of 2)

SUMMARY OF THE LEVEL ICE RESISTANCE TEST DATA (CONT'D)

Run No. (#)	WLD (m)	V (m/s)	σ_f (kPa)	Horizontal Force (F_x) Average Mean (N)	Horizontal Force (F_x) Average RMS (N)	Horizontal Force (F_x) Peak Mean (N)	Vertical Force (F_z) Average Mean (N)	Vertical Force (F_z) Average RMS (N)	Vertical Force (F_z) Peak Mean (N)	Pitching Moment (F_y) Average Mean (Nm)	Pitching Moment (F_y) Average RMS (Nm)	Pitching Moment (F_y) Peak Mean (Nm)	Piece Size[1] (m)
				Test Name: CONE13 Ice Thickness: 35.6 mm									
1	1.48	0.01	41.6	47	9	69	76	12	112	19	5	28	0.258
2	1.48	0.05	40.6	56	15	81	86	19	118	24	9	45	0.196
3	1.48	0.10	40.3	68	21	105	94	31	149	29	13	58	0.159
4	1.48	0.25	40.0	90	49	180	88	77	247	35	48	132	0.115
5	1.48	0.50	39.7	143	113	276	17	170	232	38	122	205	0.150
6	1.28	0.01	38.6	53	9	73	73	11	104	11	4	19	0.204
7	1.28	0.05	37.5	55	15	78	76	17	102	13	5	22	0.205
8	1.28	0.10	37.3	66	22	105	81	29	138	15	9	37	0.133
9	1.28	0.25	37.0	85	44	166	76	74	240	17	30	81	0.132
10	1.28	0.50	36.7	134	116	268	21	135	180	13	81	131	0.124
11	1.08	0.01	36.1	38	8	56	56	8	70	1	2	8	0.171
12	1.08	0.05	35.2	39	11	57	56	12	75	2	3	7	0.194
13	1.08	0.10	34.8	47	18	83	62	22	101	3	4	12	0.154
14	1.08	0.25	34.4	68	40	141	54	54	168	-0	14	28	0.134
15	1.08	0.50	34.1	105	87	219	23	106	146	-8	38	49	0.134
16	1.08	0.25	33.7	62	35	133	51	46	145	-0	13	27	0.128

NOTE: 1 Piece size is calculated from the dominant frequency from the resistance power density spectrum, e.g. Piece Size = Velocity/Dominant Frequency

Table 5 (2 of 2)

THE VALUES OF σ_s AND F_{sc} FOR FIGURES 17 TO 29

A. FIGURE 17: V = 0.01 M/S; WLD = 1.08 M; σ_s = 32.4 KPA

h (mm)	AVERAGE F_h (N)	AVERAGE F_v (N)	MEAN PEAK F_h (N)	MEAN PEAK F_v (N)
.055	114	119	142	145
.085	267	290	295	355
.036	37	55	54	68

B. FIGURE 18: V = 0.05 M/S; WLD = 1.08 M; σ_s = 32.4 KPA

h (mm)	AVERAGE F_h (N)	AVERAGE F_v (N)	MEAN PEAK F_h (N)	MEAN PEAK F_v (N)
.055	123	113	176	160
.085	276	301	345	365
.036	38	55	56	74

C. FIGURE 19: V = 0.10 M/S; WLD = 1.08 M; σ_s = 32.4 KPA

h (mm)	AVERAGE F_h (N)	AVERAGE F_v (N)	MEAN PEAK F_h (N)	MEAN PEAK F_v (N)
.055	297	301	383	408
.085	144	124	205	194
.036	47	62	84	101

D. FIGURE 20: V = 0.01 M/S; WLD = 1.28 M; σ_s = 35.6 KPA

h (mm)	AVERAGE F_h (N)	AVERAGE F_v (N)	MEAN PEAK F_h (N)	MEAN PEAK F_v (N)
.055	136	174	162	200
.085	255	303	303	334
.036	47	64	64	91

THE VALUES OF σ_s AND F_{sc} FOR FIGURES 17 TO 29 (CONT'D)

E. FIGURE 21: V = 0.05 M/S; WLD = 1.28 M; σ_s = 35.6 KPA

h (mm)	AVERAGE F_h (N)	AVERAGE F_V (N)	MEAN PEAK F_h (N)	MEAN PEAK F_V (N)
.055	146	172	199	229
.085	258	302	318	368
.036	50	68	70	92

F. FIGURE 22: V = 0.10 M/S; WLD = 1.28 M; σ_s = 35.6 KPA

h (mm)	AVERAGE F_h (N)	AVERAGE F_V (N)	MEAN PEAK F_h (N)	MEAN PEAK F_V (N)
.055	177	203	261	315
.085	310	344	403	465
.036	59	73	95	125

G. FIGURE 23: V = 0.01 M/S; WLD = 1.48 M; σ_s = 36.6 KPA

h (mm)	AVERAGE F_h (N)	AVERAGE F_V (N)	MEAN PEAK F_h (N)	MEAN PEAK F_V (N)
.055	151	202	190	231
.085	300	378	398	458
.036	43	70	63	103

H. FIGURE 24: V = 0.05 M/S; WLD = 1.48 M; σ_s = 36.6 KPA

h (mm)	AVERAGE F_h (N)	AVERAGE F_V (N)	MEAN PEAK F_h (N)	MEAN PEAK F_V (N)
.055	169	210	233	286
.085	355	446	438	546
.036	52	81	76	111

THE VALUES OF σ_s AND F_{sc} FOR FIGURES 17 TO 29 (CONT'D)

I. FIGURE 25: V = 0.10 M/S; WLD = 1.48 M; σ_s = 36.6 KPA

h (mm)	AVERAGE F_h (N)	AVERAGE F_V (N)	MEAN PEAK F_h (N)	MEAN PEAK F_V (N)
.055	177	201	246	304
.085	360	433	467	587
.036	64	88	99	141

J. FIGURES 26 TO 29: V = 0.01 M/S; WLD = 1.28 M; σ_s = 35.6 KPA

h^2 (mm^2)	AVERAGE F_h (N)	AVERAGE F_V (N)	MEAN PEAK F_h (N)	MEAN PEAK F_V (N)
PRESENT TESTS				
.00303	136	174	162	200
.00723	255	303	303	334
.00130	47	64	64	91
PREVIOUS TESTS				
.00464	283	383	291	411
.00106	46	70	57	72
.00262	134	144	135	159

K. FIGURES 26 TO 29: V = 0.05 M/S; WLD = 1.28 M; σ_s = 35.6 KPA

h^2 (mm^2)	AVERAGE F_h (N)	AVERAGE F_V (N)	MEAN PEAK F_h (N)	MEAN PEAK F_V (N)
PRESENT TESTS				
.00303	146	172	199	229
.00723	258	302	318	368
.00130	50	68	70	92
PREVIOUS TESTS				
.00464	267	366	311	420
.00106	59	81	66	80
.00262	129	149	161	176

THE VALUES OF σ_s AND F_{sc} FOR FIGURES 17 TO 29 (CONT'D)

L. FIGURES 26 TO 29: V = 0.10 M/S; WLD = 1.28 M; σ_s = 35.6 KPA

h^2 (mm^2)	AVERAGE F_h (N)	AVERAGE F_v (N)	MEAN PEAK F_h (N)	MEAN PEAK F_v (N)
PRESENT TESTS				
.00303	177	203	261	315
.00723	310	344	403	465
.00130	59	73	95	125
PREVIOUS TESTS				
.00464	295	397	368	526
.00106	76	99	95	110
.00262	158	180	233	241

Table 7

EQUATIONS OF STRENGTH CURVES (AVERAGE PEAK FORCES)[1]

V	F_h		F_v	
	B	C	B	C
(m/s)	(N/kPa)	(N)	(N/kPa)	(N)
0.01	0.83	12.9	1.13	17.1
0.05	1.01	16.6	1.16	22.6
0.10	1.33	19.8	1.50	24.6
0.25	1.61	36.6	1.50	16.1
0.50	1.69	80.0	1.46	-24.8

NOTE: 1) Test condition:

Cone angle = 45°
Water line dia. = 1.28 m
Friction = 0.15
Ice thickness = 33.5 mm

Equation:

$$\text{Force(N)} = B \times \sigma_f(\text{kPa}) + C$$

Table 8

SUMMARY[1] OF ICE BREAKING,
ICE CLEARING AND OPEN WATER RESISTANCES OF SELECTED TESTS

V (m/s)	Solid Ice F_h (N)	Solid Ice F_V (N)	Presawn Ice F_h (N)	Presawn Ice F_V (N)	Force Components: Open Water F_h (N)	Open Water F_V (N)	Breaking F_h (N)	Breaking F_V (N)	Clearing F_h (N)	Clearing F_V (N)
0.01	46.1	62.3	15	16	1.3	2.8	31.1	46.3	13.7	13.2
0.05	57.0	69.0	20	22	2.0	3.9	37.0	47.0	18.0	18.1
0.10	73.0	84.6	22	23	2.9	4.7	51.0	61.6	19.1	18.3
0.25	101.0	76.1	45	20	11.2	-6.4	56.0	56.1	33.8	26.4
0.50	147.6	33.6	82	-28	31.3	-56.8	65.6	61.6	50.7	55.2

NOTE: 1) Test condition:

Cone angle	= 45°
Water line dia.	= 1.28 m
Friction	= 0.15
Ice thickness	= 33.5 mm
Flexural strength	= 40 kPa

Table 9

SUMMARY OF OPEN WATER RESISTANCE TEST DATA

Run No.	V (m/s)	Hori. Force Mean (N)	Hori. Force RMS (N)	Vert. Force Mean (N)	Vert. Force RMS (N)	Pitch Moment Mean (Nm)	Pitch Moment RMS (Nm)
			WLD = 1.28 m				
1	0.01	1.3	3.9	2.8	5.7	-0.1	2.0
2	0.05	2.0	3.1	3.9	6.7	-0.1	0.9
3	0.10	2.9	3.8	4.7	11.0	-0.1	0.3
4	0.25	11.2	6.3	-6.4	13.0	0.2	3.3
5	0.50	31.3	9.9	-56.8	27.8	2.2	4.2
			WLD = 1.48 m				
6	0.01	0.6	3.7	-9.6	9.4	0.8	1.6
7	0.05	2.0	3.2	-13.3	7.6	1.0	0.8
8	0.10	3.7	4.2	-17.0	8.5	1.2	1.4
9	0.25	13.0	10.9	-42.0	12.6	3.2	2.6
10	0.50	37.8	11.8	-116.7	26.5	10.0	4.2
			WLD = 1.08 m				
11	0.01	-0.4	3.8	-4.3	11.0	0.0	1.5
12	0.05	-0.8	3.3	-1.8	10.9	0.1	1.4
13	0.10	2.1	4.0	-2.5	8.5	-0.1	1.6
14	0.25	7.9	6.2	-14.8	9.2	-1.1	4.6
15	0.50	22.5	8.9	-52.9	18.2	-2.4	4.1
			WLD = 1.28 m				
16[1]	0.25	9.4	*	-31.7	*	-0.4	*
17[1]	0.50	31.1	*	-76.4	*	1.4	*

NOTE: 1) Restricted channel water resistance

SUMMARY OF THE MULTI-YEAR RIDGE RESISTANCE TEST DATA

Run No. (#)	W_T (m)	σ_R[1] (kPa)	Horizontal Force (F_x) #4[2] (N)	#5 (N)	#6 (N)	Vertical Force (F_z) #4 (N)	#5 (N)	#6 (N)	Pitching Moment (M_y) #4 (N)	#5 (N)	#6 (N)	Broken Ridge Size[3] A_R (m)	B_R (m)	α_R (Deg)	Mode[4] (#)
Test Name: CONE10 WLD: 1.28 m Ridge Thickness: 75.8 mm															
1	0.17	88.6	154	181	219	193	260	239	63	88	71	1.13	1.40	52	1
2	0.31	87.8	242	328	292	254	444	295	92	167	97	0.83	1.50	43	1
3	0.48	87.2	344	278	256	277	400	371	101	181	133	*	1.11	*	3
5	0.58	85.9	367	460	379	381	531	377	139	226	108	0.84	1.36	66	1
6	0.77	82.9	332	480	433	351	533	423	129	223	144	*	*	*	3
7	0.88	82.2	468	506	468	459	693	480	165	202	160	*	0.70	*	3
Test Name: CONE10 WLD: 1.48 m Ridge Thickness: 75.8 mm															
9	0.19	80.2	145	188	181	194	250	211	85	132	103	0.94	1.17	59	2
10	0.36	79.7	140	282	263	182	370	289	88	200	150	1.07	1.43	64	2
11	0.44	79.1	262	315	303	294	422	324	154	220	165	1.11	1.71	56	2
12	0.65	78.8	376	471	408	400	610	419	211	265	209	0.79	1.60	58	1
13	0.74	78.0	353	469	443	359	648	452	209	338	257	2.28	0.81	45	3
14	1.00	77.7	315	491	484	362	592	512	198	328	272	2.88	0.88	45	3
Test Name: CONE12 WLD: 1.48 m Ridge Thickness: 106.5 mm															
1	0.44	117.3	470	758	725	539	932	755	295	452	404	1.40	1.76	68	2
2	0.60	115.9	795	1123	871	799	1139	923	432	687	461	1.58	2.21	62	2
3	0.83	115.4	727	958	1065	774	1341	1043	453	630	544	1.52	2.64	56	2

Table 10 (1 of 2)

SUMMARY OF THE MULTI-YEAR RIDGE RESISTANCE TEST DATA (CONT'D)

Run No. (#)	W_T (m)	σ_B[1] (kPa)	Horizontal Force (F_x) #4[2] (N)	#5 (N)	#6 (N)	Vertical Force (F_z) #4 (N)	#5 (N)	#6 (N)	Pitching Moment (M_y) #4 (N)	#5 (N)	#6 (N)	Broken Ridge Size[3] A_R (m)	B_R (m)	α_R (Deg)	Mode[4] (#)
Test Name: CONE12 WLD: 1.28 m Ridge Thickness: 106.5 mm															
5	0.24	110.9	172	316	444	195	340	428	74	143	150	1.42	1.61	68	2
6	0.41	110.2	632	736	661	587	798	680	214	378	222	1.87	2.35	60	2
7	0.59	109.7	515	773	814	514	839	789	206	378	278	1.76	2.16	71	2
8	0.81	109.1	981	1143	1142	949	1170	1070	342	449	361	1.73	2.95	53	2
Test Name: CONE12 WLD: 1.08 m Ridge Thickness: 106.5 mm															
10	0.26	107.3	388	498	475	369	562	437	74	130	85	1.07	1.29	72	2
11	0.45	106.4	613	971	751	539	760	645	103	214	110	1.58	2.04	63	2
12	0.59	105.8	623	892	850	597	864	820	148	227	151	1.42	1.85	70	2
13	0.81	105.3	1011	1260	1010	933	1372	932	163	164	163	1.80	3.06	52	2

NOTE:
1 Downward breaking flexural strength of ridge ice
2 Events of a particular failure scenario as defined in Section 3.2.1
3 Dimensions of broken ridge fragments

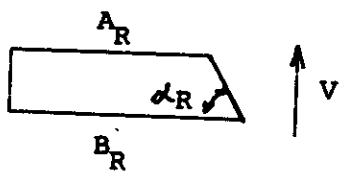

4 Failure scenarios as defined in Section 3.2.1.

Table 10 (2 of 2)

SUMMARY OF THE RIDGE PLATE RESISTANCE TEST DATA (MULTI-YEAR RIDGE RESISTANCE TESTS)

Run No. (#)	WLD (m)	σ_f (kPa)	Horizontal Force (F_x) Average Mean (N)	Horizontal Force (F_x) Average RMS (N)	Horizontal Force (F_x) Peak Mean (N)	Vertical Force (F_z) Average Mean (N)	Vertical Force (F_z) Average RMS (N)	Vertical Force (F_z) Peak Mean (N)	Pitching Moment (M_y) Average Mean (Nm)	Pitching Moment (M_y) Average RMS (Nm)	Pitching Moment (M_y) Peak Mean (Nm)	No. of Peaks
Test Name: CONE10 Ridge Plate Thickness: 75.8 mm												
8	1.28	81.2	326	177	493	354	185	518	95	62	161	9
15	1.48	77.0	341	174	518	279	196	578	170	98	279	7
Test Name: CONE12 Ridge Plate Thickness: 106.5 mm												
4	1.48	114.7	1059	494	1510	1103	492	1495	419	216	618	13
9	1.28	108.7	874	531	1388	884	517	1368	186	136	345	12
14	1.08	104.6	1034	512	1508	985	473	1408	16	84	116	11

Table 11

SUMMARY OF THE ANALYTICAL PREDICTIONS

Run No. (#)	n	z^1 (m)	I_R (m**4)	l_R (m)	$\tilde{\sigma}_c$ (kPa)	$\tilde{\sigma}_f$ (kPa)	Mode[2] (#)	S_c[3] (kPa)	S_t (kPa)	F_H (N)	F_V (N)
		Test Name: CONE10 WLD: 1.28 m Ridge Thickness: 75.8 mm									
1	0.169	0.0367	0.54E+07	0.966	184	35.6	1	184	28.1	236	175
2	0.166	0.0321	0.73E+07	0.955	183	34.8	2	174	34.8	348	257
3	0.164	0.0308	0.10E+08	0.966	182	34.2	2	148	34.2	427	316
5	0.161	0.0288	0.10E+08	0.931	181	33.0	2	136	33.0	438	324
6	0.153	0.0267	0.11E+08	0.890	176	30.2	2	119	30.2	461	341
7	0.151	0.0263	0.12E+08	0.885	175	29.6	2	114	39.6	491	363
		Test Name: CONE10 WLD: 1.48 m Ridge Thickness: 75.8 mm									
9	0.146	0.0343	0.52E+07	0.942	172	27.9	2	158	27.9	233	172
10	0.145	0.0308	0.77E+07	0.936	172	27.6	2	140	27.6	313	231
11	0.144	0.0296	0.83E+07	0.922	171	27.1	2	130	27.1	333	246
12	0.143	0.0275	0.10E+08	0.895	170	26.8	2	115	26.8	394	291
13	0.132	0.0266	0.10E+08	0.880	170	24.5	2	107	24.5	401	296
14	0.131	0.0252	0.12E+08	0.853	169	24.3	2	100	24.3	468	346

Table 12 (1 of 2)

SUMMARY OF THE ANALYTICAL PREDICTIONS

Run No. (#)	n	z^1 (m)	I_R ($m^{**}4$)	l_R (m)	σ_c (kPa)	σ_f (kPa)	Mode[2] (#)	S_c[3] (kPa)	S_t (kPa)	F_H (N)	F_V (N)
		Test Name: CONE12 WLD: 1.48 m Ridge Thickness: 106.5 mm									
1	0.124	0.0382	0.20E+08	1.409	243	40.4	2	205	40.4	638	472
2	0.120	0.0353	0.22E+08	1.370	240	39.6	2	183	39.6	703	520
3	0.119	0.0330	0.25E+08	1.327	239	39.3	2	166	39.3	804	594
		Test Name: CONE12 WLD: 1.28 m Ridge Thickness: 106.5 mm									
5	0.107	0.0420	0.14E+08	1.470	230	36.7	2	225	36.7	434	321
6	0.105	0.0362	0.17E+08	1.405	228	36.3	2	200	36.3	551	407
7	0.104	0.0332	0.19E+08	1.354	227	36.1	2	176	36.1	629	465
8	0.103	0.0309	0.22E+08	1.306	226	35.8	2	159	35.8	713	527
		Test Name: CONE12 WLD: 1.08 m Ridge Thickness: 106.5 mm									
10	0.095	0.0392	0.13E+08	1.454	222	33.6	2	208	33.6	423	313
11	0.093	0.0337	0.16E+08	1.376	220	33.2	2	185	33.2	523	386
12	0.092	0.0316	0.17E+08	1.335	219	32.9	2	168	32.9	571	422
13	0.091	0.0294	0.19E+08	1.284	218	32.6	2	138	32.6	648	479

NOTE:
1 Distance from the bottom of ridge to neutral axis.
2 Failure criterion: 2 - tensile failure at top surface of ice sheet, 1- compressive failure at the bottom of ridge.
3 Stress at failure: S_c - compressive stress at bottom surface of ridge, S_t- tensile stress at the surface of ice sheet.

Table 12 (2 of 2)

Table 13

COMPARISON OF MEASURED AND PREDICTED FORCES

Failure[1] Run No. (#)	Measured F_H (N)	Measured F_V (N)	Predicted F_H (N)	Predicted F_V (N)	Predicted/Measured F_H	Predicted/Measured F_V	Mode (N)
Test Name: CONE10 WLD: 1.28 m Ridge Thickness: 75.8 mm							
1	194	212	236	175	1.22	0.82	1
2	267	268	348	257	1.30	0.96	1
5	354	350	438	324	1.24	0.93	1
Test Name: CONE10 WLD: 1.48 m Ridge Thickness: 75.8 mm							
9	145	173	233	172	1.61	1.00	2
10	227	251	313	231	1.38	0.92	2
11	267	286	333	246	1.25	0.86	2
12	372	381	394	291	1.06	0.77	1

NOTE: 1) Failure scenarios as defined in Section 3.2.1.

Table 14

SUMMARY OF NON-DIMENSIONAL ANALYSIS

Run No. (#)	σ_{gov} (kPa)	H_e (m)	F_H (N)	F_V (N)	Non-Dimensional[1] F_H	Non-Dimensional[1] F_V	W_T (m)	l_R (m)	Non-Dim.[2] W_T
Test Name: CONE10 WLD: 1.28 m Ridge Thickness: 75.8 mm									
1	184	0.073	194	212	0.19	0.21	0.170	0.966	0.18
2	174	0.065	267	268	0.35	0.35	0.314	0.955	0.33
5	136	0.060	354	350	0.71	0.70	0.584	0.931	0.63
Test Name: CONE10 WLD: 1.48 m Ridge Thickness: 75.8 mm									
9	172	0.069	145	173	0.17	0.20	0.191	0.942	0.20
10	140	0.063	227	251	0.39	0.43	0.361	0.936	0.39
11	130	0.061	267	286	0.53	0.57	0.437	0.922	0.47
12	115	0.057	372	381	0.96	0.98	0.647	0.895	0.72

NOTE: 1) The forces are non-dimensionalized by multiplying $0.97/(\sigma_{gov} * H_e^2)$

2) The width is non-dimensionalized by dividing l_R

PLATE 1. VIEW OF ICE BASIN SHOWING SERVICE CARRIAGE

PLATE 2. IN-SITU CANTILEVER BEAM TESTS TO MEASURE THE FLEXURAL STRENGTH OF ICE

PLATE 3. PLATE DEFLECTION METHOD TO MEASURE THE ELASTIC MODULUS OF ICE

PLATE 4. APPARATUS FOR COMPRESSIVE AND SHEAR STRENGTH TESTS

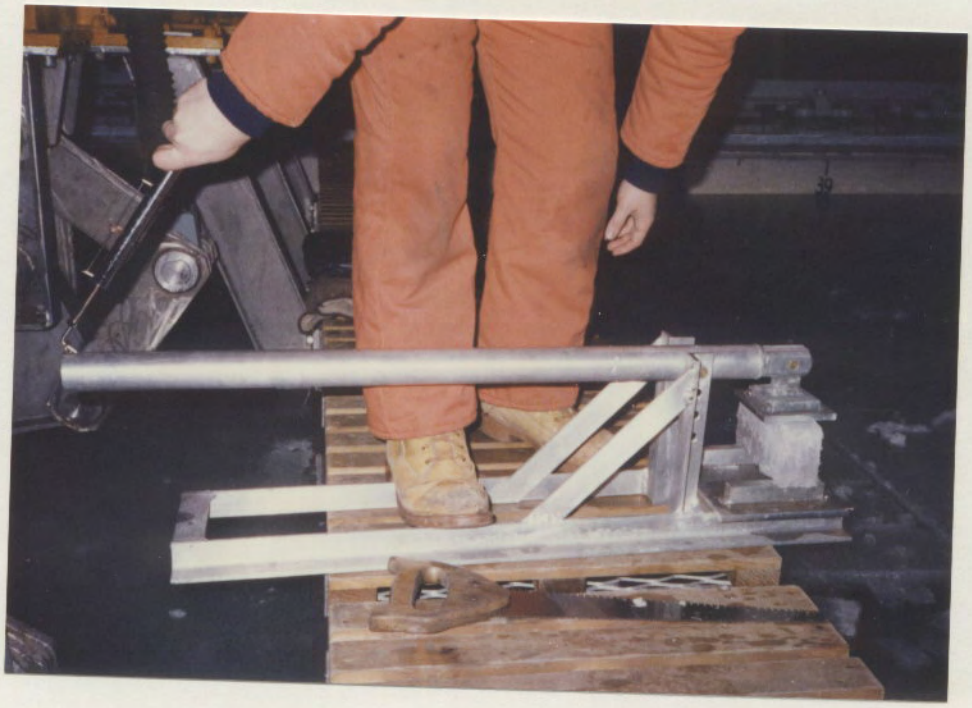

PLATE 5. PARENTAL RIDGE BEAMS CUT TO SPECIFIC WIDTHS

PLATE 6. PARENTAL RIDGE BEAMS PUSHED TO SPECIFIC LOCATIONS DURING SECOND SEEDING

PLATE 7. SEEDING FOR ICE SHEET IN BETWEEN RIDGE BEAMS

PLATE 8. TYPICAL VERTICAL CROSS-SECTION OF MODEL RIDGE

PLATE 9. 45 DEGREE MODEL CONE CONNECTED TO THE TEST FRAME THROUGH A 6-COMPONENT LOAD CELL

PLATE 10. TYPICAL BROKEN RIDGE FRAGMENTS ASSOCIATED WITH FAILURE MODES 1 AND 2 (TEST CONE12, RUN NO. 1)

PLATE 11. TYPICAL BROKEN RIDGE FRAGMENTS ASSOCIATED WITH FAILURE MODE 3 (TEST CONE10, RUN NO. 6)

PLATE 12. FAILURE MODES 1 AND 2 - EVENT 1: CIRCUMFERENTIAL CRACK FORMED AT THE SHEET RIDGE INTERFACE

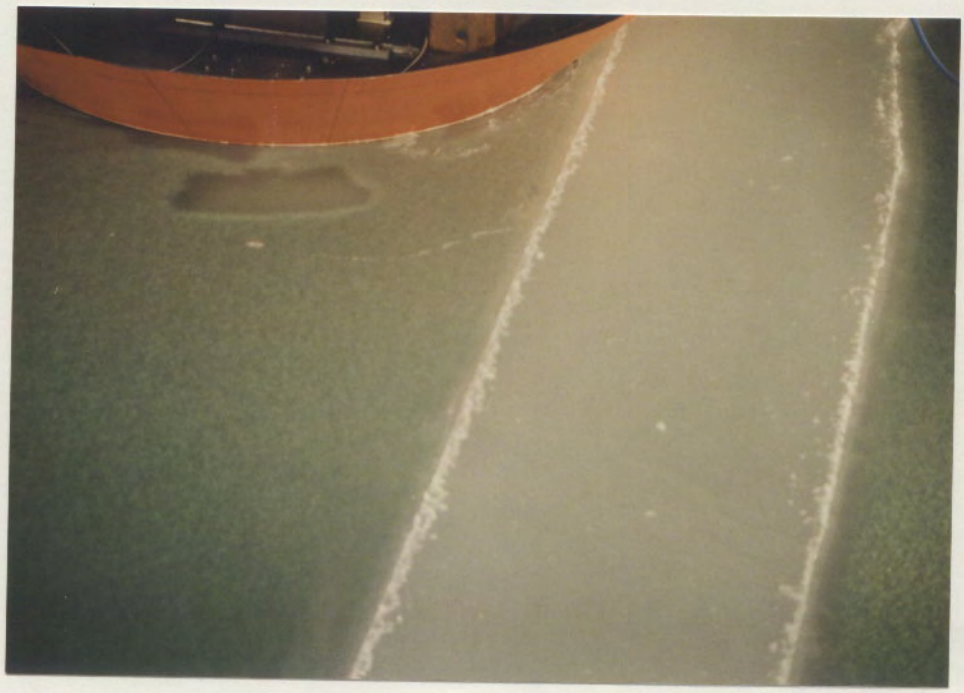

PLATE 13. FAILURE MODES 1 AND 2 - EVENT 2:
FORMATION OF THE CENTER CRACK

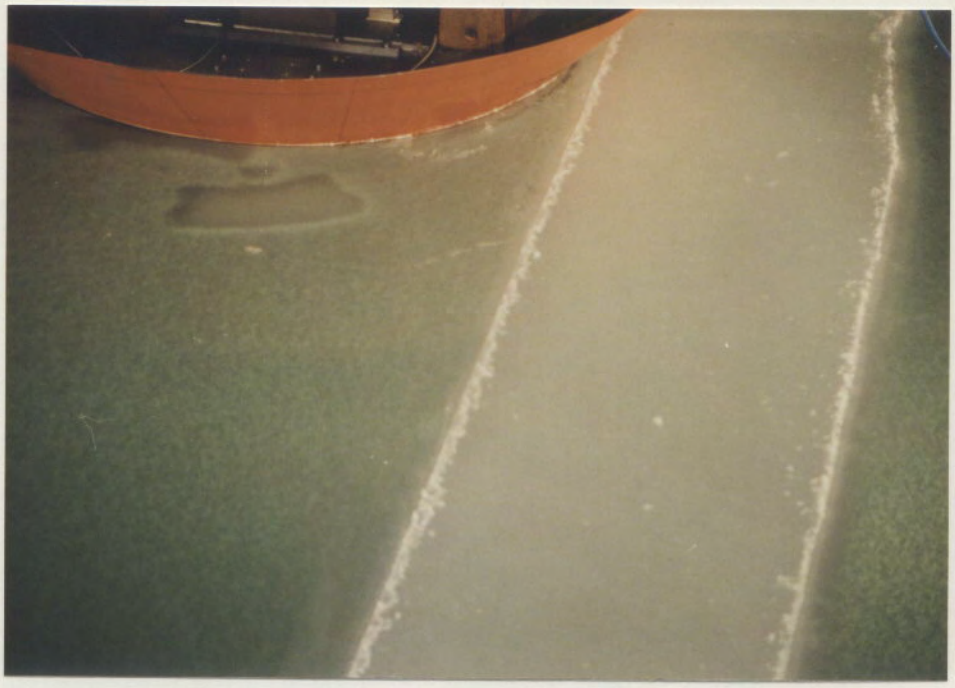

PLATE 14. FAILURE MODES 1 AND 2 - EVENT 3:
FIRST APPEARANCE OF HINGE CRACK

PLATE 15. FAILURE MODES 1 AND 2 - EVENT 3: SECOND HINGE CRACK FORMED ADJACENT TO THE FIRST HINGE CRACK

PLATE 16. FAILURE MODE 1 - EVENT 6: FAILURE BY HINGE CRACK EXTENSION INTO ICE SHEET (TEST CONE10, RUN NO. 2)

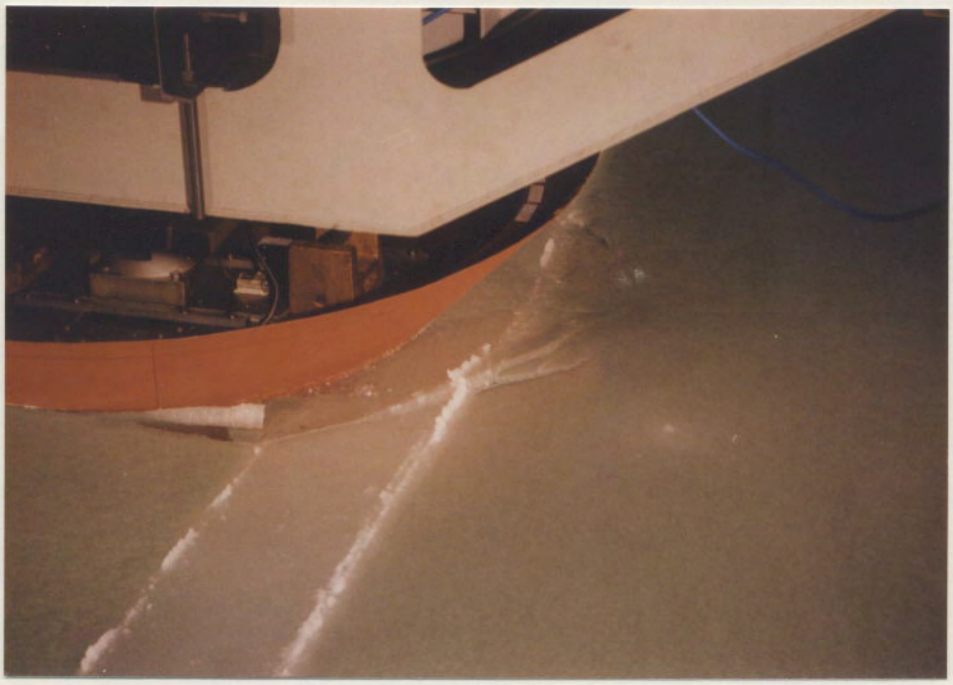

PLATE 17. FAILURE MODE 2 - EVENT 6: FAILURE BY RIDGE/SHEET SEPARATION (TEST CONE12, RUN NO. 2)

PLATE 18. FAILURE MODE 3: MIXED BEAM/SHEET FAILURE (TEST CONE10 RUN NO. 3)

Figure 1

CROSS-SECTIONAL PROFILE OF MODEL RIDGE

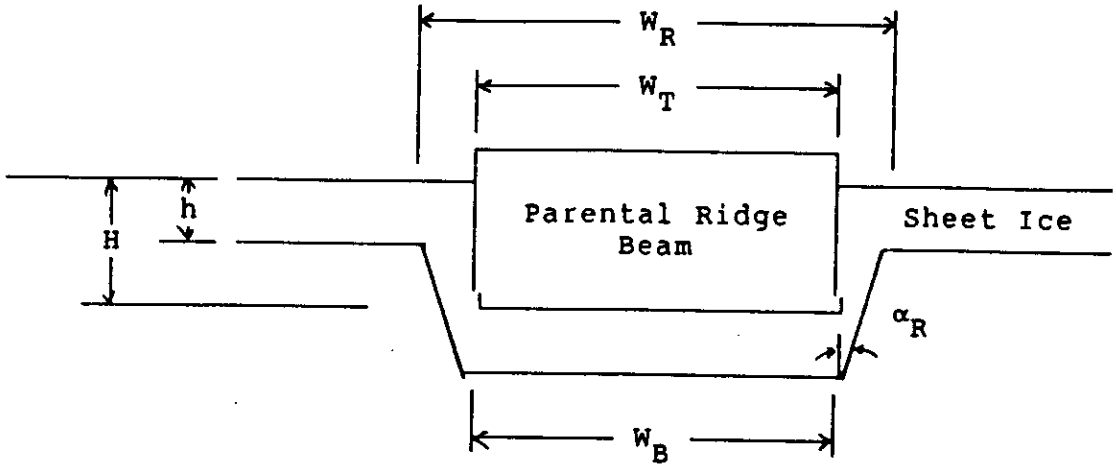

Figure 2

MODEL GEOMETRIES AND EXPERIMENTAL SETUP (NOTE: NOT OF SCALE)

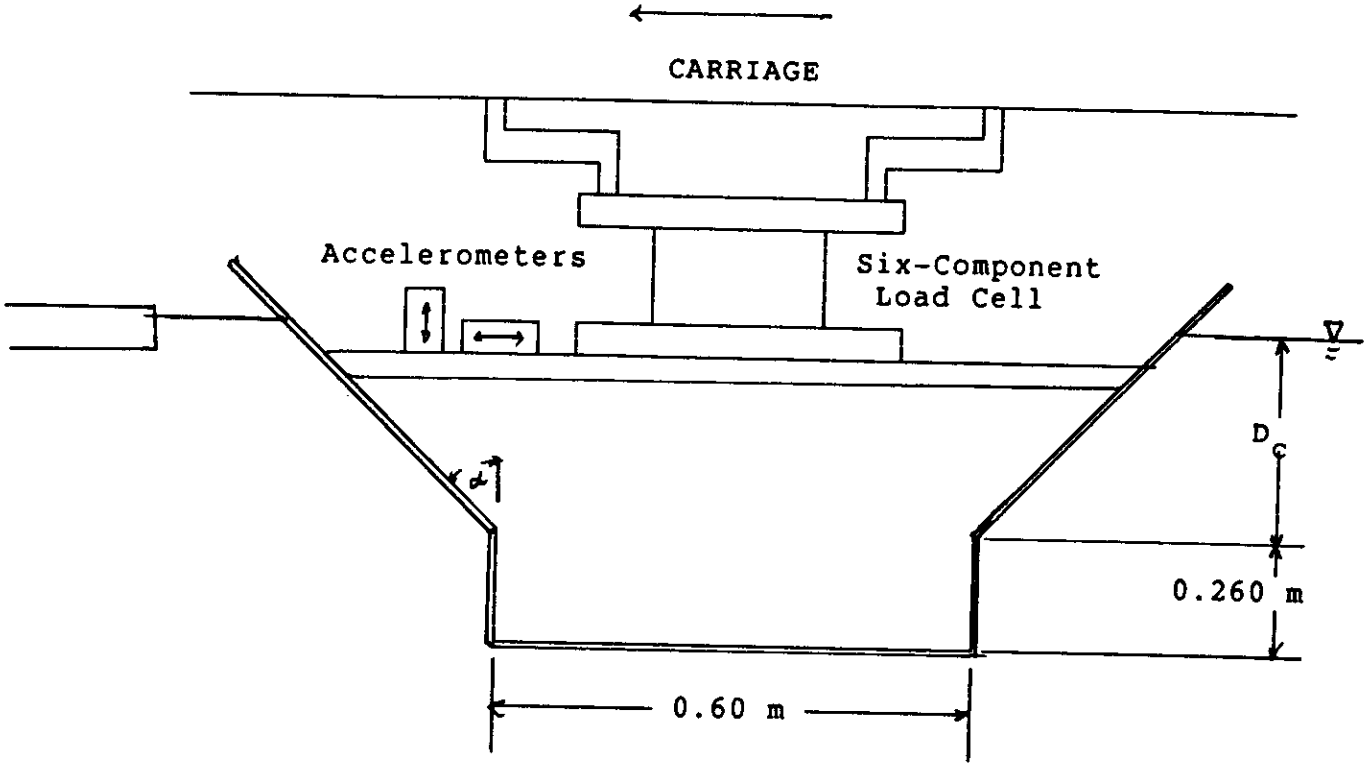

α(°)	WLD(m)	D_c(m)
45	1.08	0.24
	1.28	0.34
	1.48	0.44

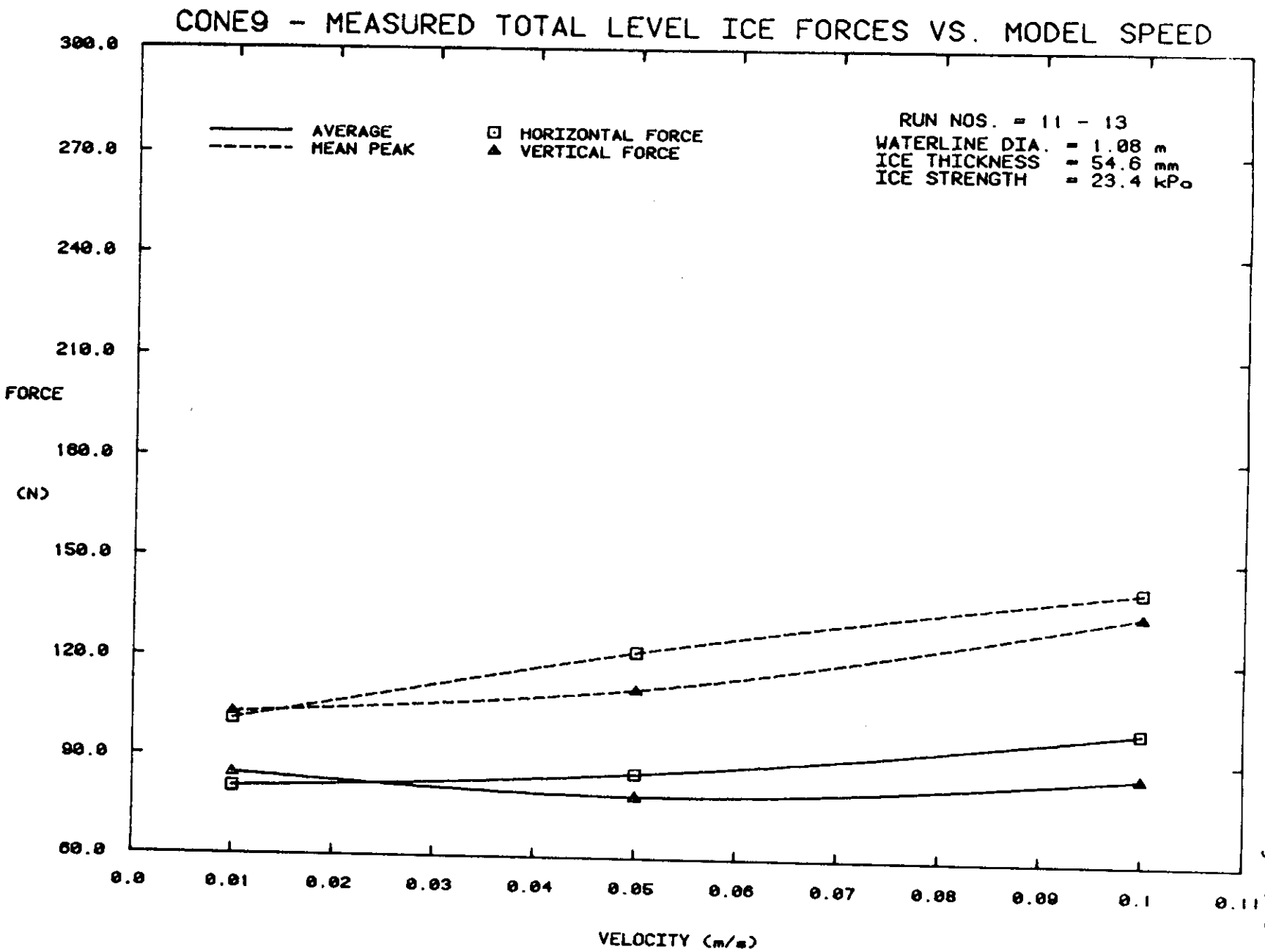
CONE9 - MEASURED TOTAL LEVEL ICE FORCES VS. MODEL SPEED
AVERAGE
MEAN PEAK
HORIZONTAL FORCE
VERTICAL FORCE
RUN NOS. = 11 - 13
WATERLINE DIA. = 1.08 m
ICE THICKNESS = 54.6 mm
ICE STRENGTH = 23.4 kPa
300.0
270.0
240.0
210.0
FORCE
180.0
(N)
150.0
120.0
90.0
60.0
0.0
0.01
0.02
0.03
0.04
0.05
0.06
0.07
0.08
0.09
0.1
0.11
VELOCITY (m/s)

Figure 4

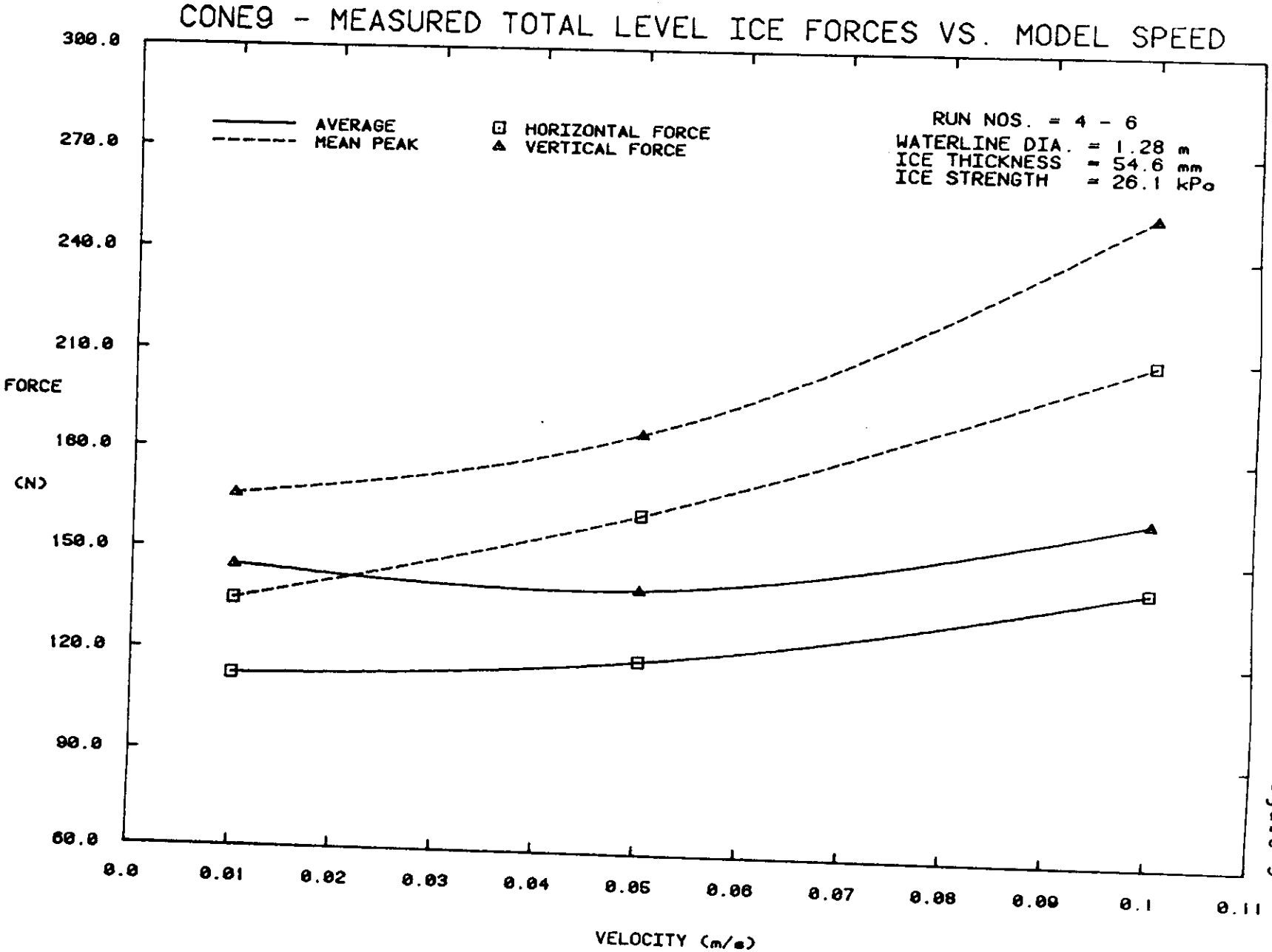
CONE9 - MEASURED TOTAL LEVEL ICE FORCES VS. MODEL SPEED
AVERAGE
MEAN PEAK
HORIZONTAL FORCE
VERTICAL FORCE
RUN NOS. = 4 - 6
WATERLINE DIA. = 1.28 m
ICE THICKNESS = 54.6 mm
ICE STRENGTH = 26.1 kPa
FORCE
(N)
300.0
270.0
240.0
210.0
180.0
150.0
120.0
90.0
60.0
0.0
0.01
0.02
0.03
0.04
0.05
0.06
0.07
0.08
0.09
0.1
0.11
VELOCITY (m/s)

Figure 5

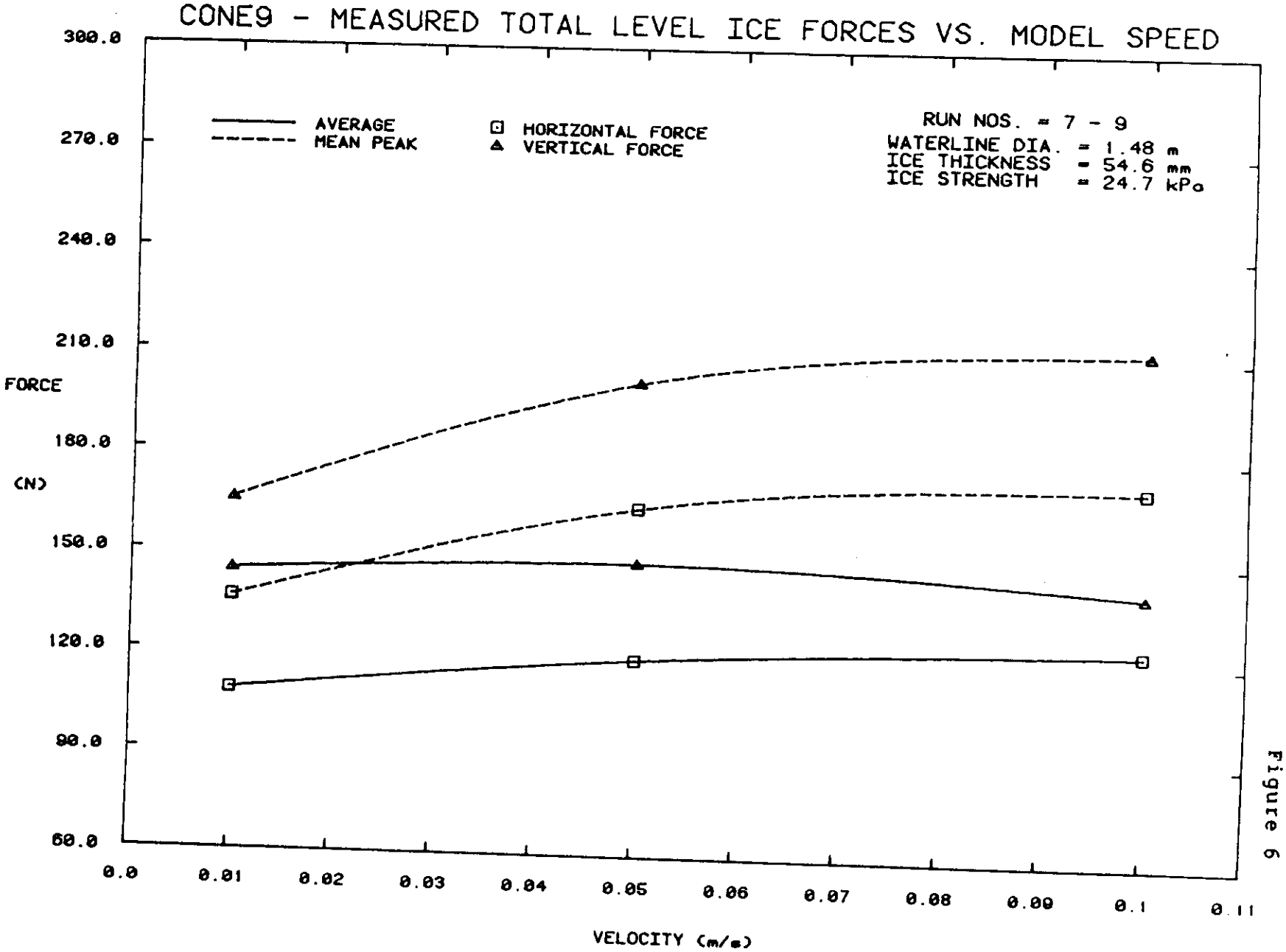
CONE9 - MEASURED TOTAL LEVEL ICE FORCES VS. MODEL SPEED
AVERAGE
MEAN PEAK
HORIZONTAL FORCE
VERTICAL FORCE
RUN NOS. = 7 - 9
WATERLINE DIA. = 1.48 m
ICE THICKNESS = 54.6 mm
ICE STRENGTH = 24.7 kPa
FORCE
(N)
300.0
270.0
240.0
210.0
180.0
150.0
120.0
90.0
60.0
0.0
0.01
0.02
0.03
0.04
0.05
0.06
0.07
0.08
0.09
0.1
0.11
VELOCITY (m/s)

Figure 6

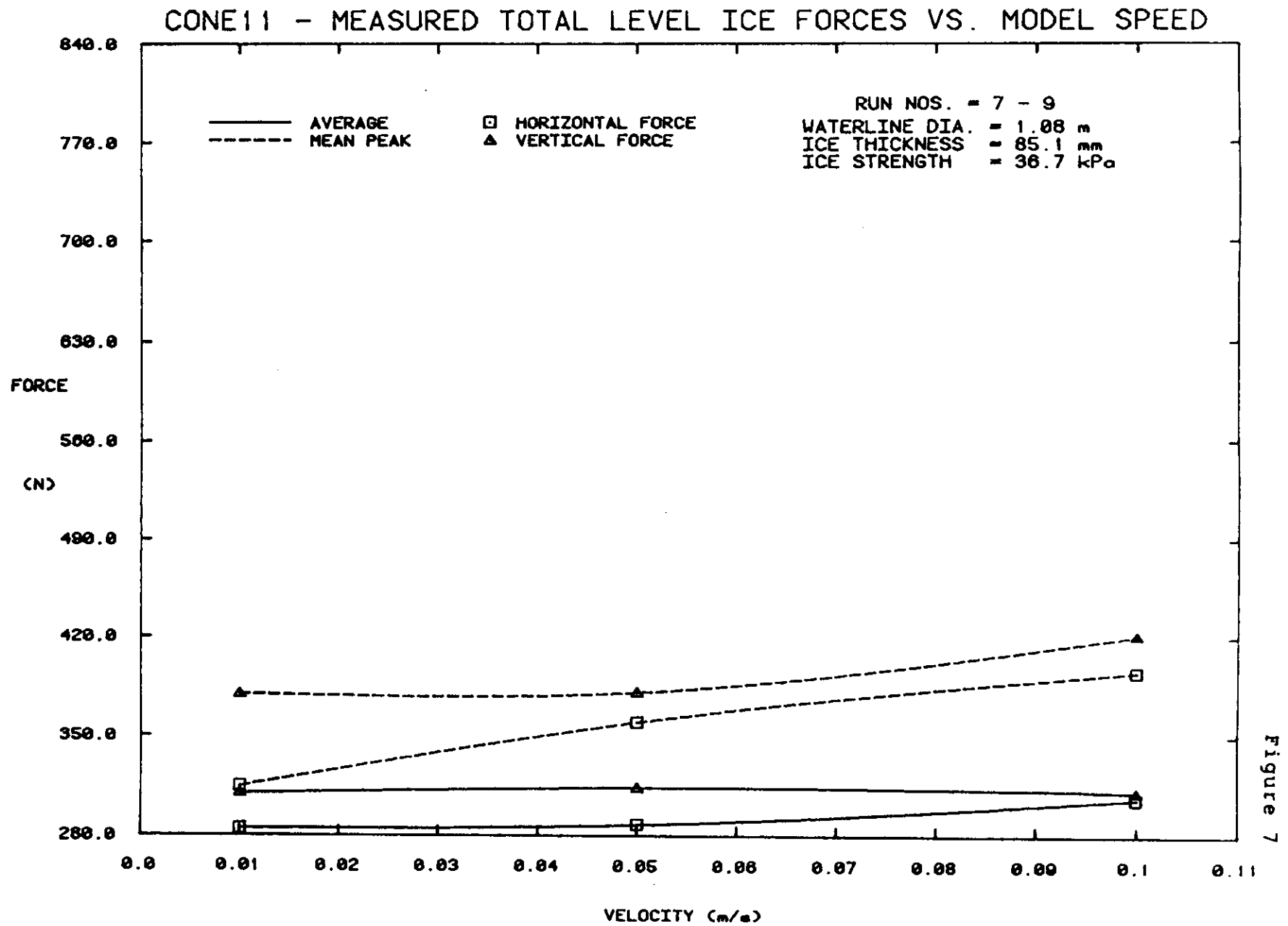
CONE11 - MEASURED TOTAL LEVEL ICE FORCES VS. MODEL SPEED
AVERAGE
MEAN PEAK
HORIZONTAL FORCE
VERTICAL FORCE
RUN NOS. = 7 - 9
WATERLINE DIA. = 1.08 m
ICE THICKNESS = 85.1 mm
ICE STRENGTH = 36.7 kPa
840.0
770.0
700.0
630.0
FORCE
560.0
(N)
490.0
420.0
350.0
280.0
0.0
0.01
0.02
0.03
0.04
0.05
0.06
0.07
0.08
0.09
0.1
0.11
VELOCITY (m/s)

Figure 7

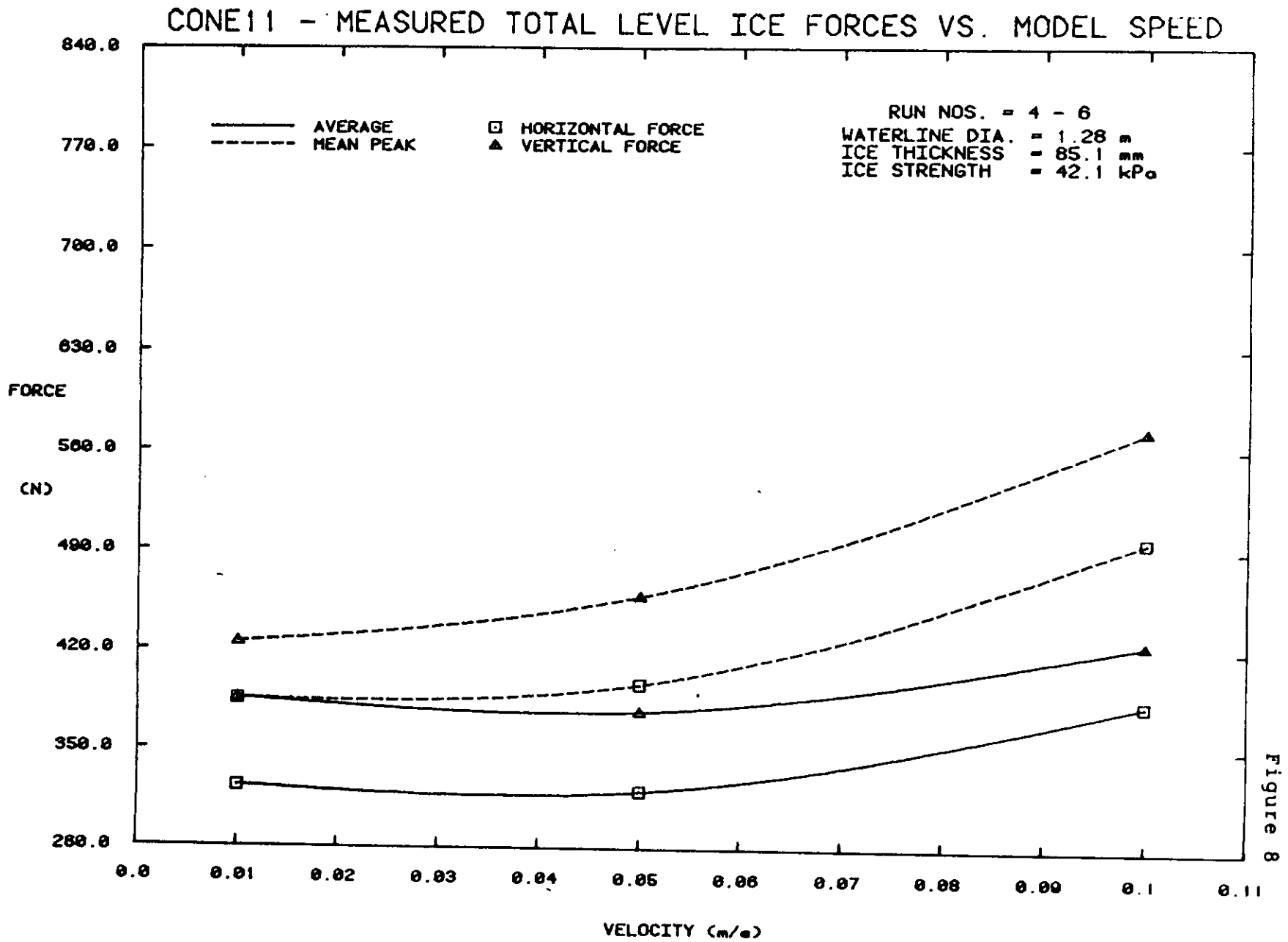
CONE11 - MEASURED TOTAL LEVEL ICE FORCES VS. MODEL SPEED
AVERAGE
MEAN PEAK
HORIZONTAL FORCE
VERTICAL FORCE
RUN NOS. = 4 - 6
WATERLINE DIA. = 1.28 m
ICE THICKNESS = 85.1 mm
ICE STRENGTH = 42.1 kPa
840.0
770.0
700.0
630.0
FORCE
560.0
(N)
490.0
420.0
350.0
280.0
0.0
0.01
0.02
0.03
0.04
0.05
0.06
0.07
0.08
0.09
0.1
0.11
VELOCITY (m/s)

Figure 8

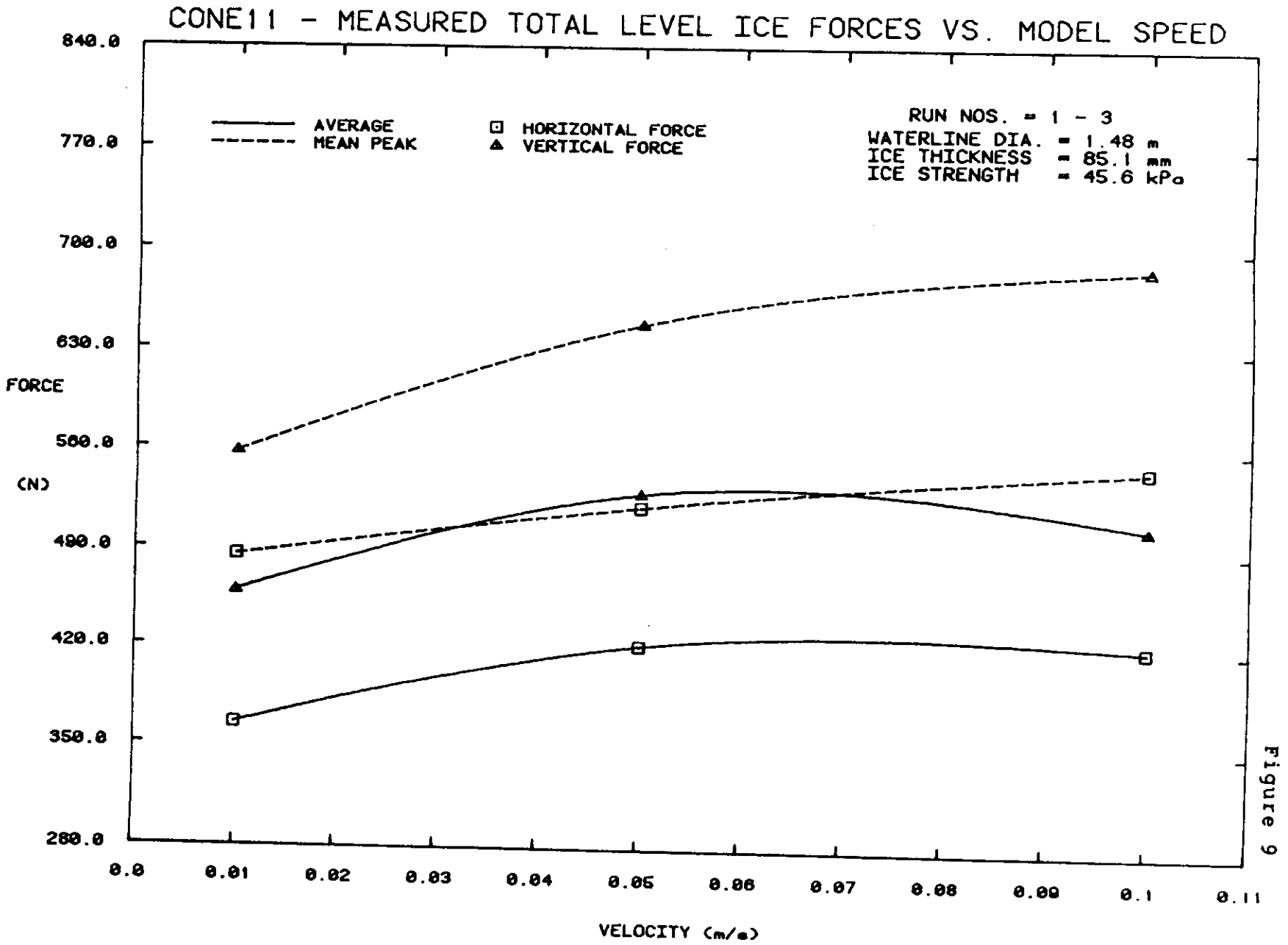
CONE11 - MEASURED TOTAL LEVEL ICE FORCES VS. MODEL SPEED
AVERAGE
MEAN PEAK
HORIZONTAL FORCE
VERTICAL FORCE
RUN NOS. = 1 - 3
WATERLINE DIA. = 1.48 m
ICE THICKNESS = 85.1 mm
ICE STRENGTH = 45.6 kPa
840.0
770.0
700.0
630.0
FORCE
560.0
(N)
490.0
420.0
350.0
280.0
0.0
0.01
0.02
0.03
0.04
0.05
0.06
0.07
0.08
0.09
0.1
0.11
VELOCITY (m/s)

Figure 9

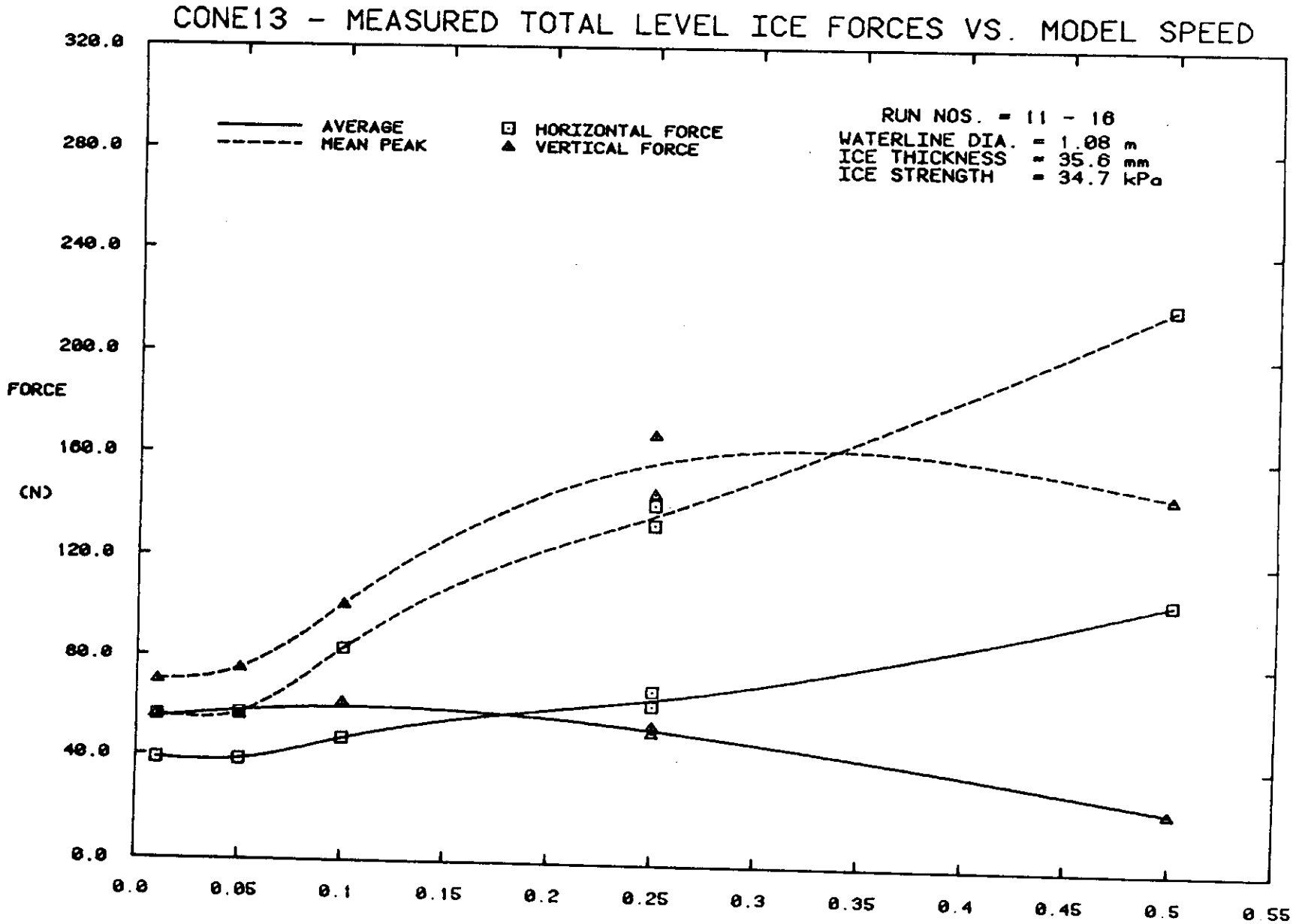
CONE13 - MEASURED TOTAL LEVEL ICE FORCES VS. MODEL SPEED
AVERAGE
MEAN PEAK
HORIZONTAL FORCE
VERTICAL FORCE
RUN NOS. = 11 - 18
WATERLINE DIA. = 1.08 m
ICE THICKNESS = 35.6 mm
ICE STRENGTH = 34.7 kPa
FORCE
(N)
320.0
280.0
240.0
200.0
160.0
120.0
80.0
40.0
0.0
0.0
0.05
0.1
0.15
0.2
0.25
0.3
0.35
0.4
0.45
0.5
0.55

Figure 10

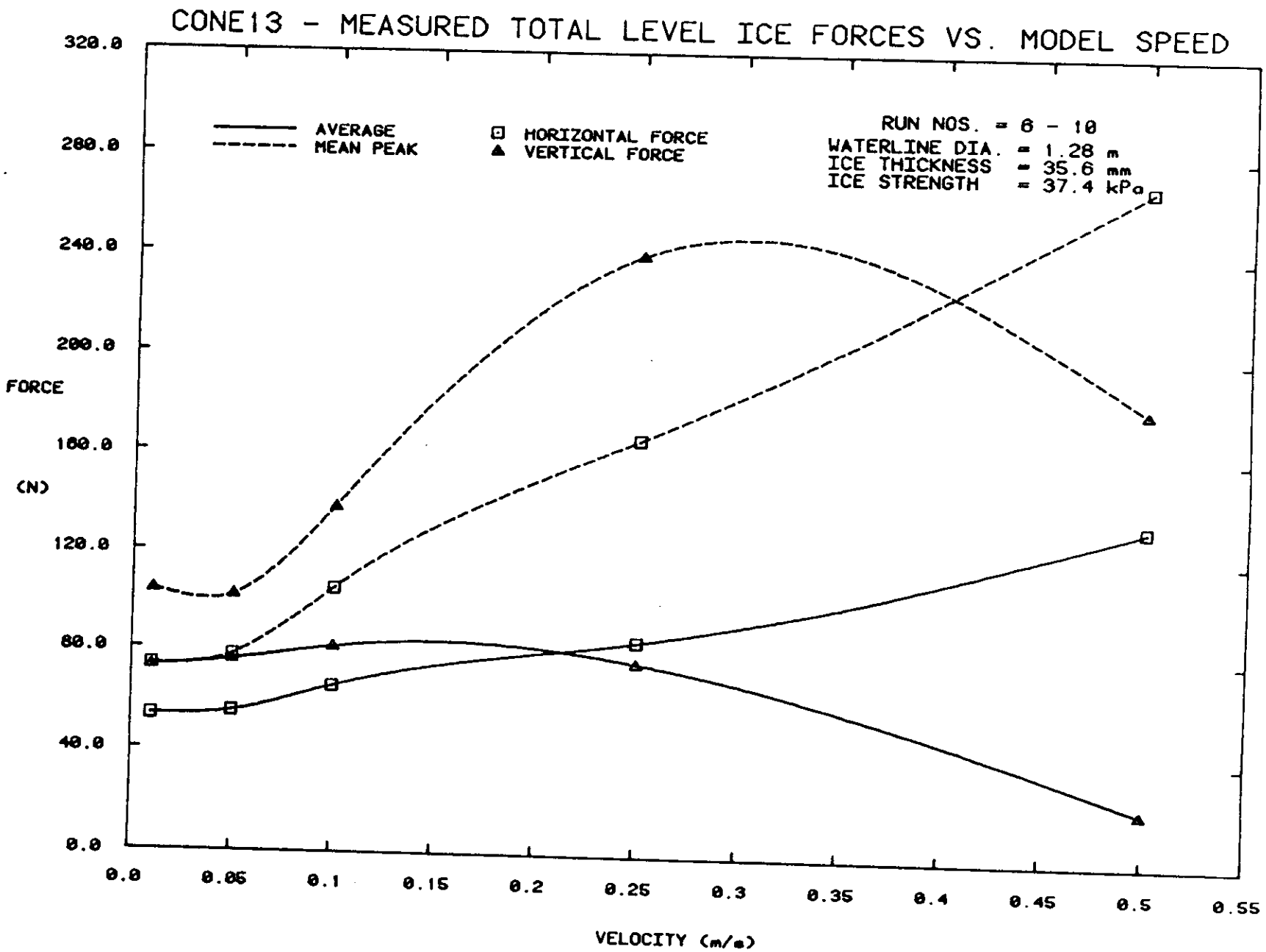
CONE13 - MEASURED TOTAL LEVEL ICE FORCES VS. MODEL SPEED
AVERAGE
MEAN PEAK
HORIZONTAL FORCE
VERTICAL FORCE
RUN NOS. = 6 - 10
WATERLINE DIA. = 1.28 m
ICE THICKNESS = 35.6 mm
ICE STRENGTH = 37.4 kPa
320.0
280.0
240.0
200.0
160.0
120.0
80.0
40.0
0.0
FORCE
(N)
0.0
0.05
0.1
0.15
0.2
0.25
0.3
0.35
0.4
0.45
0.5
0.55
VELOCITY (m/s)

Figure 11

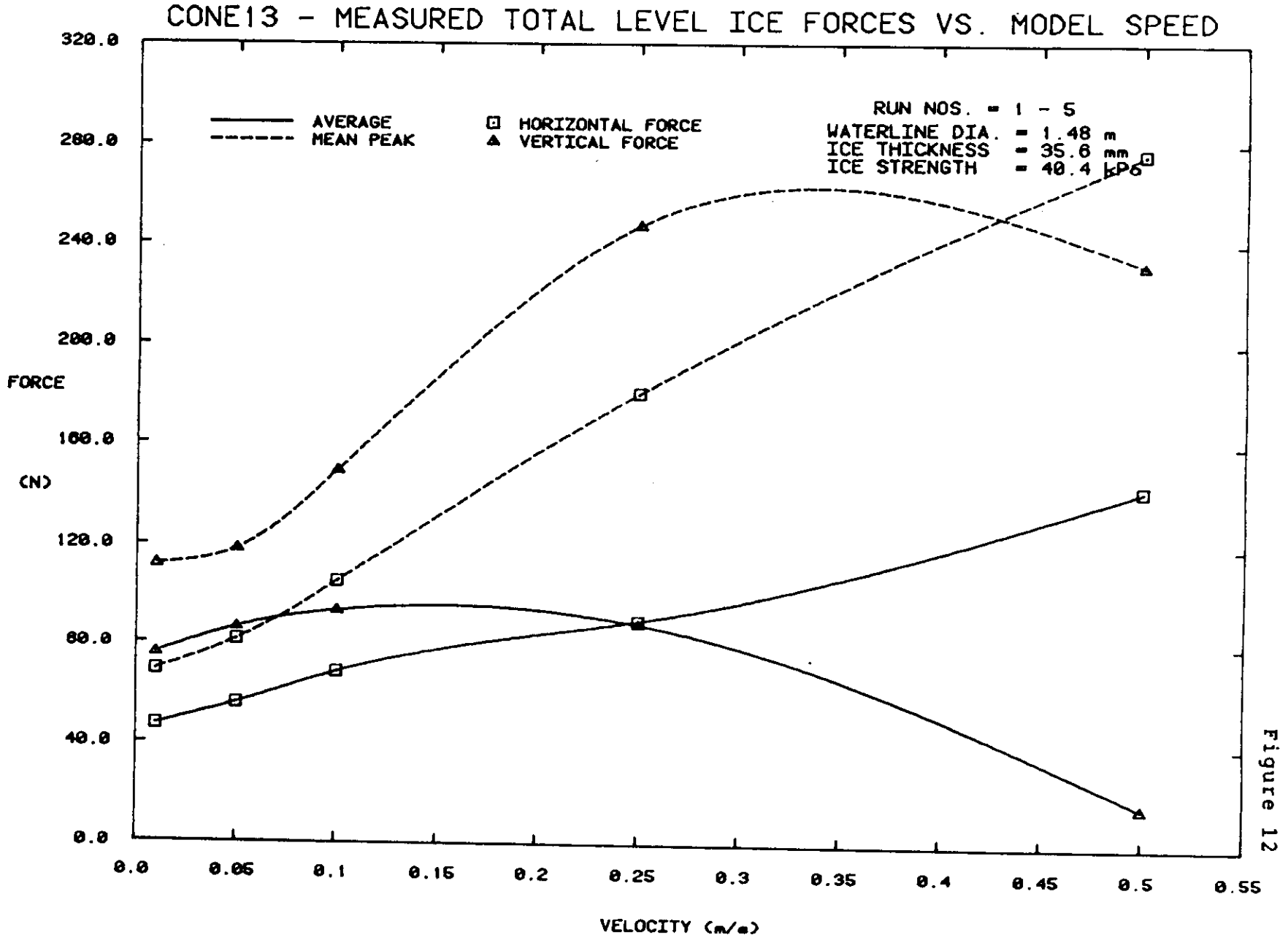
CONE13 - MEASURED TOTAL LEVEL ICE FORCES VS. MODEL SPEED
AVERAGE
MEAN PEAK
HORIZONTAL FORCE
VERTICAL FORCE
RUN NOS. = 1 - 5
WATERLINE DIA. = 1.48 m
ICE THICKNESS = 35.6 mm
ICE STRENGTH = 40.4 kPa
FORCE
(N)
320.0
280.0
240.0
200.0
160.0
120.0
80.0
40.0
0.0
0.0
0.05
0.1
0.15
0.2
0.25
0.3
0.35
0.4
0.45
0.5
0.55
VELOCITY (m/s)

Figure 12

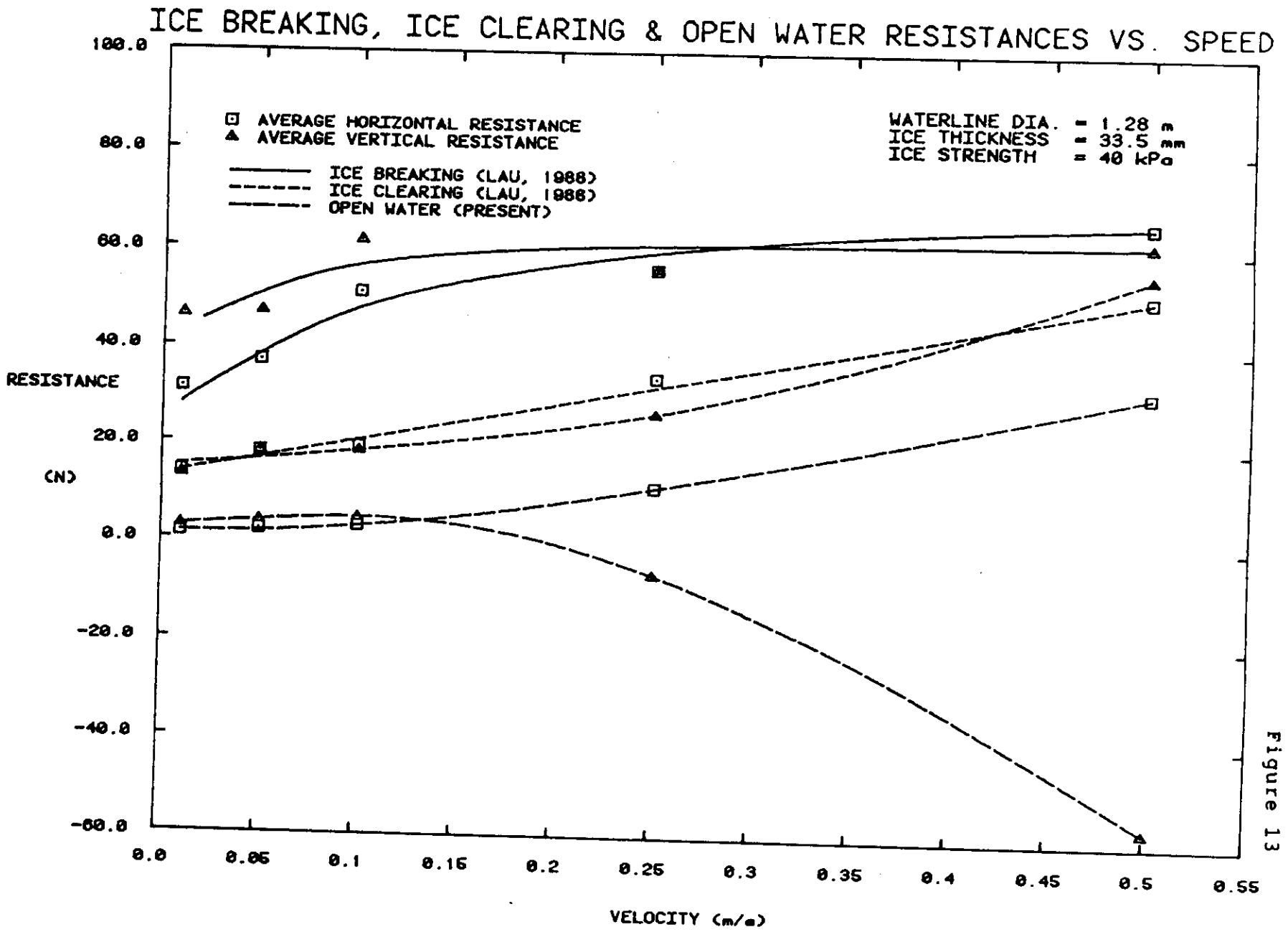
ICE BREAKING, ICE CLEARING & OPEN WATER RESISTANCES VS. SPEED
AVERAGE HORIZONTAL RESISTANCE
AVERAGE VERTICAL RESISTANCE
ICE BREAKING (LAU, 1988)
ICE CLEARING (LAU, 1986)
OPEN WATER (PRESENT)
WATERLINE DIA. = 1.28 m
ICE THICKNESS = 33.5 mm
ICE STRENGTH = 40 kPa
RESISTANCE
(N)
100.0
80.0
60.0
40.0
20.0
0.0
-20.0
-40.0
-60.0
0.0
0.05
0.1
0.15
0.2
0.25
0.3
0.35
0.4
0.45
0.5
0.55
VELOCITY (m/s)

Figure 13

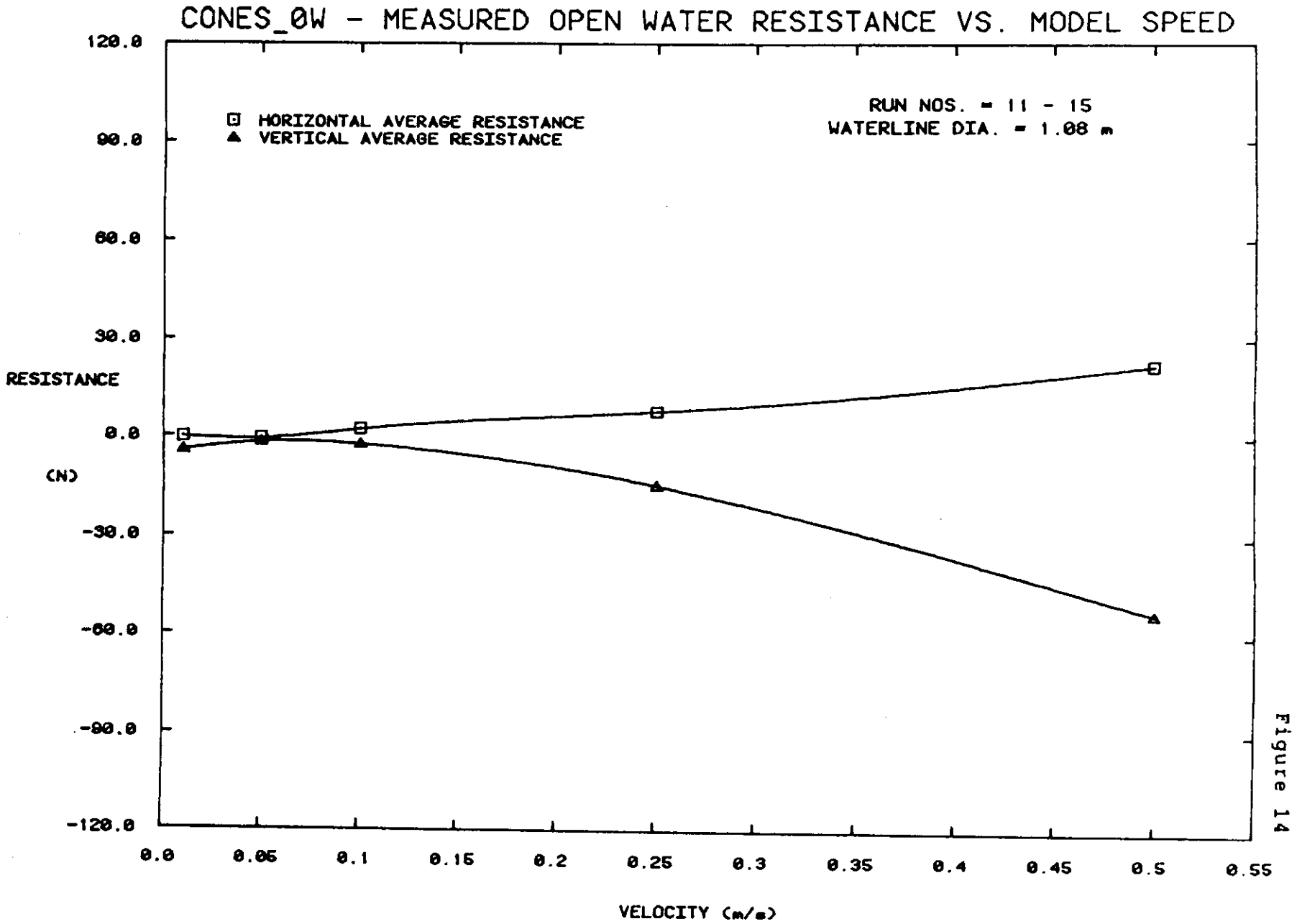
CONES_0W - MEASURED OPEN WATER RESISTANCE VS. MODEL SPEED
HORIZONTAL AVERAGE RESISTANCE
VERTICAL AVERAGE RESISTANCE
RUN NOS. = 11 - 15
WATERLINE DIA. = 1.08 m
120.0
90.0
60.0
30.0
0.0
-30.0
-60.0
-90.0
-120.0
RESISTANCE
(N)
0.0
0.05
0.1
0.15
0.2
0.25
0.3
0.35
0.4
0.45
0.5
0.55
VELOCITY (m/s)

Figure 14

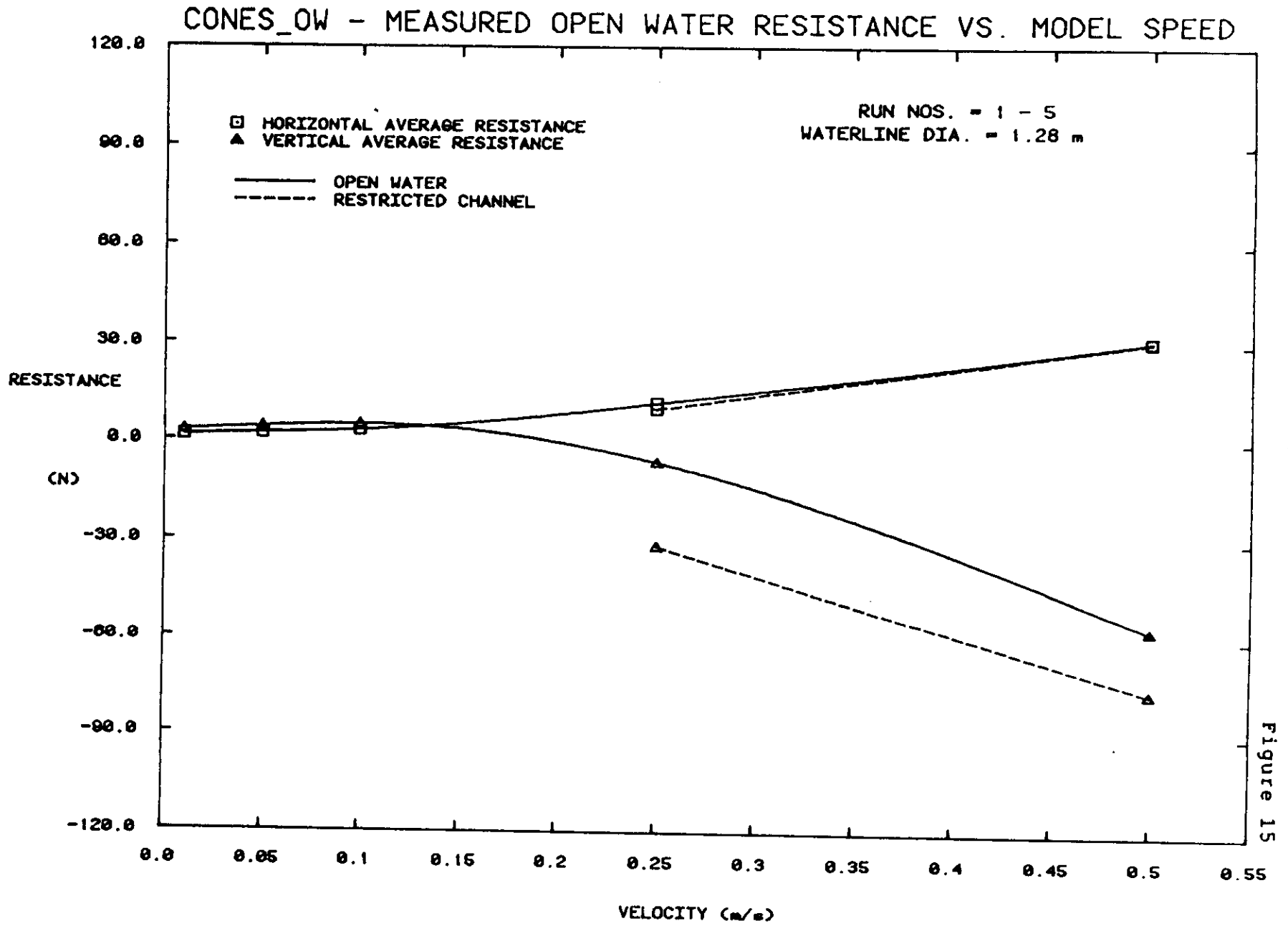
CONES_OW - MEASURED OPEN WATER RESISTANCE VS. MODEL SPEED
HORIZONTAL AVERAGE RESISTANCE
VERTICAL AVERAGE RESISTANCE
OPEN WATER
RESTRICTED CHANNEL
RUN NOS. = 1 - 5
WATERLINE DIA. = 1.28 m
RESISTANCE
(N)
120.0
90.0
60.0
30.0
0.0
-30.0
-60.0
-90.0
-120.0
0.0
0.05
0.1
0.15
0.2
0.25
0.3
0.35
0.4
0.45
0.5
0.55
VELOCITY (m/s)

Figure 15

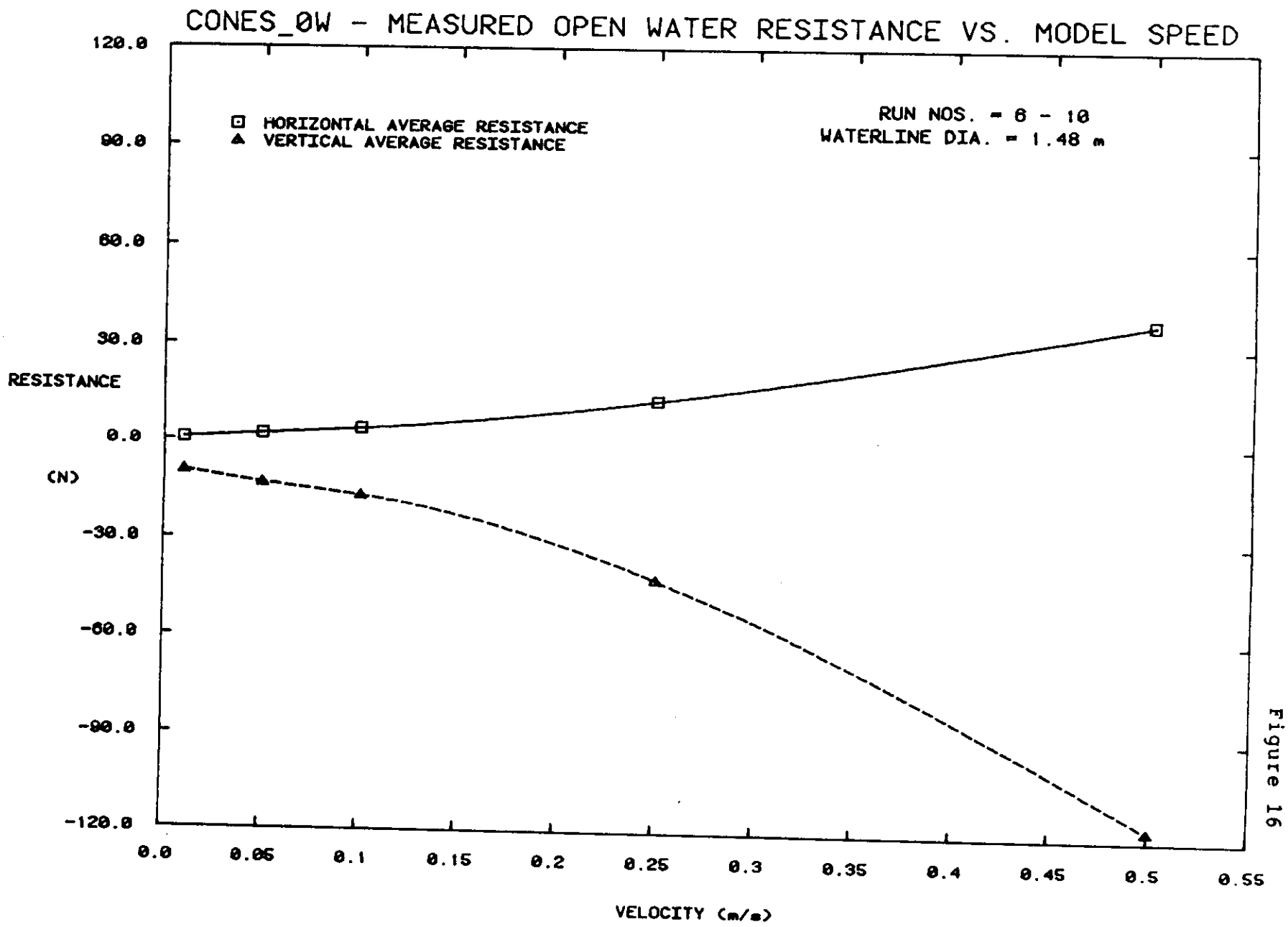
CONES_0W - MEASURED OPEN WATER RESISTANCE VS. MODEL SPEED
HORIZONTAL AVERAGE RESISTANCE
VERTICAL AVERAGE RESISTANCE
RUN NOS. = 6 - 10
WATERLINE DIA. = 1.48 m
120.0
90.0
60.0
30.0
0.0
-30.0
-60.0
-90.0
-120.0
RESISTANCE
(N)
0.0
0.05
0.1
0.15
0.2
0.25
0.3
0.35
0.4
0.45
0.5
0.55
VELOCITY (m/s)

Figure 16

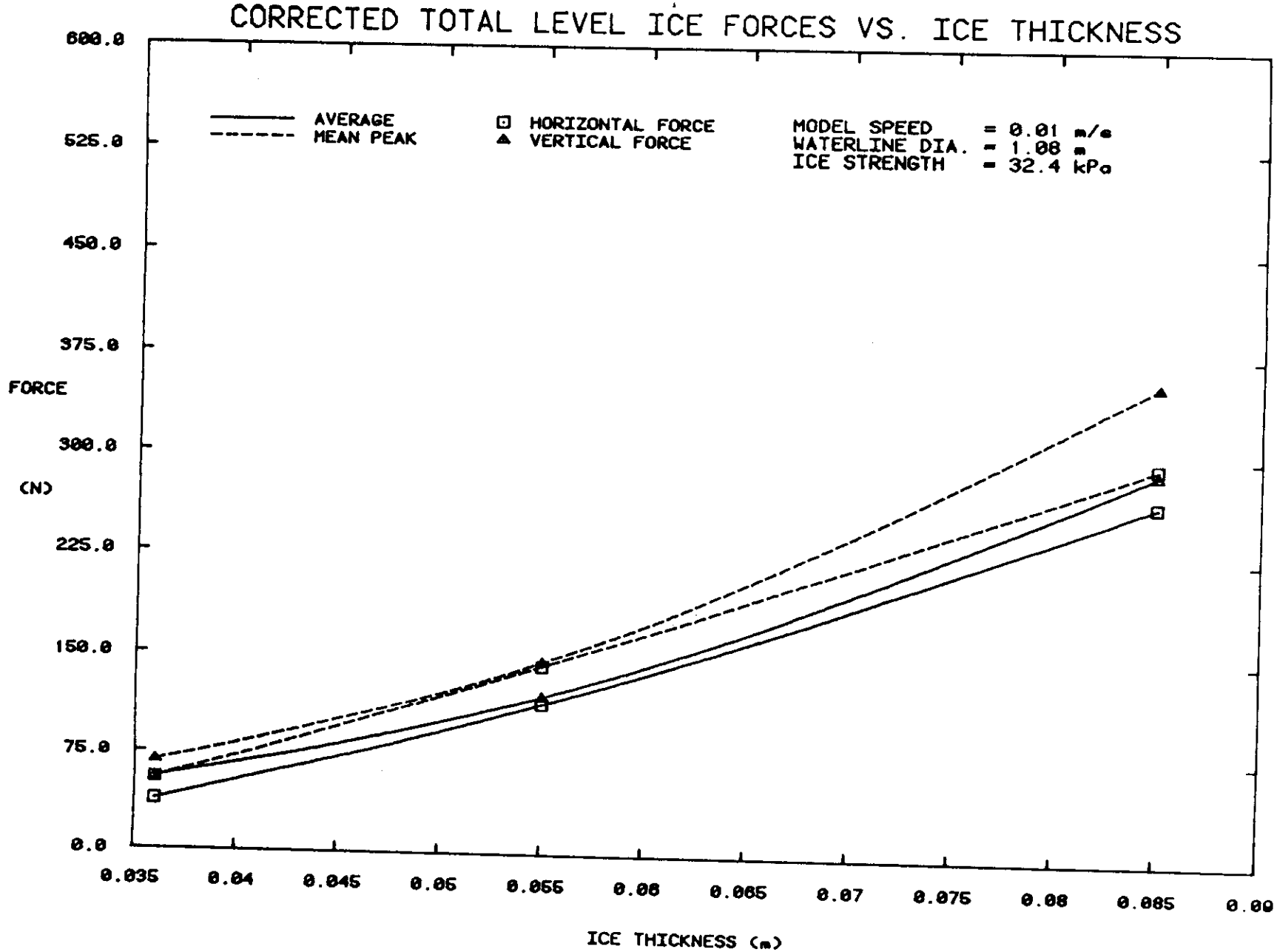
CORRECTED TOTAL LEVEL ICE FORCES VS. ICE THICKNESS
AVERAGE
MEAN PEAK
HORIZONTAL FORCE
VERTICAL FORCE
MODEL SPEED = 0.01 m/s
WATERLINE DIA. = 1.08 m
ICE STRENGTH = 32.4 kPa
600.0
525.0
450.0
375.0
FORCE
300.0
(N)
225.0
150.0
75.0
0.0
0.035
0.04
0.045
0.05
0.055
0.06
0.065
0.07
0.075
0.08
0.085
0.09
ICE THICKNESS (m)

Figure 17

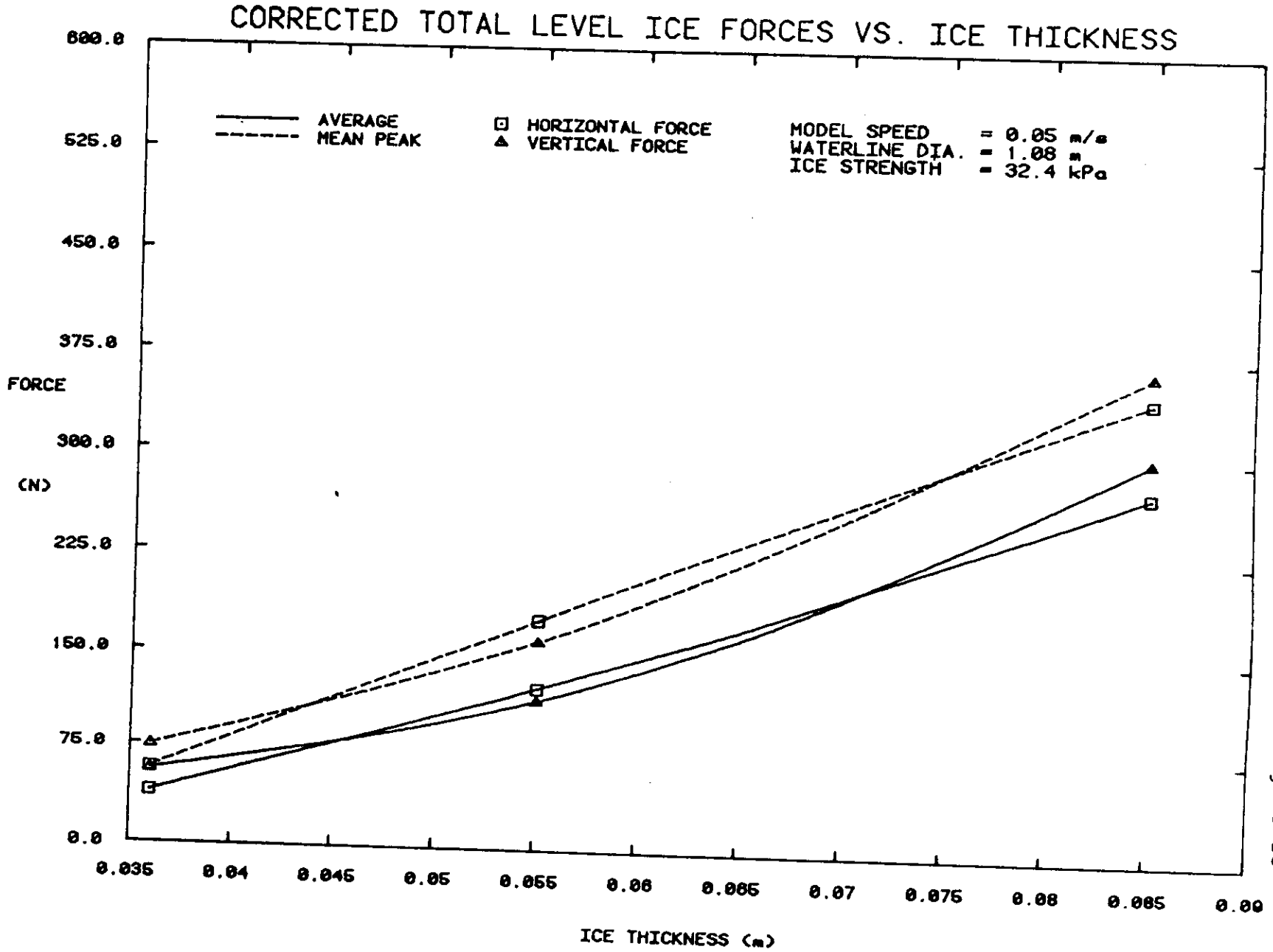
CORRECTED TOTAL LEVEL ICE FORCES VS. ICE THICKNESS
AVERAGE
MEAN PEAK
HORIZONTAL FORCE
VERTICAL FORCE
MODEL SPEED = 0.05 m/s
WATERLINE DIA. = 1.08 m
ICE STRENGTH = 32.4 kPa
600.0
525.0
450.0
375.0
FORCE
300.0
(N)
225.0
150.0
75.0
0.0
0.035
0.04
0.045
0.05
0.055
0.06
0.065
0.07
0.075
0.08
0.085
0.09
ICE THICKNESS (m)

Figure 18

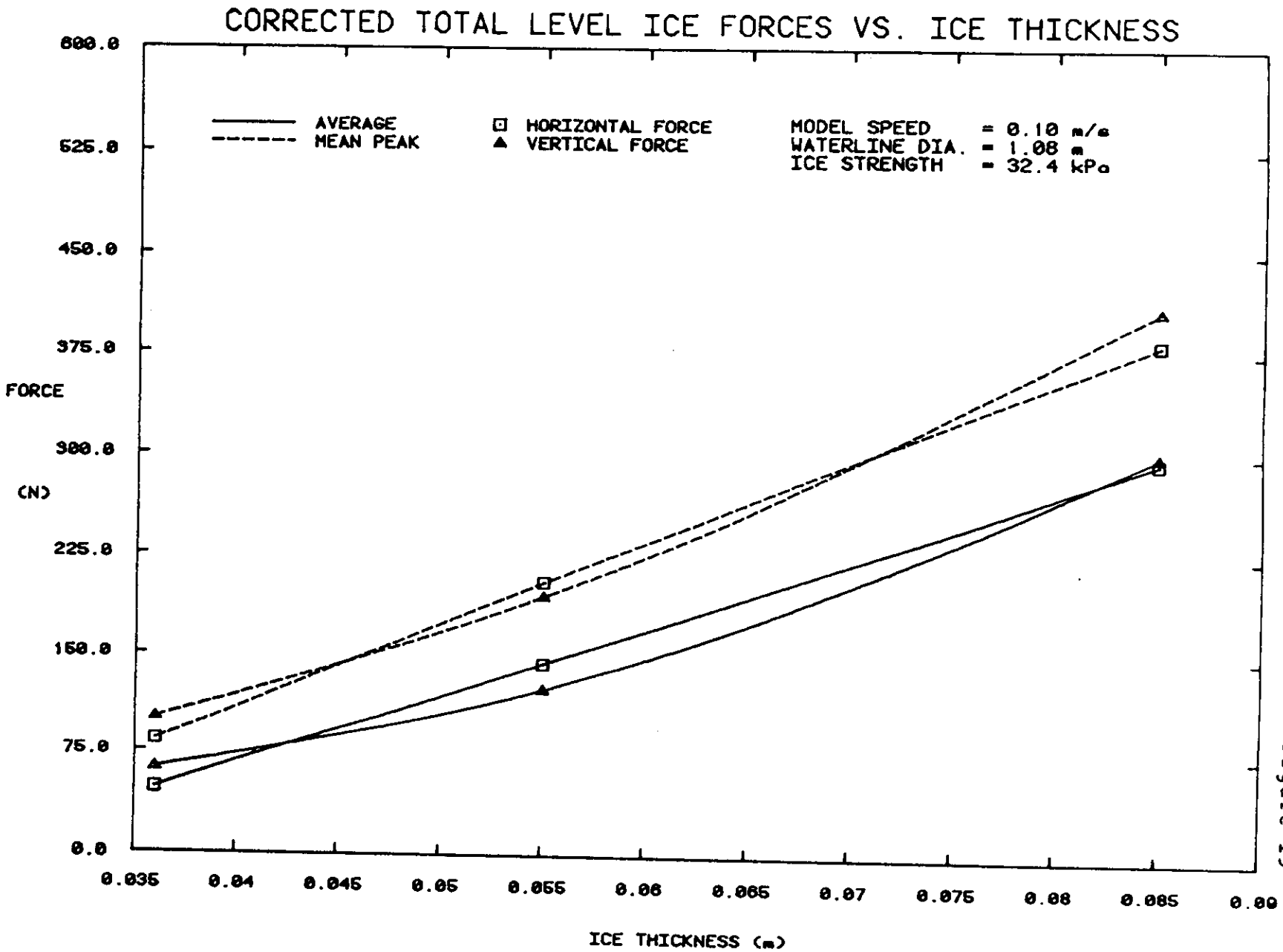
CORRECTED TOTAL LEVEL ICE FORCES VS. ICE THICKNESS
AVERAGE
MEAN PEAK
HORIZONTAL FORCE
VERTICAL FORCE
MODEL SPEED = 0.10 m/s
WATERLINE DIA. = 1.08 m
ICE STRENGTH = 32.4 kPa
FORCE
(N)
600.0
525.0
450.0
375.0
300.0
225.0
150.0
75.0
0.0
0.035
0.04
0.045
0.05
0.055
0.06
0.065
0.07
0.075
0.08
0.085
0.09
ICE THICKNESS (m)

Figure 19

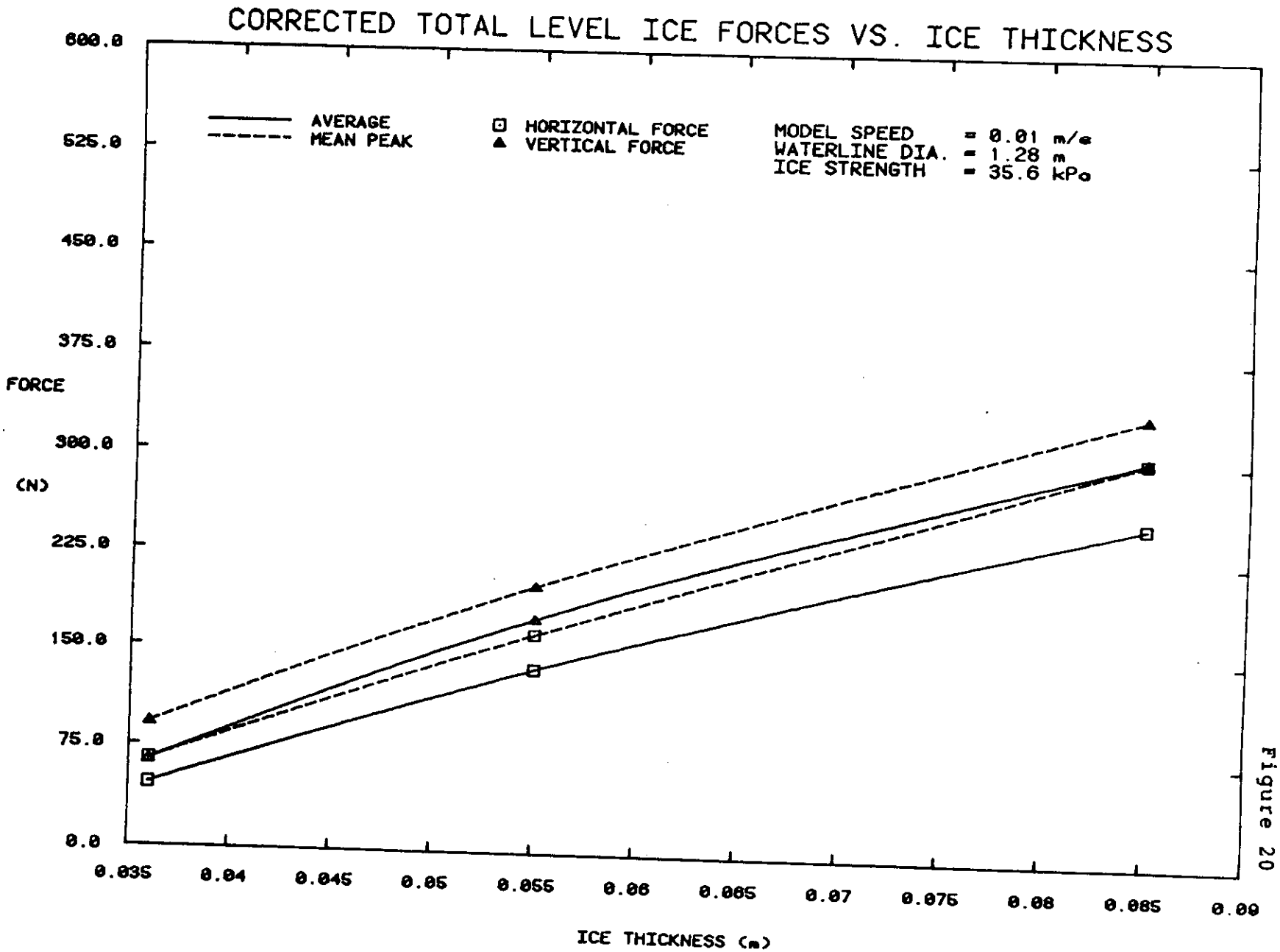
CORRECTED TOTAL LEVEL ICE FORCES VS. ICE THICKNESS
AVERAGE
MEAN PEAK
HORIZONTAL FORCE
VERTICAL FORCE
MODEL SPEED = 0.01 m/s
WATERLINE DIA. = 1.28 m
ICE STRENGTH = 35.6 kPa
600.0
525.0
450.0
375.0
FORCE
300.0
(N)
225.0
150.0
75.0
0.0
0.035
0.04
0.045
0.05
0.055
0.06
0.065
0.07
0.075
0.08
0.085
0.09
ICE THICKNESS (m)

Figure 20

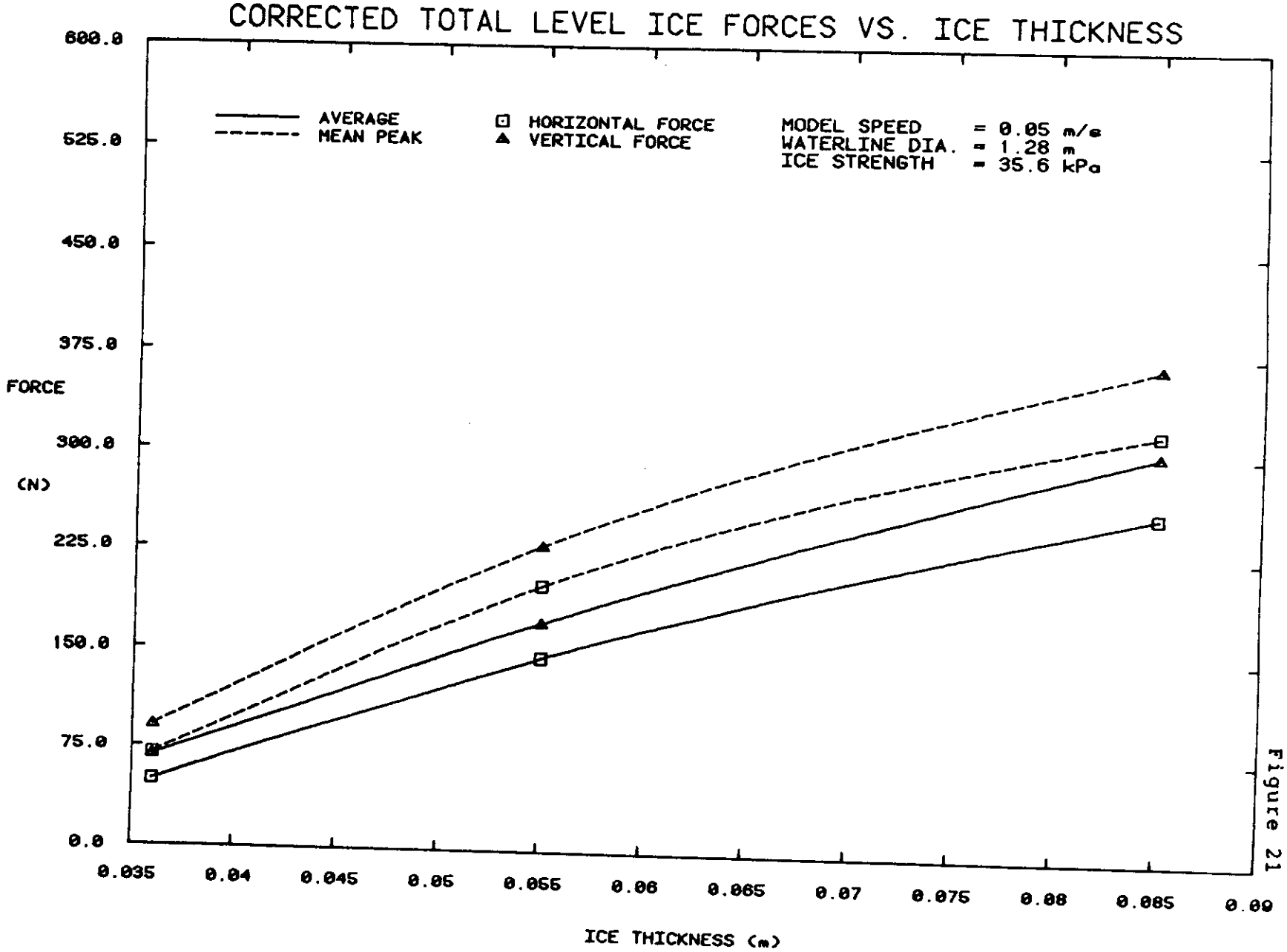
CORRECTED TOTAL LEVEL ICE FORCES VS. ICE THICKNESS
AVERAGE
MEAN PEAK
HORIZONTAL FORCE
VERTICAL FORCE
MODEL SPEED = 0.05 m/s
WATERLINE DIA. = 1.28 m
ICE STRENGTH = 35.6 kPa
600.0
525.0
450.0
375.0
FORCE
300.0
(N)
225.0
150.0
75.0
0.0
0.035
0.04
0.045
0.05
0.055
0.06
0.065
0.07
0.075
0.08
0.085
0.09
ICE THICKNESS (m)

Figure 21

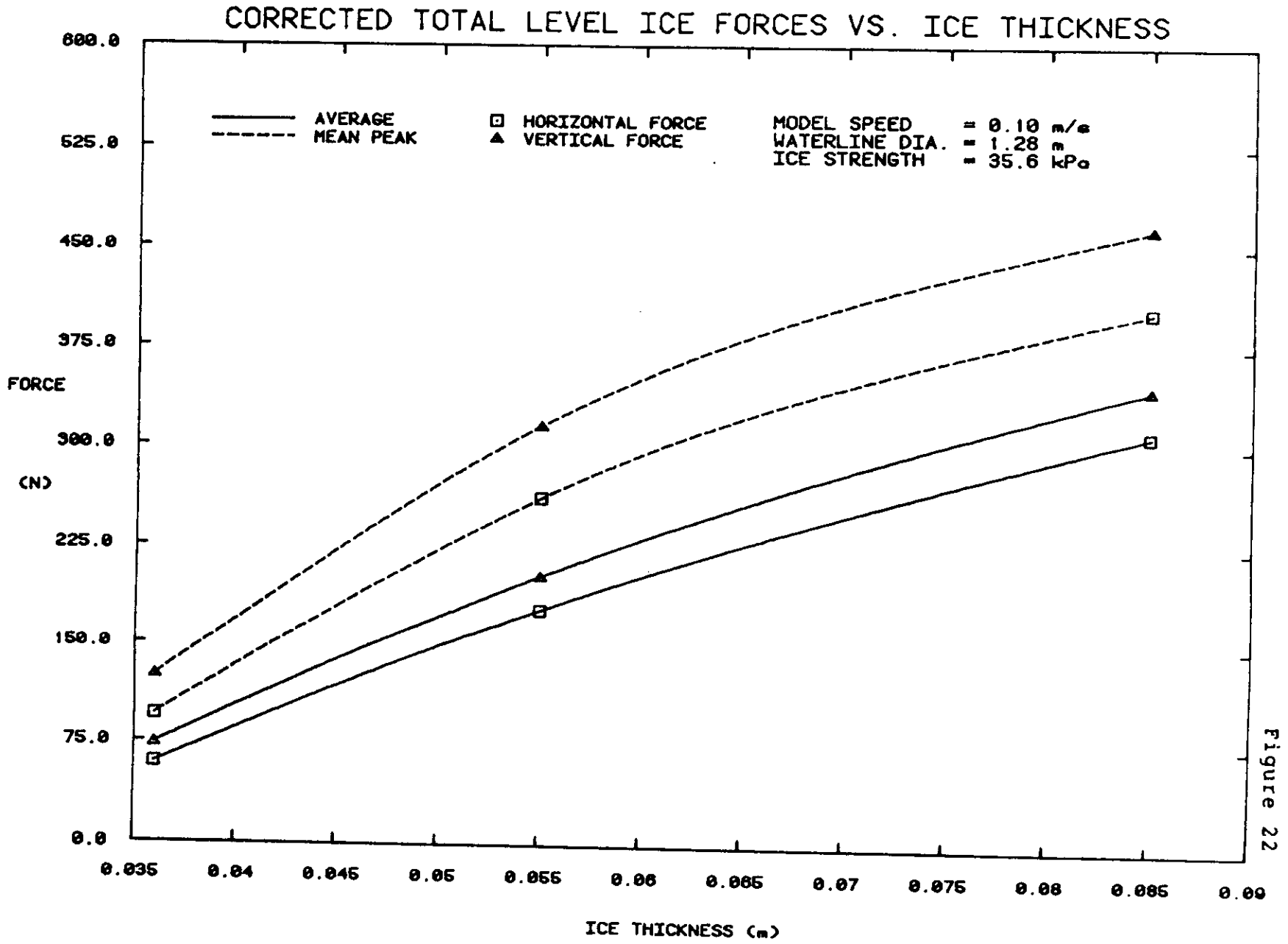
CORRECTED TOTAL LEVEL ICE FORCES VS. ICE THICKNESS
AVERAGE
MEAN PEAK
HORIZONTAL FORCE
VERTICAL FORCE
MODEL SPEED = 0.10 m/s
WATERLINE DIA. = 1.28 m
ICE STRENGTH = 35.6 kPa
600.0
525.0
450.0
375.0
FORCE
300.0
(N)
225.0
150.0
75.0
0.0
0.035
0.04
0.045
0.05
0.055
0.06
0.065
0.07
0.075
0.08
0.085
0.09
ICE THICKNESS (m)

Figure 22

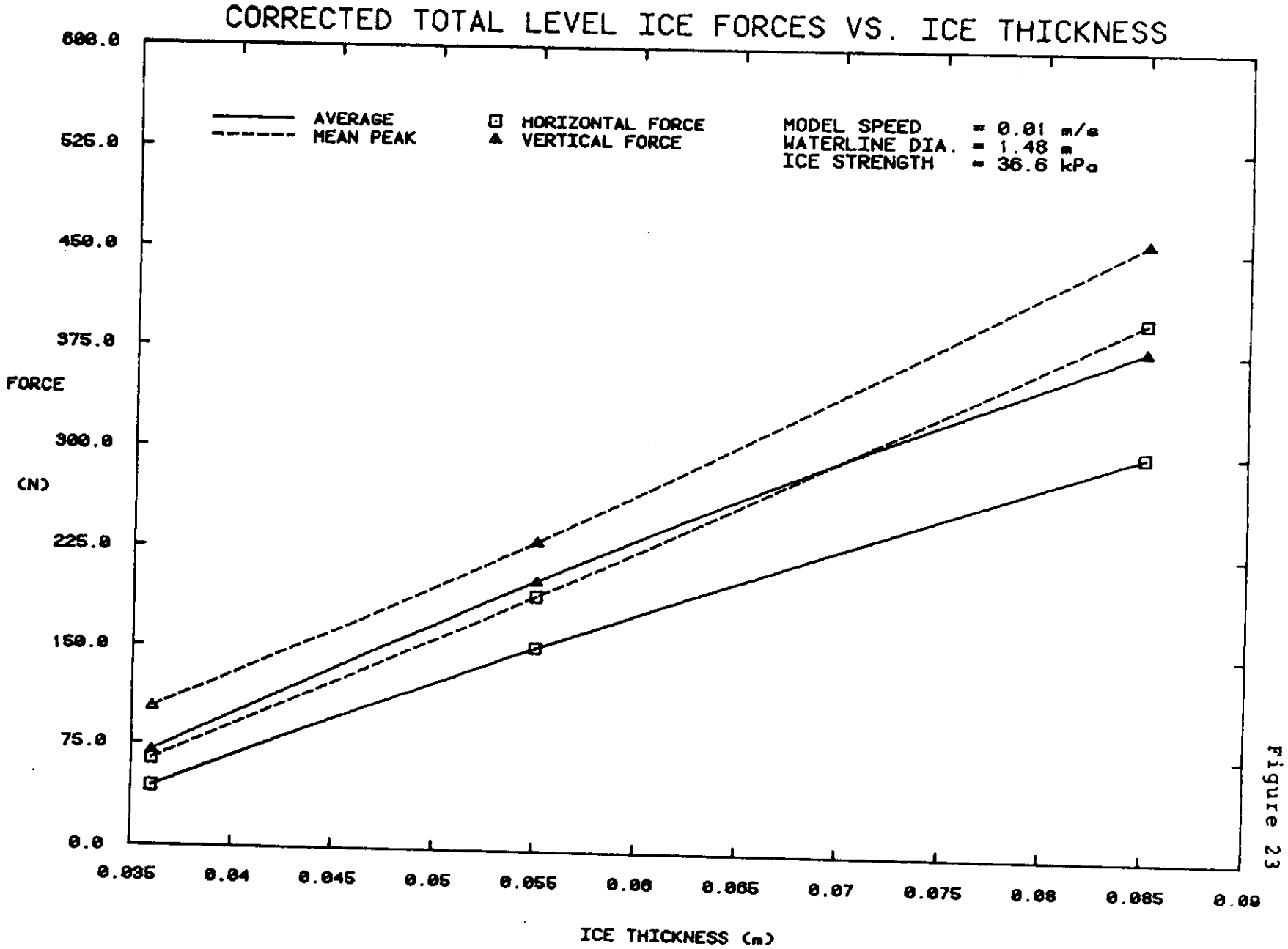
CORRECTED TOTAL LEVEL ICE FORCES VS. ICE THICKNESS
AVERAGE
MEAN PEAK
HORIZONTAL FORCE
VERTICAL FORCE
MODEL SPEED = 0.01 m/s
WATERLINE DIA. = 1.48 m
ICE STRENGTH = 36.6 kPa
600.0
525.0
450.0
375.0
FORCE
300.0
(N)
225.0
150.0
75.0
0.0
0.035
0.04
0.045
0.05
0.055
0.06
0.065
0.07
0.075
0.08
0.085
0.09
ICE THICKNESS (m)

Figure 23

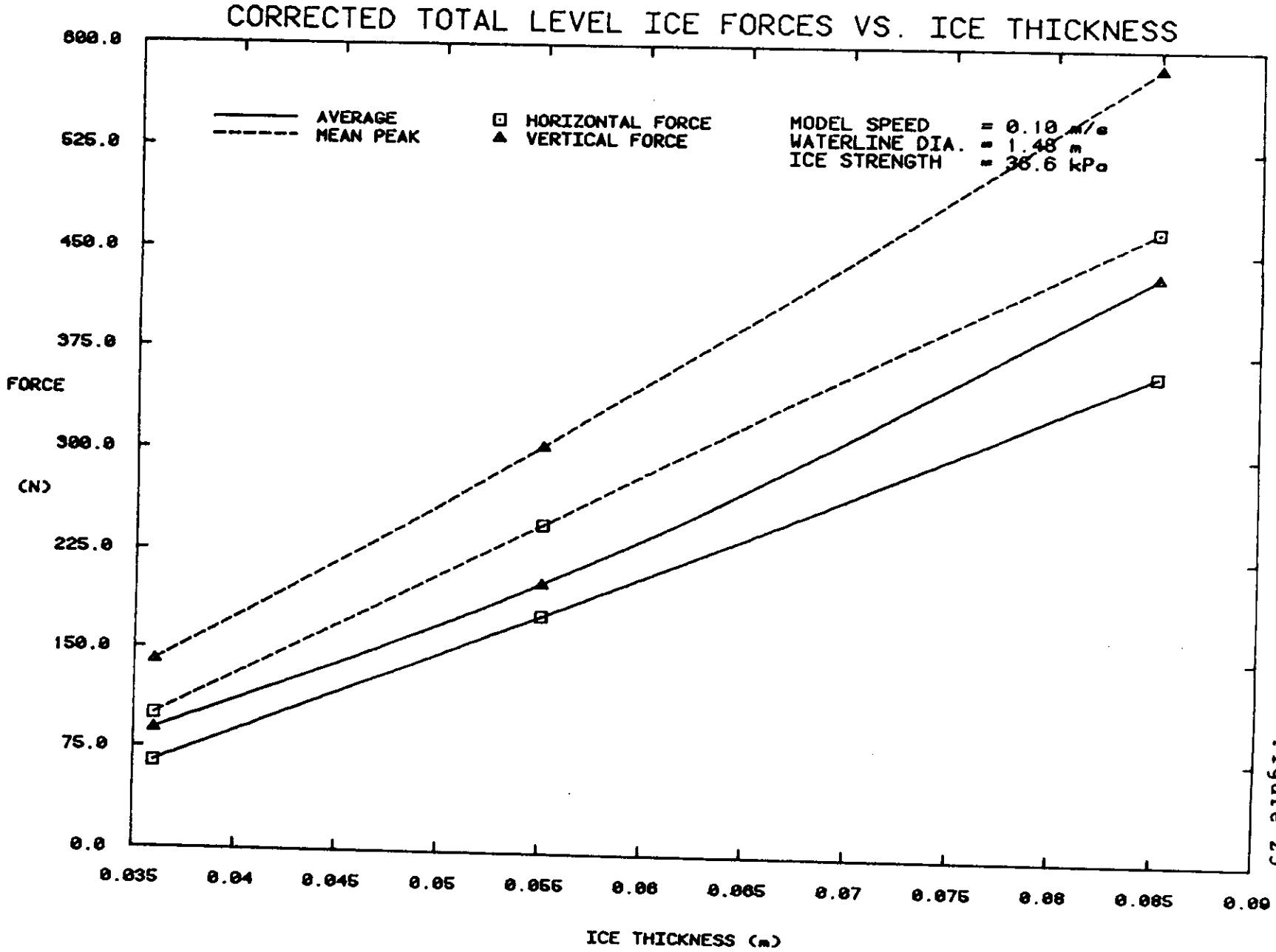
CORRECTED TOTAL LEVEL ICE FORCES VS. ICE THICKNESS
AVERAGE
MEAN PEAK
HORIZONTAL FORCE
VERTICAL FORCE
MODEL SPEED = 0.10 m/s
WATERLINE DIA. = 1.48 m
ICE STRENGTH = 36.6 kPa
600.0
525.0
450.0
375.0
FORCE
300.0
(N)
225.0
150.0
75.0
0.0
0.035
0.04
0.045
0.05
0.055
0.06
0.065
0.07
0.075
0.08
0.085
0.09
ICE THICKNESS (m)

Figure 25

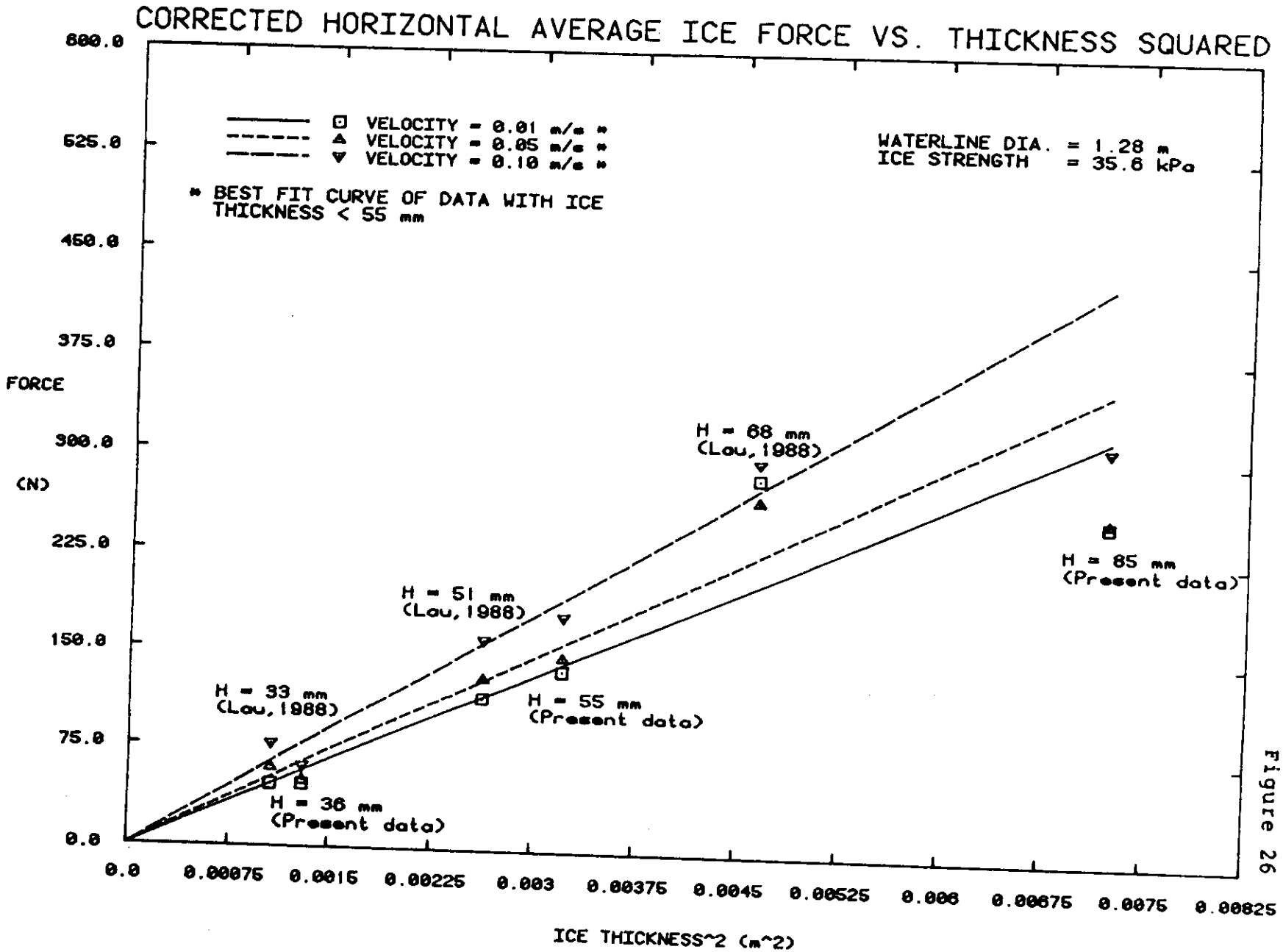
CORRECTED HORIZONTAL AVERAGE ICE FORCE VS. THICKNESS SQUARED
VELOCITY = 0.01 m/s *
VELOCITY = 0.05 m/s *
VELOCITY = 0.10 m/s *
* BEST FIT CURVE OF DATA WITH ICE THICKNESS < 55 mm
WATERLINE DIA. = 1.28 m
ICE STRENGTH = 35.6 kPa
H = 68 mm (Lau, 1988)
H = 85 mm (Present data)
H = 51 mm (Lau, 1988)
H = 33 mm (Lau, 1988)
H = 55 mm (Present data)
H = 36 mm (Present data)
FORCE (N)
600.0
525.0
450.0
375.0
300.0
225.0
150.0
75.0
0.0
0.0
0.00075
0.0015
0.00225
0.003
0.00375
0.0045
0.00525
0.006
0.00675
0.0075
0.00825
ICE THICKNESS^2 (m^2)

Figure 26

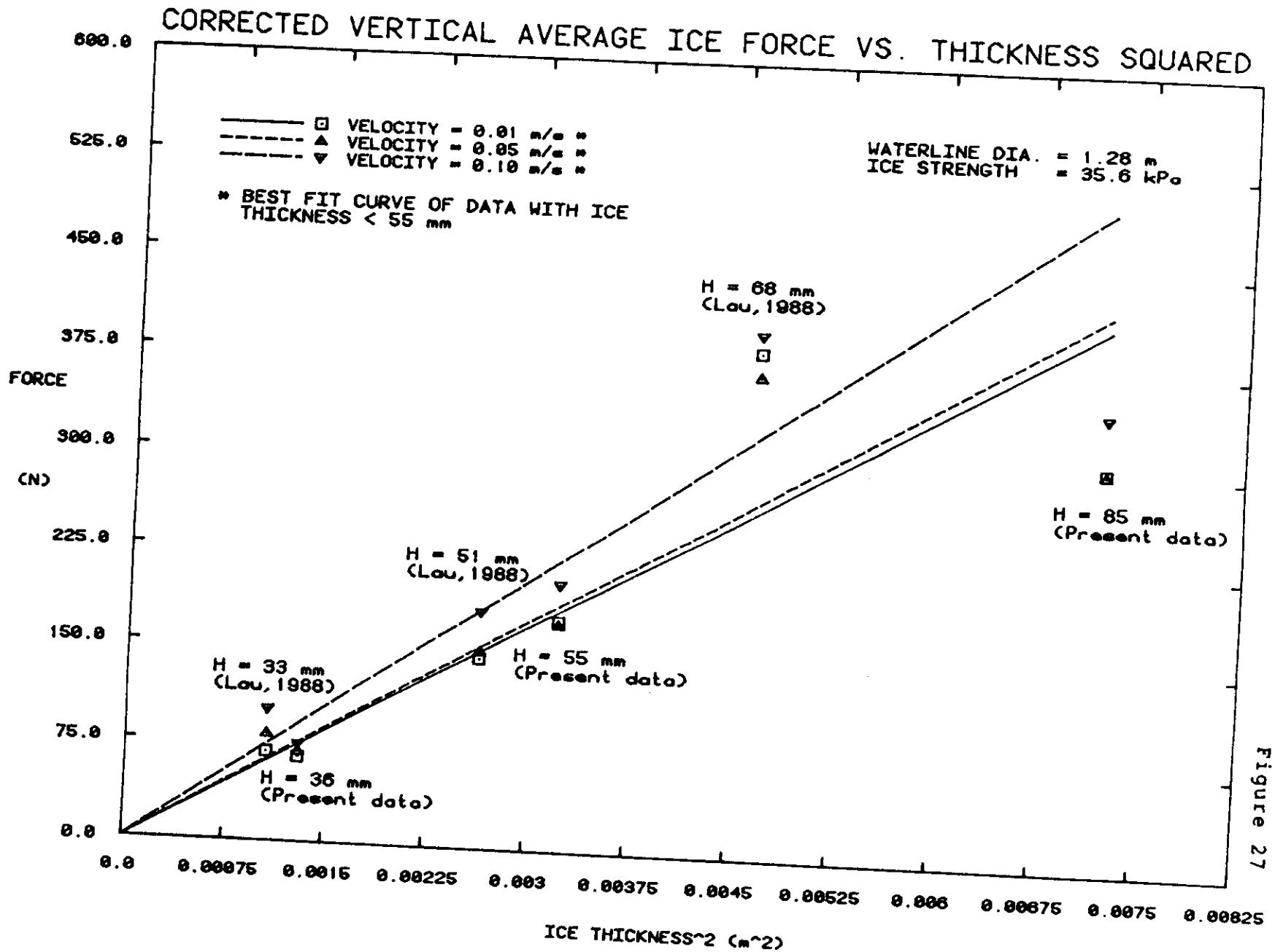
CORRECTED VERTICAL AVERAGE ICE FORCE VS. THICKNESS SQUARED
VELOCITY = 0.01 m/s *
VELOCITY = 0.05 m/s *
VELOCITY = 0.10 m/s *
* BEST FIT CURVE OF DATA WITH ICE THICKNESS < 55 mm
WATERLINE DIA. = 1.28 m
ICE STRENGTH = 35.6 kPa
H = 68 mm (Lau, 1988)
H = 85 mm (Present data)
H = 51 mm (Lau, 1988)
H = 55 mm (Present data)
H = 33 mm (Lau, 1988)
H = 36 mm (Present data)
FORCE (N)
600.0
525.0
450.0
375.0
300.0
225.0
150.0
75.0
0.0
0.0
0.00075
0.0015
0.00225
0.003
0.00375
0.0045
0.00525
0.006
0.00675
0.0075
0.00825
ICE THICKNESS^2 (m^2)

Figure 27

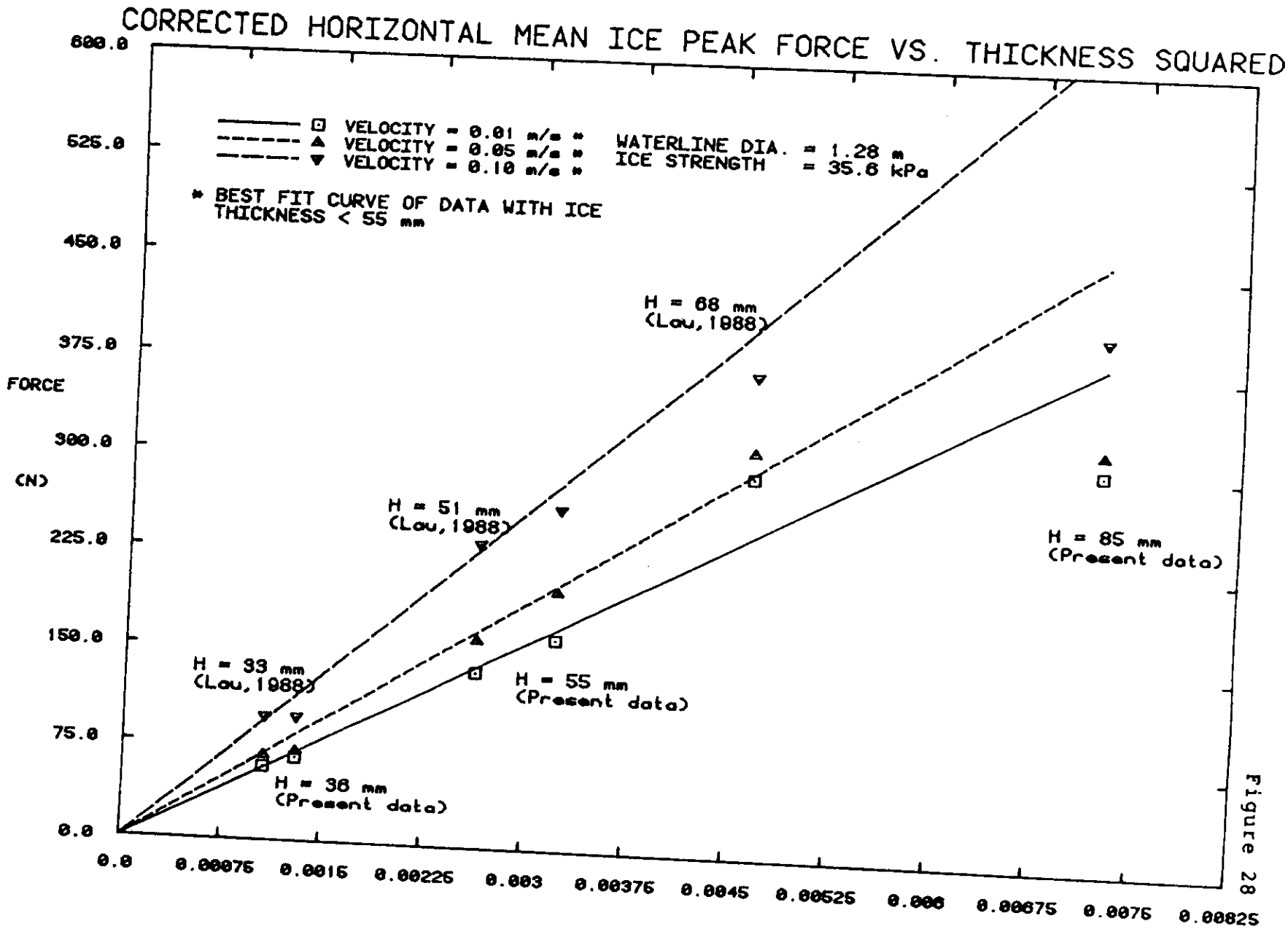
CORRECTED HORIZONTAL MEAN ICE PEAK FORCE VS. THICKNESS SQUARED
VELOCITY = 0.01 m/s *
VELOCITY = 0.05 m/s *
VELOCITY = 0.10 m/s *
WATERLINE DIA. = 1.28 m
ICE STRENGTH = 35.6 kPa
* BEST FIT CURVE OF DATA WITH ICE THICKNESS < 55 mm
H = 68 mm (Lau, 1988)
H = 51 mm (Lau, 1988)
H = 33 mm (Lau, 1988)
H = 85 mm (Present data)
H = 55 mm (Present data)
H = 36 mm (Present data)
FORCE (N)
600.0
525.0
450.0
375.0
300.0
225.0
150.0
75.0
0.0
0.0
0.00075
0.0015
0.00225
0.003
0.00375
0.0045
0.00525
0.006
0.00675
0.0075
0.00825

Figure 28

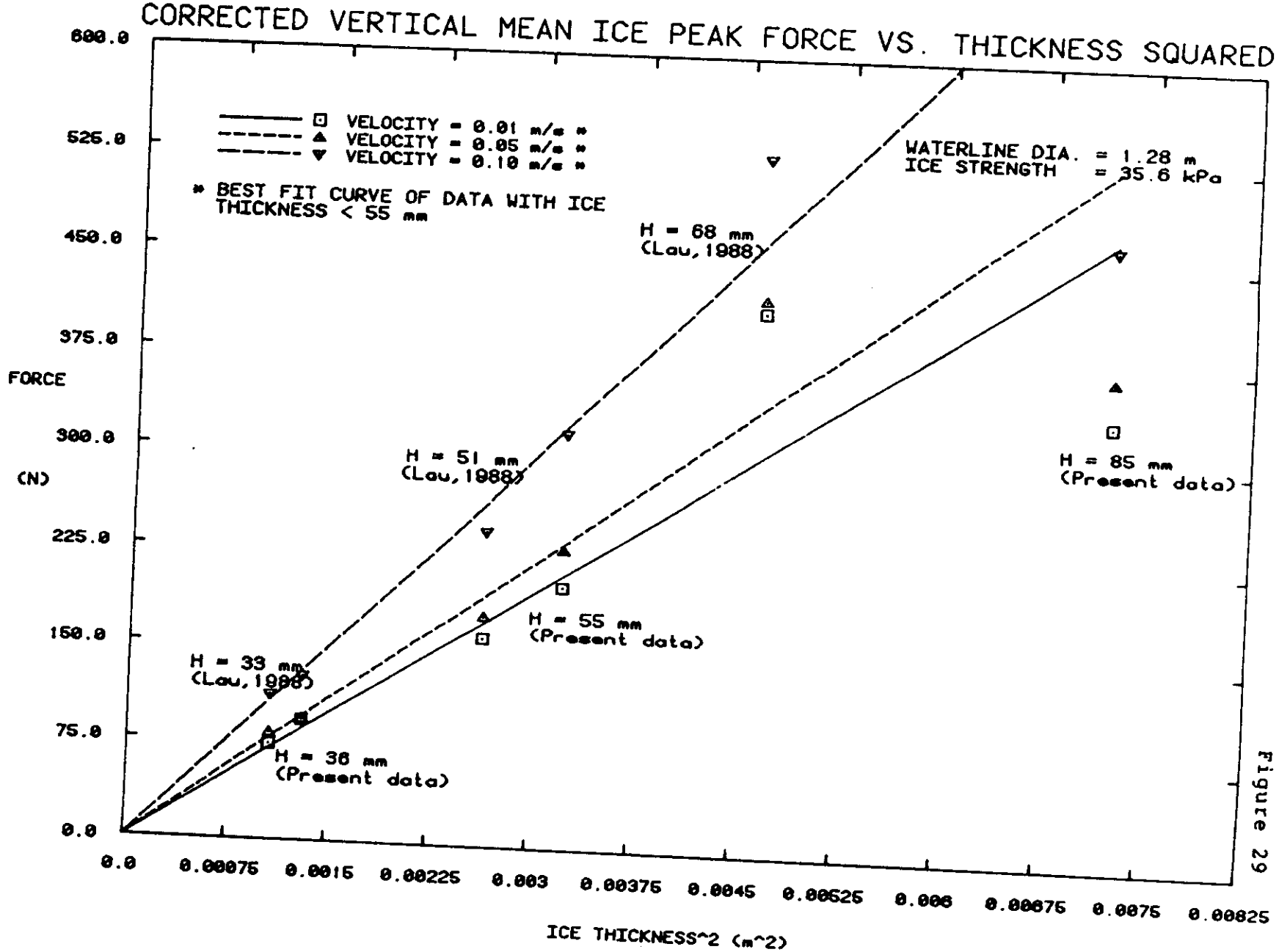
CORRECTED VERTICAL MEAN ICE PEAK FORCE VS. THICKNESS SQUARED
VELOCITY = 0.01 m/s *
VELOCITY = 0.05 m/s *
VELOCITY = 0.10 m/s *
* BEST FIT CURVE OF DATA WITH ICE THICKNESS < 55 mm
WATERLINE DIA. = 1.28 m
ICE STRENGTH = 35.6 kPa
H = 68 mm (Lau, 1988)
H = 51 mm (Lau, 1988)
H = 33 mm (Lau, 1988)
H = 85 mm (Present data)
H = 55 mm (Present data)
H = 38 mm (Present data)
FORCE (N)
600.0
525.0
450.0
375.0
300.0
225.0
150.0
75.0
0.0
0.0
0.00075
0.0015
0.00225
0.003
0.00375
0.0045
0.00525
0.006
0.00675
0.0075
0.00825
ICE THICKNESS^2 (m^2)

Figure 29

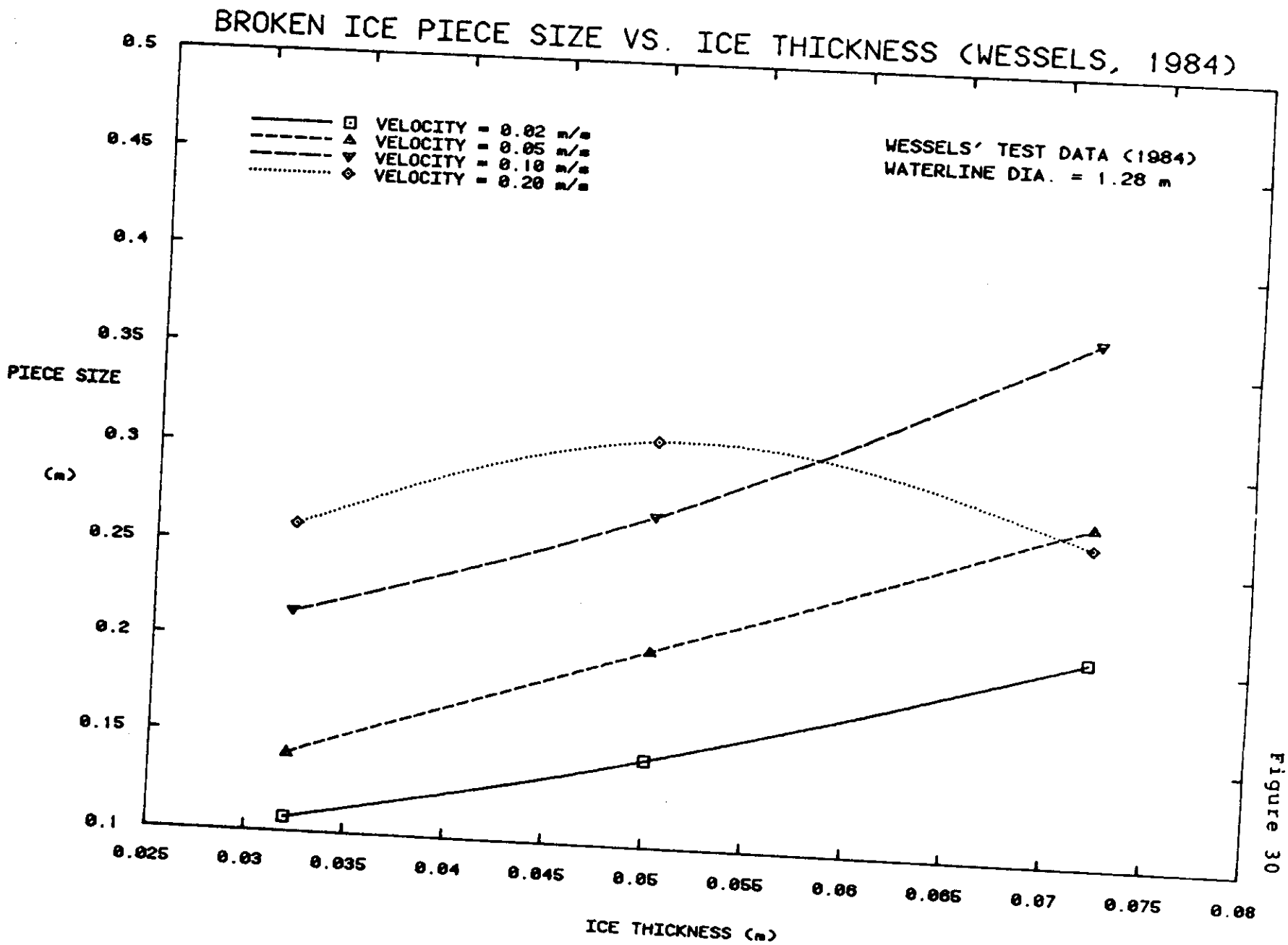
BROKEN ICE PIECE SIZE VS. ICE THICKNESS (WESSELS, 1984)
VELOCITY = 0.02 m/s
VELOCITY = 0.05 m/s
VELOCITY = 0.10 m/s
VELOCITY = 0.20 m/s
WESSELS' TEST DATA (1984)
WATERLINE DIA. = 1.28 m
PIECE SIZE
(m)
0.5
0.45
0.4
0.35
0.3
0.25
0.2
0.15
0.1
0.025
0.03
0.035
0.04
0.045
0.05
0.055
0.06
0.065
0.07
0.075
0.08
ICE THICKNESS (m)

Figure 30

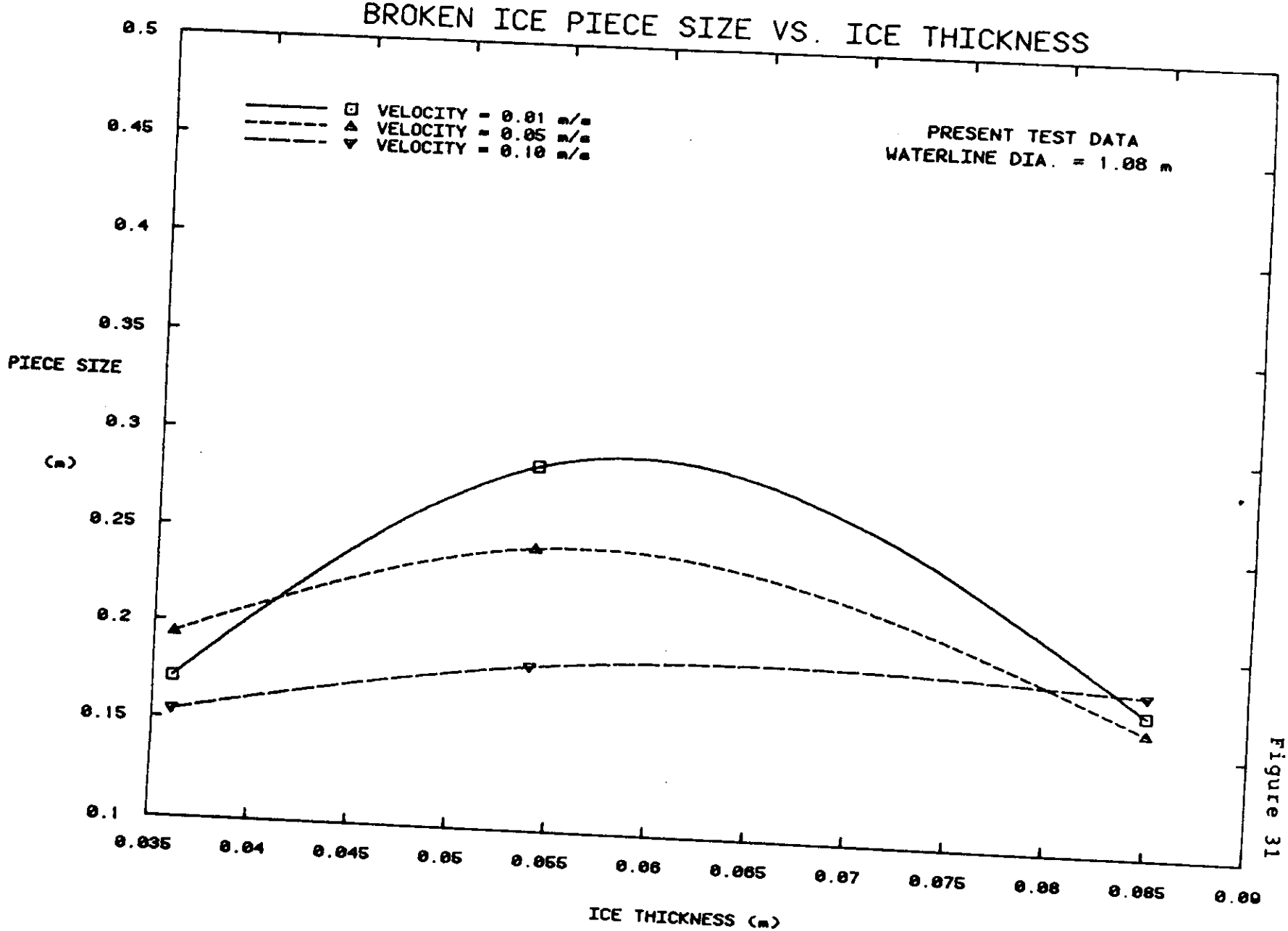
BROKEN ICE PIECE SIZE VS. ICE THICKNESS
VELOCITY = 0.01 m/s
VELOCITY = 0.05 m/s
VELOCITY = 0.10 m/s
PRESENT TEST DATA
WATERLINE DIA. = 1.08 m
PIECE SIZE
(m)
0.5
0.45
0.4
0.35
0.3
0.25
0.2
0.15
0.1
0.035
0.04
0.045
0.05
0.055
0.06
0.065
0.07
0.075
0.08
0.085
0.09
ICE THICKNESS (m)

Figure 31

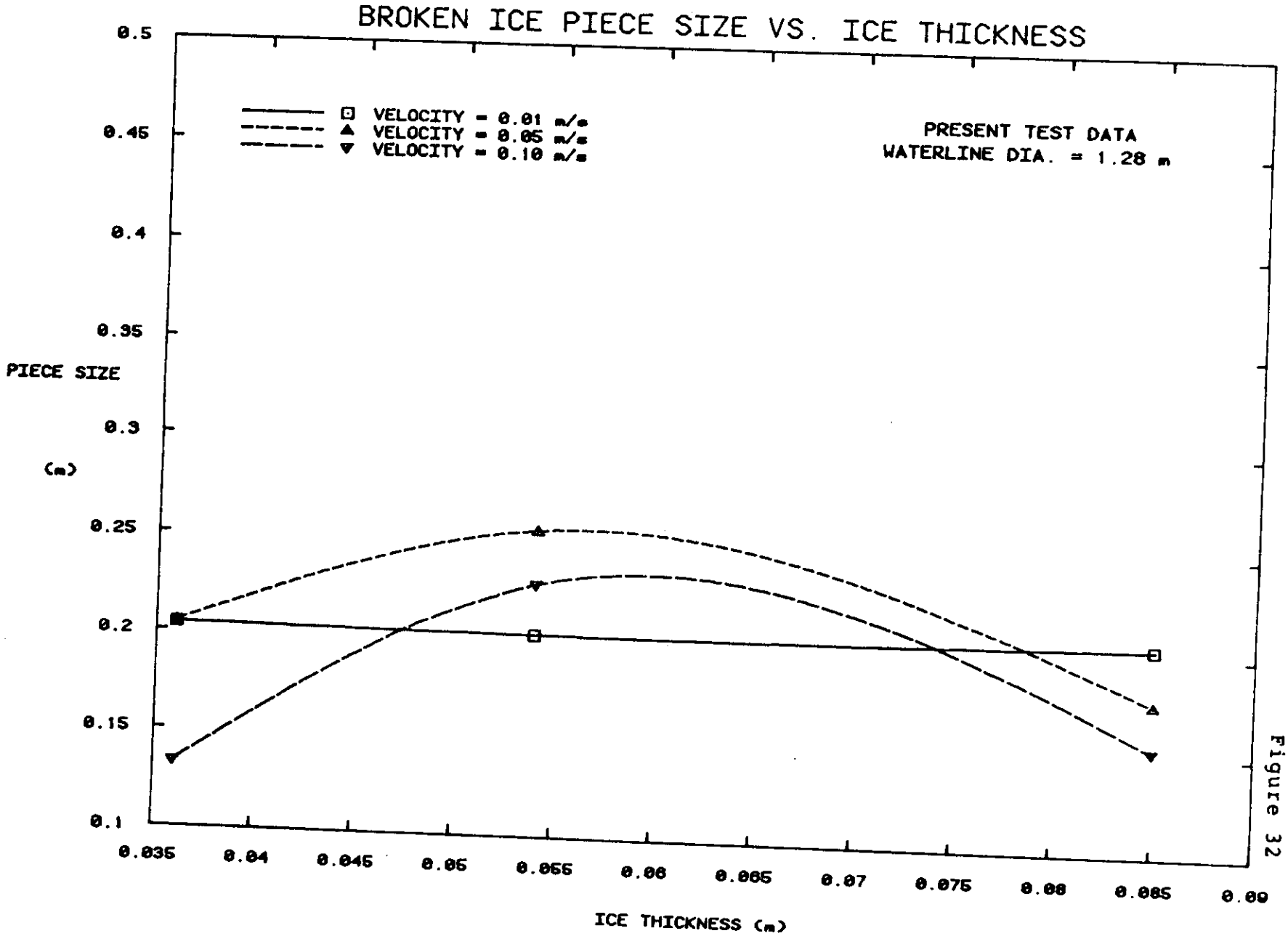
BROKEN ICE PIECE SIZE VS. ICE THICKNESS
VELOCITY = 0.01 m/s
VELOCITY = 0.05 m/s
VELOCITY = 0.10 m/s
PRESENT TEST DATA
WATERLINE DIA. = 1.28 m
PIECE SIZE
(m)
0.5
0.45
0.4
0.35
0.3
0.25
0.2
0.15
0.1
0.035
0.04
0.045
0.05
0.055
0.06
0.065
0.07
0.075
0.08
0.085
0.09
ICE THICKNESS (m)

Figure 32

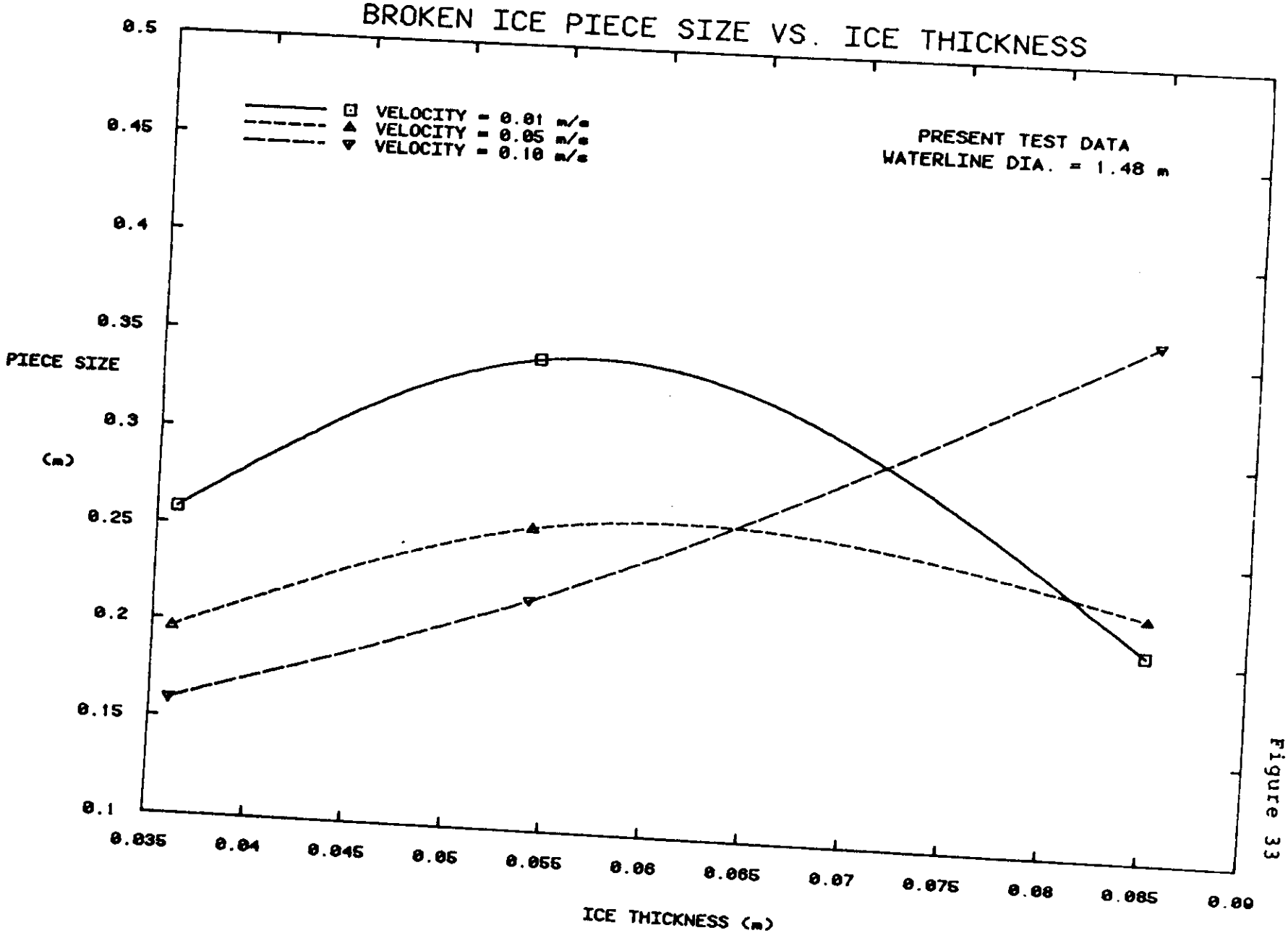
BROKEN ICE PIECE SIZE VS. ICE THICKNESS
VELOCITY = 0.01 m/s
VELOCITY = 0.05 m/s
VELOCITY = 0.10 m/s
PRESENT TEST DATA
WATERLINE DIA. = 1.48 m
PIECE SIZE
(m)
0.5
0.45
0.4
0.35
0.3
0.25
0.2
0.15
0.1
0.035
0.04
0.045
0.05
0.055
0.06
0.065
0.07
0.075
0.08
0.085
0.09
ICE THICKNESS (m)

Figure 33

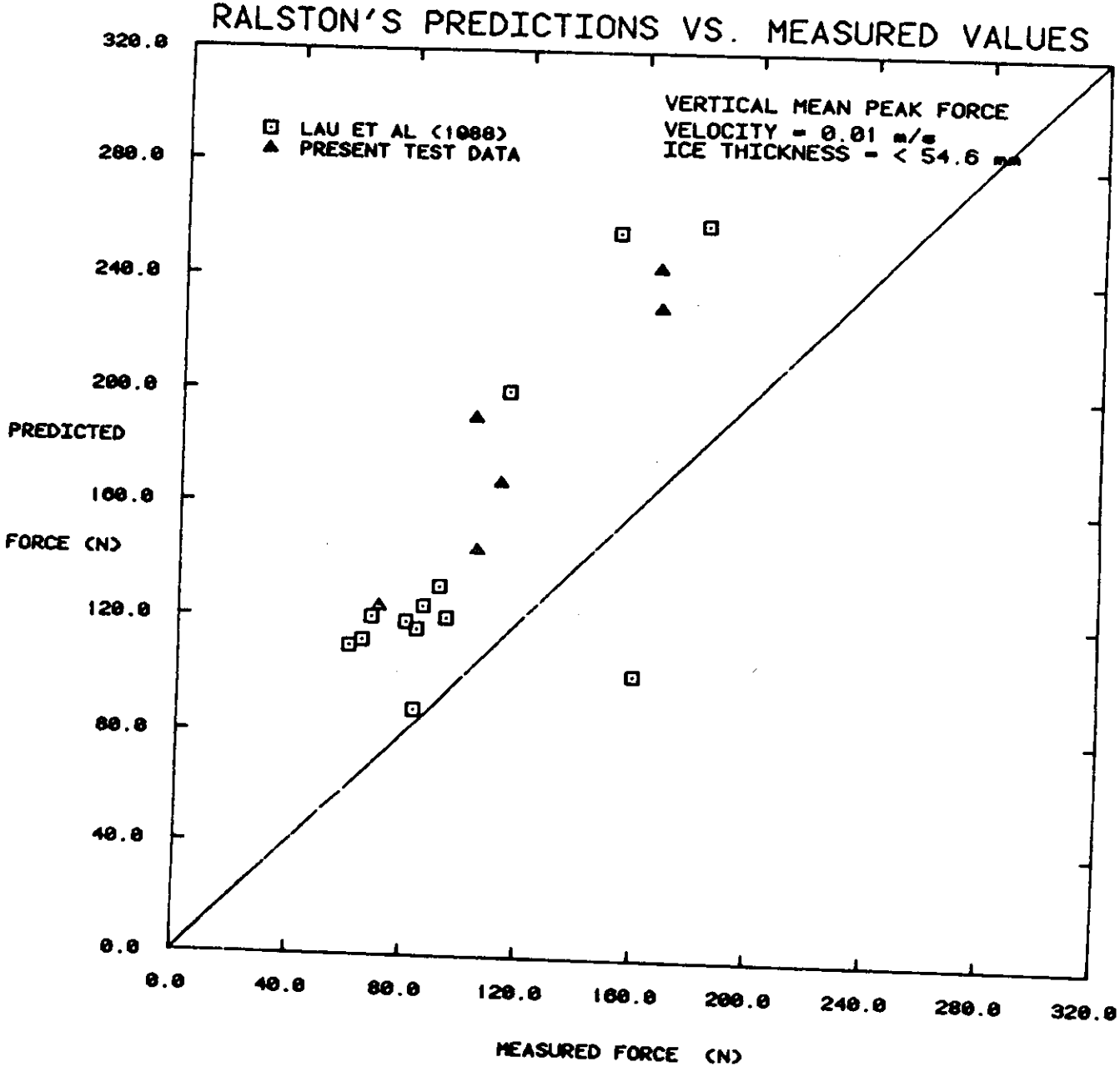
RALSTON'S PREDICTIONS VS. MEASURED VALUES
LAU ET AL (1988)
PRESENT TEST DATA
VERTICAL MEAN PEAK FORCE
VELOCITY = 0.01 m/s
ICE THICKNESS = < 54.6 mm
PREDICTED
FORCE (N)
MEASURED FORCE (N)
0.0
40.0
80.0
120.0
160.0
200.0
240.0
280.0
320.0

Figure 34

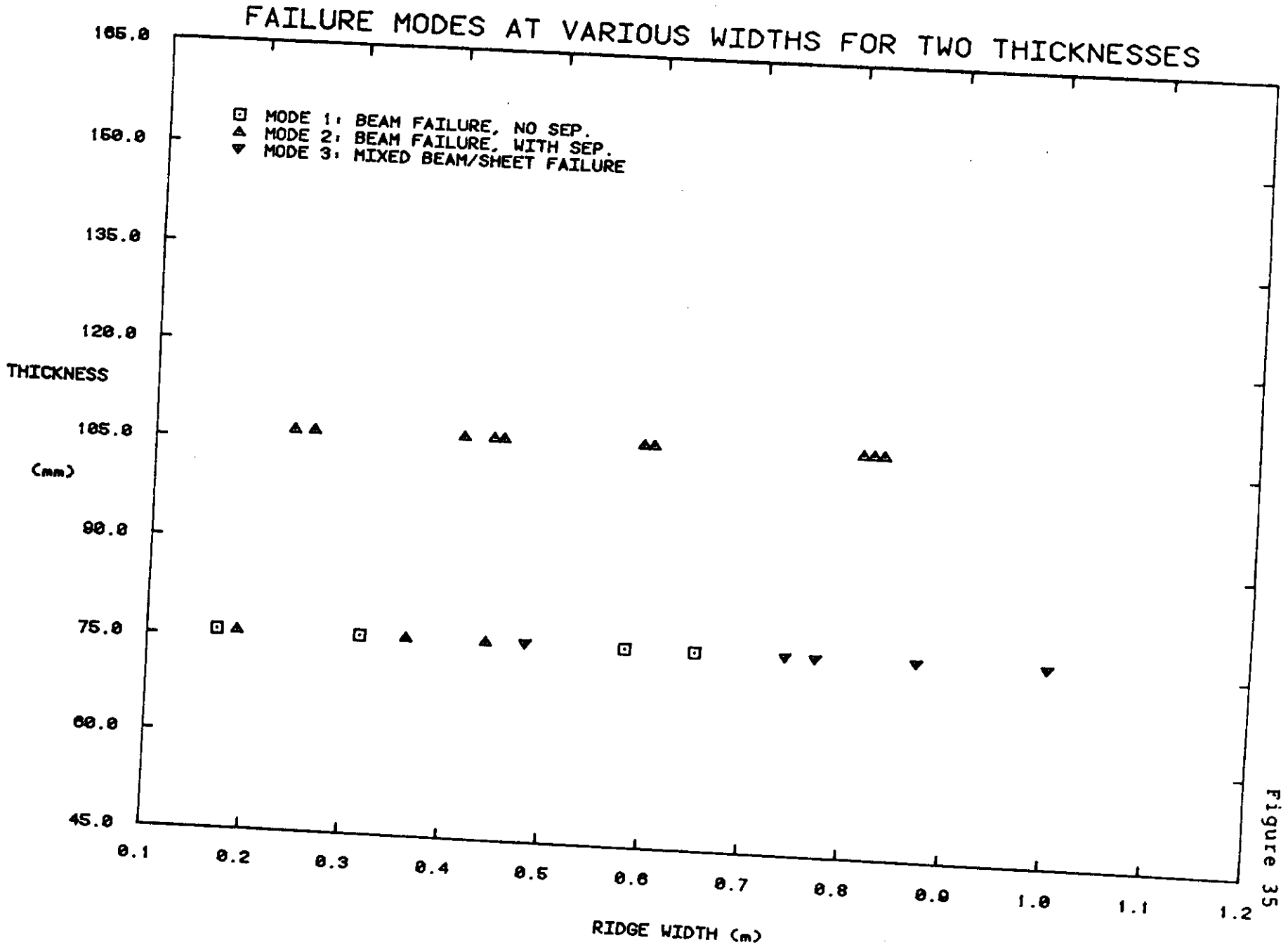
FAILURE MODES AT VARIOUS WIDTHS FOR TWO THICKNESSES
MODE 1: BEAM FAILURE, NO SEP.
MODE 2: BEAM FAILURE, WITH SEP.
MODE 3: MIXED BEAM/SHEET FAILURE
165.0
150.0
135.0
120.0
THICKNESS
105.0
(mm)
90.0
75.0
60.0
45.0
0.1
0.2
0.3
0.4
0.5
0.6
0.7
0.8
0.9
1.0
1.1
1.2
RIDGE WIDTH (m)

Figure 35

TYPICAL FORCE-TIME HISTORY OF TEST ASSOCIATED WITH FAILURE SCENARIO 1

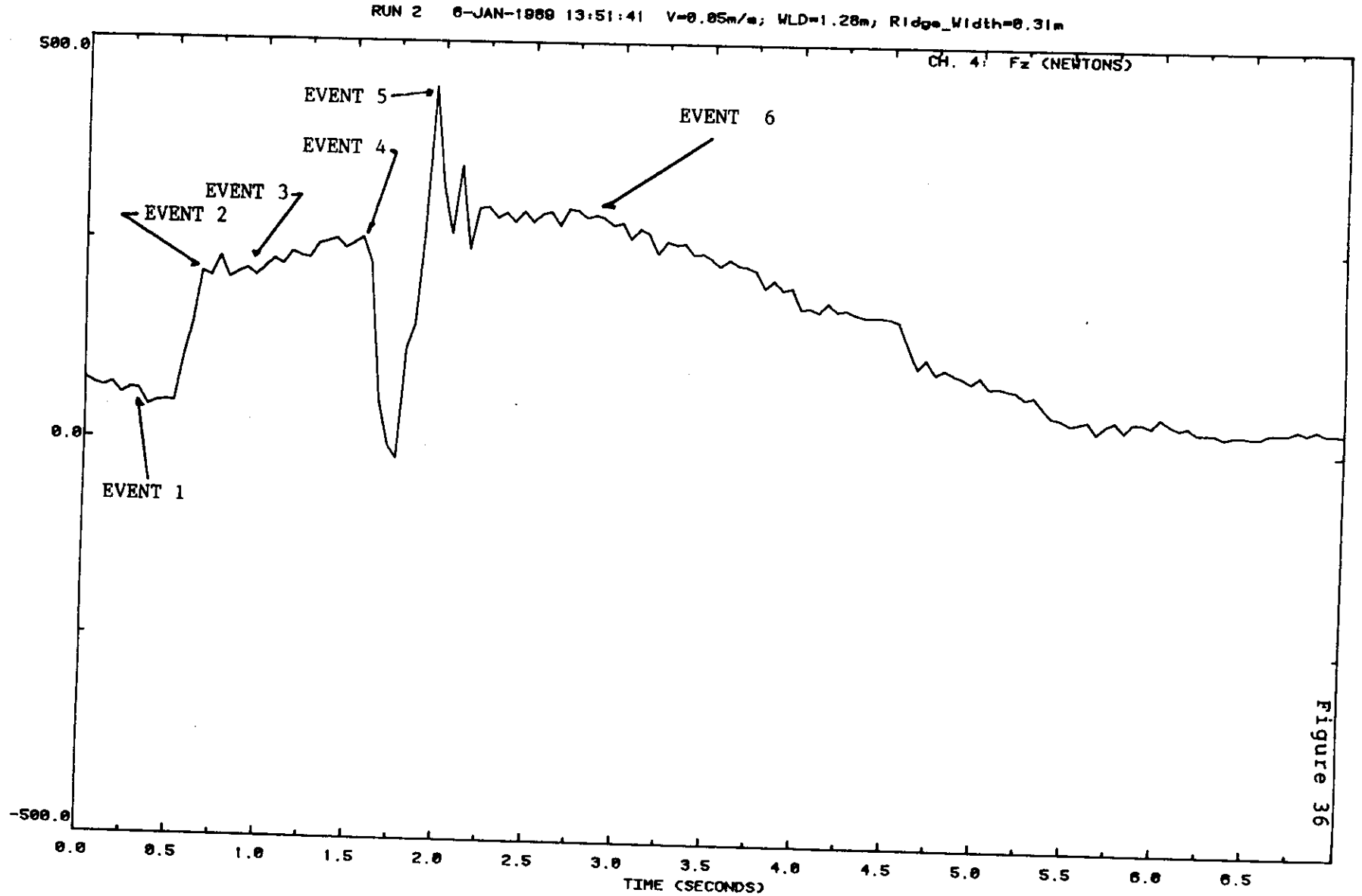

Figure 36

Figure 37

FAILURE SEQUENCE FOR SCENARIO 1

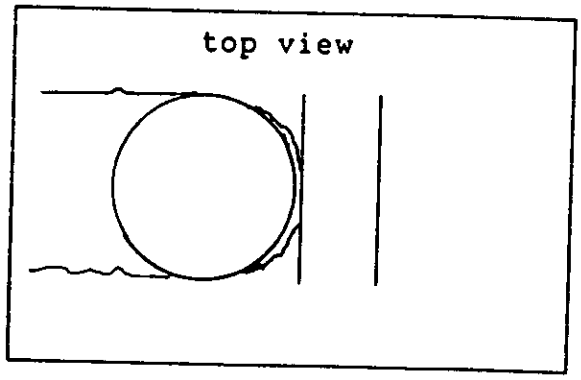

A. EVENT 1: SHEET FAILURE OF ICE SHEET

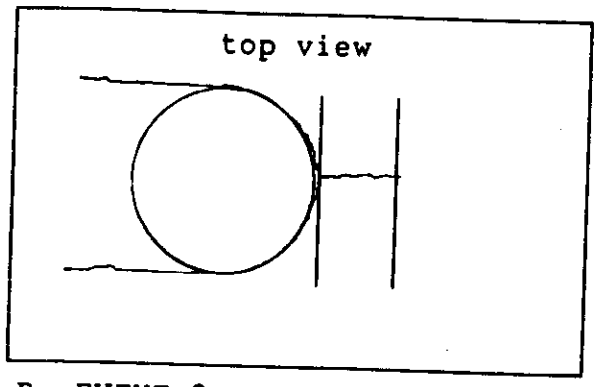

B. EVENT 2: CENTER CRACK FORMATION

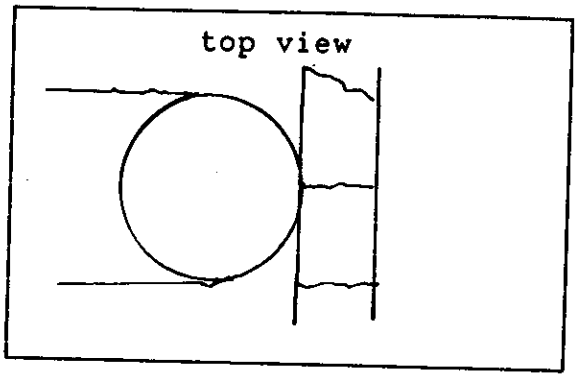

C. EVENT 3: APPEARANCE OF THE FIRST HINGE CRACK

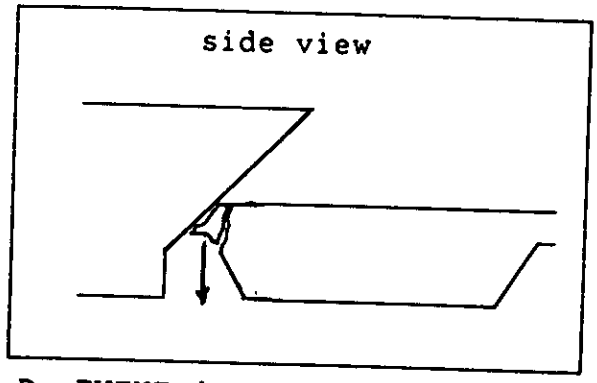

D. EVENT 4: SHEAR FAILURE AT FRONT EDGE OF RIDGE

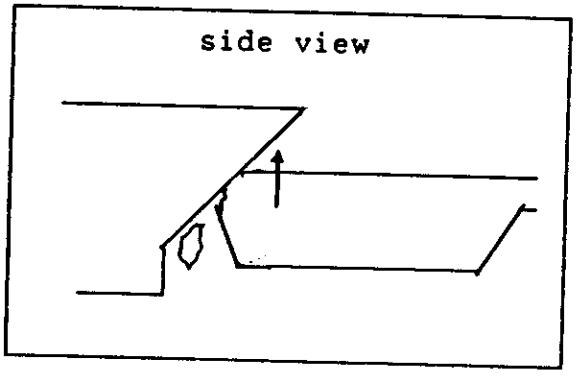

E. EVENT 5: REBOUND OF THE RIDGE

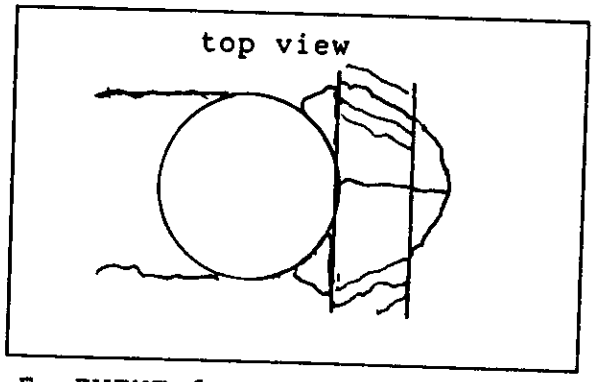

F. EVENT 6: FAILURE BY HINGE CRACK EXTENSION

TYPICAL FORCE-TIME HISTORY OF TEST ASSOCIATED WITH FAILURE SCENARIO 2

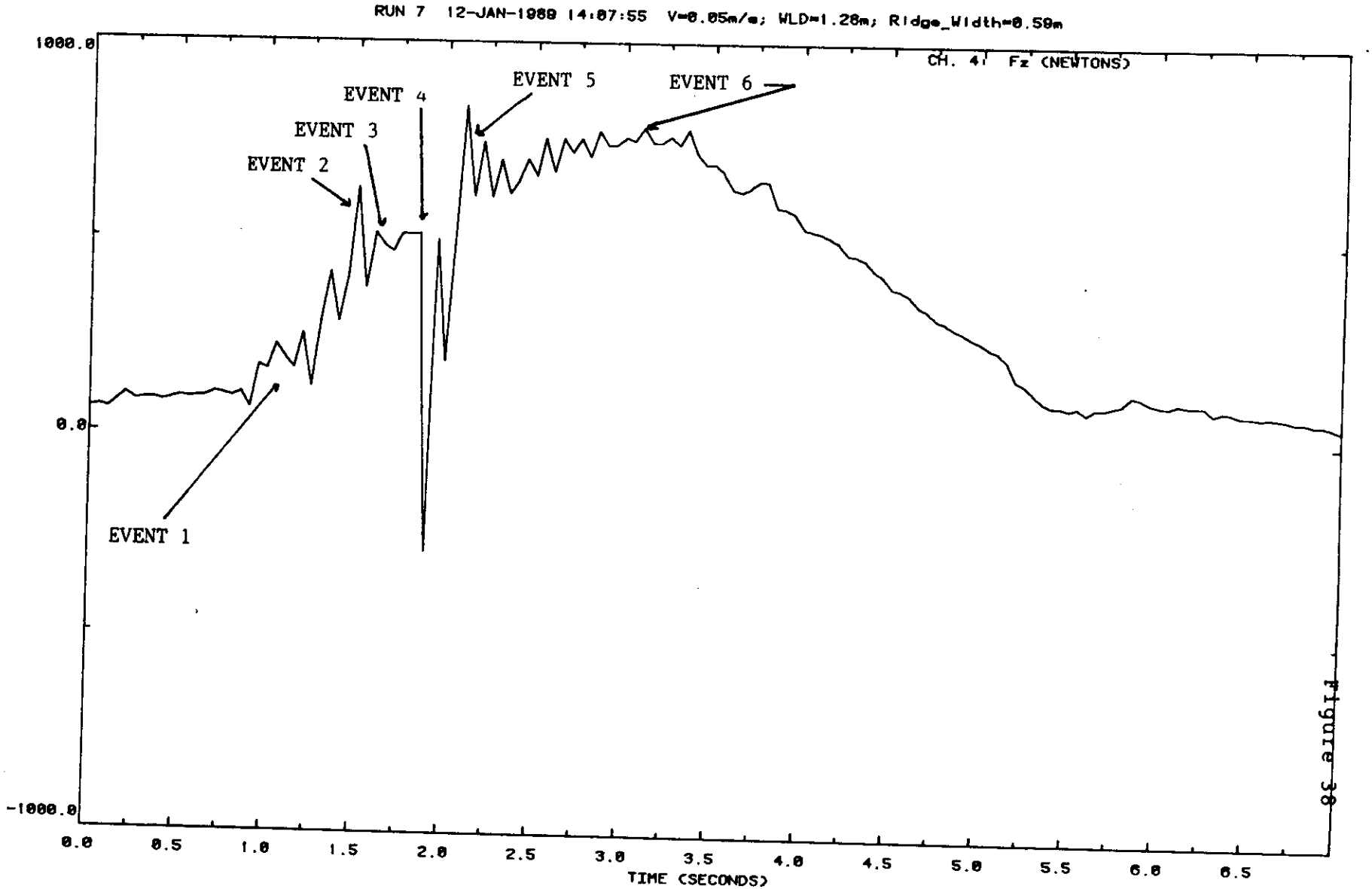

Figure 38

TYPICAL FORCE-TIME HISTORY OF TEST ASSOCIATED WITH FAILURE SCENARIO 3

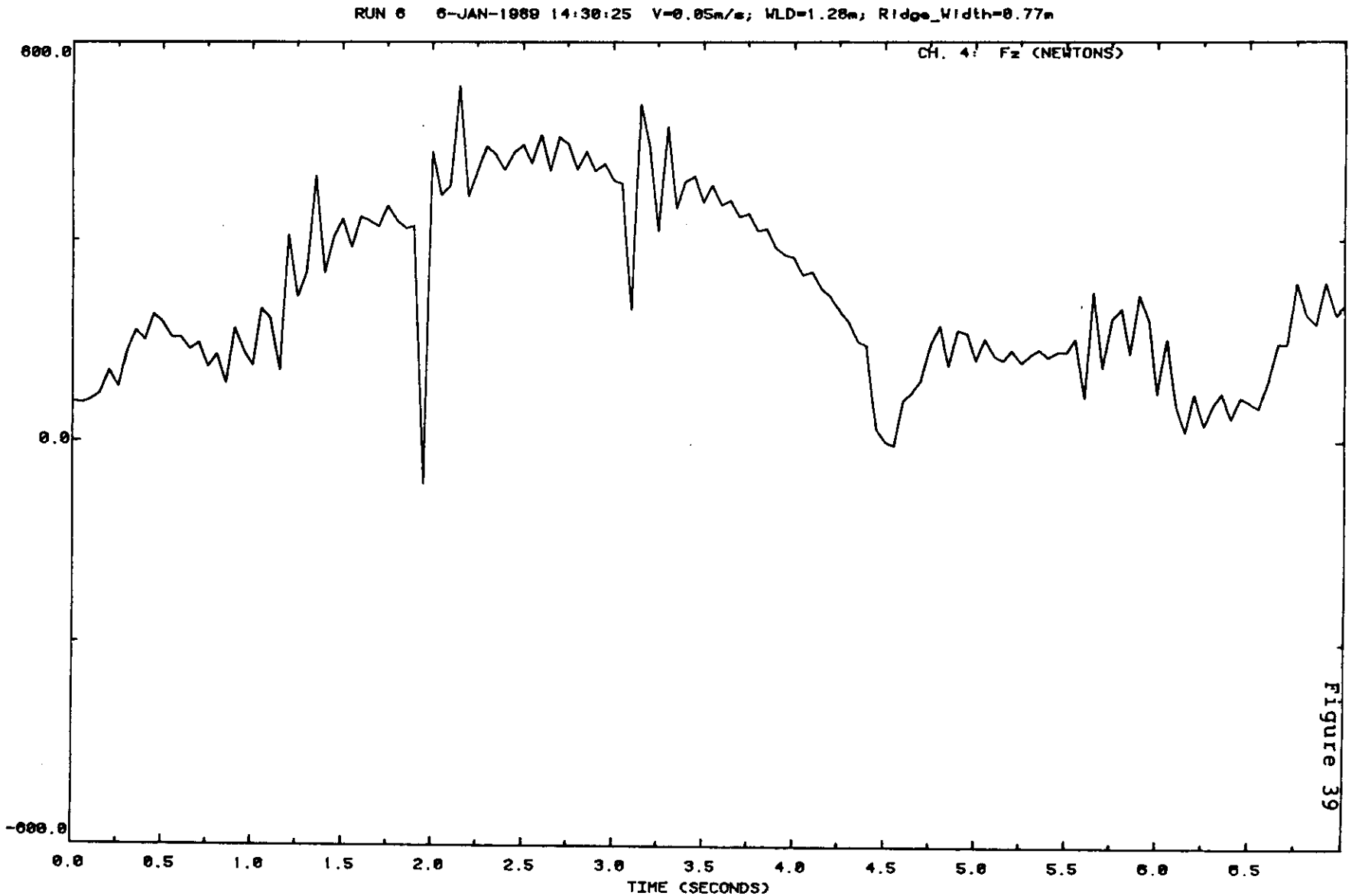

Figure 39

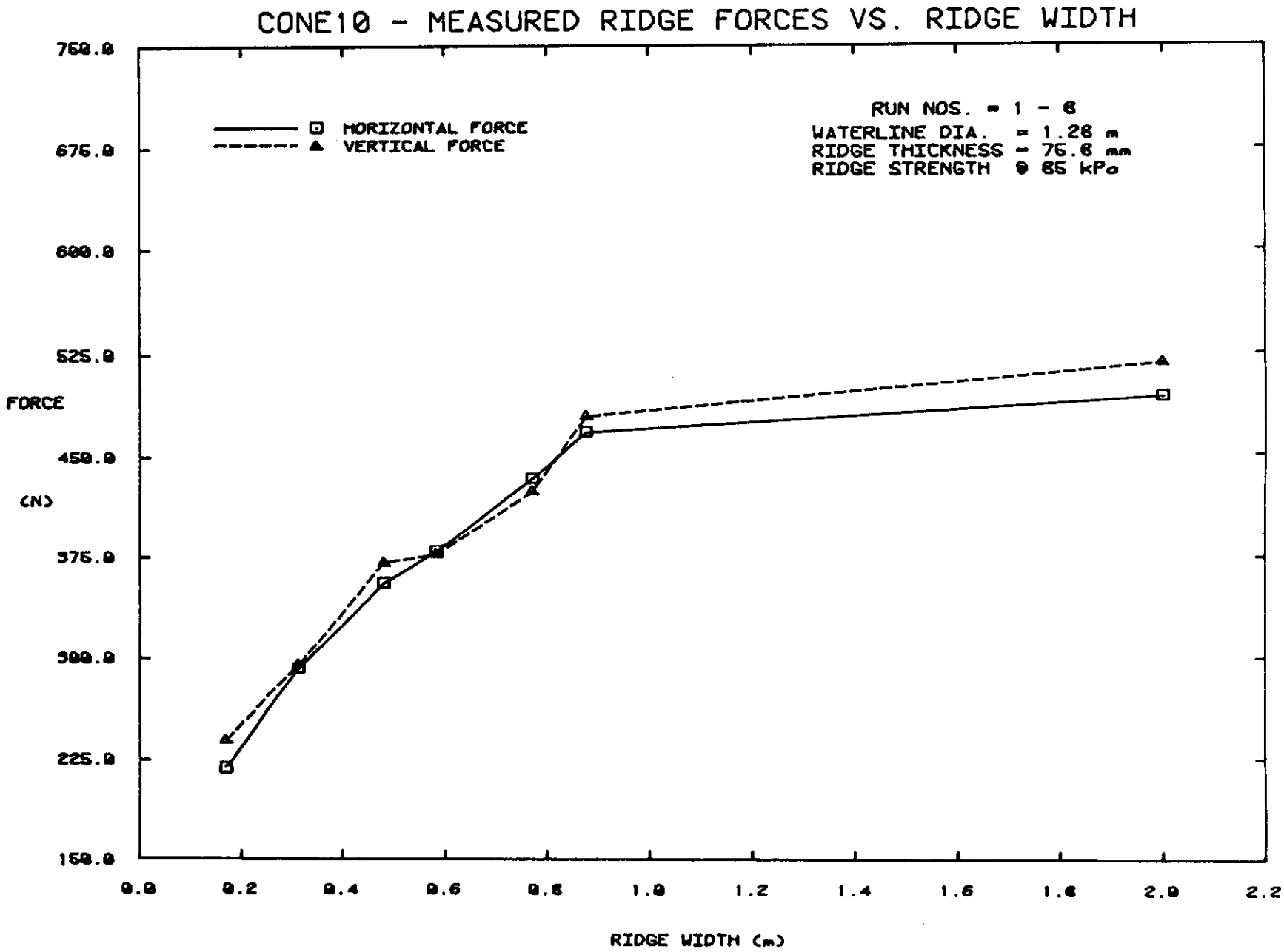
CONE10 - MEASURED RIDGE FORCES VS. RIDGE WIDTH
HORIZONTAL FORCE
VERTICAL FORCE
RUN NOS. = 1 - 6
WATERLINE DIA. = 1.26 m
RIDGE THICKNESS = 76.6 mm
RIDGE STRENGTH @ 65 kPa
FORCE
(N)
750.0
675.0
600.0
525.0
450.0
375.0
300.0
225.0
150.0
0.0
0.2
0.4
0.6
0.8
1.0
1.2
1.4
1.6
1.8
2.0
2.2
RIDGE WIDTH (m)

Figure 40

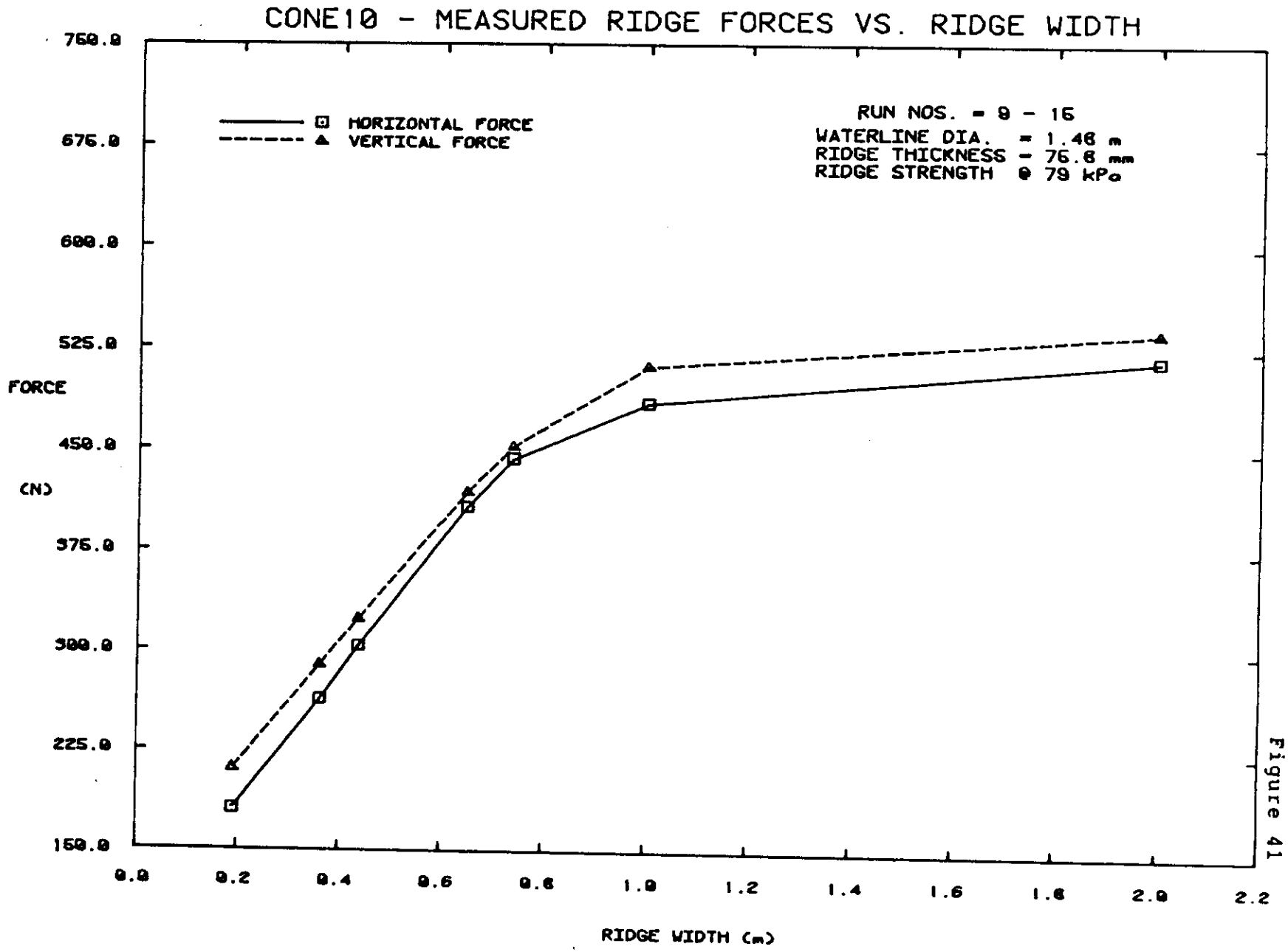
CONE10 - MEASURED RIDGE FORCES VS. RIDGE WIDTH
HORIZONTAL FORCE
VERTICAL FORCE
RUN NOS. = 9 - 15
WATERLINE DIA. = 1.46 m
RIDGE THICKNESS = 76.8 mm
RIDGE STRENGTH @ 79 kPa
750.0
675.0
600.0
525.0
FORCE
450.0
(N)
375.0
300.0
225.0
150.0
0.0
0.2
0.4
0.6
0.8
1.0
1.2
1.4
1.6
1.8
2.0
2.2
RIDGE WIDTH (m)

Figure 41

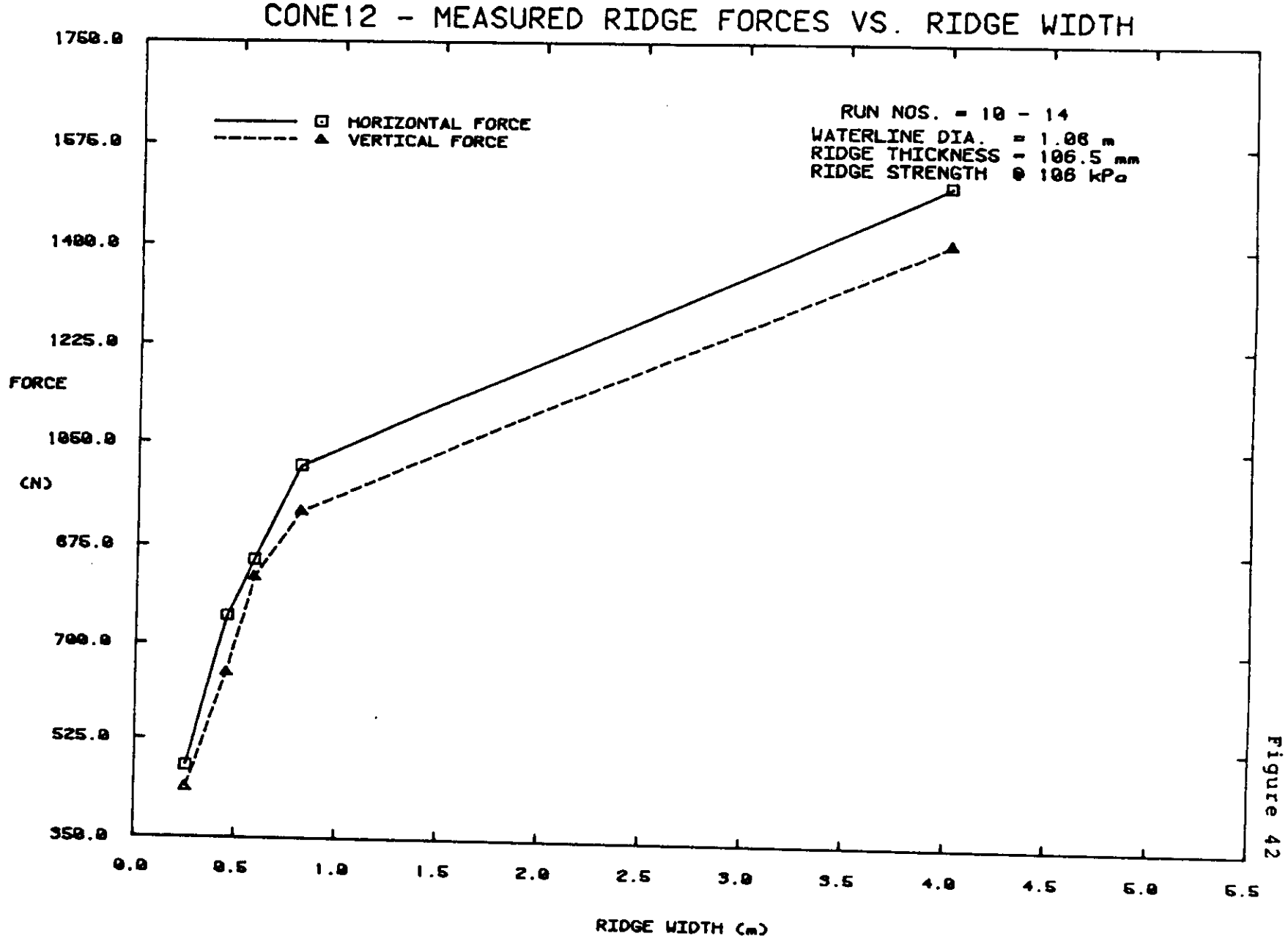
CONE12 - MEASURED RIDGE FORCES VS. RIDGE WIDTH
HORIZONTAL FORCE
VERTICAL FORCE
RUN NOS. = 10 - 14
WATERLINE DIA. = 1.06 m
RIDGE THICKNESS = 106.5 mm
RIDGE STRENGTH @ 106 kPa
1750.0
1575.0
1400.0
1225.0
FORCE
1050.0
(N)
875.0
700.0
525.0
350.0
0.0
0.5
1.0
1.5
2.0
2.5
3.0
3.5
4.0
4.5
5.0
5.5
RIDGE WIDTH (m)

Figure 42

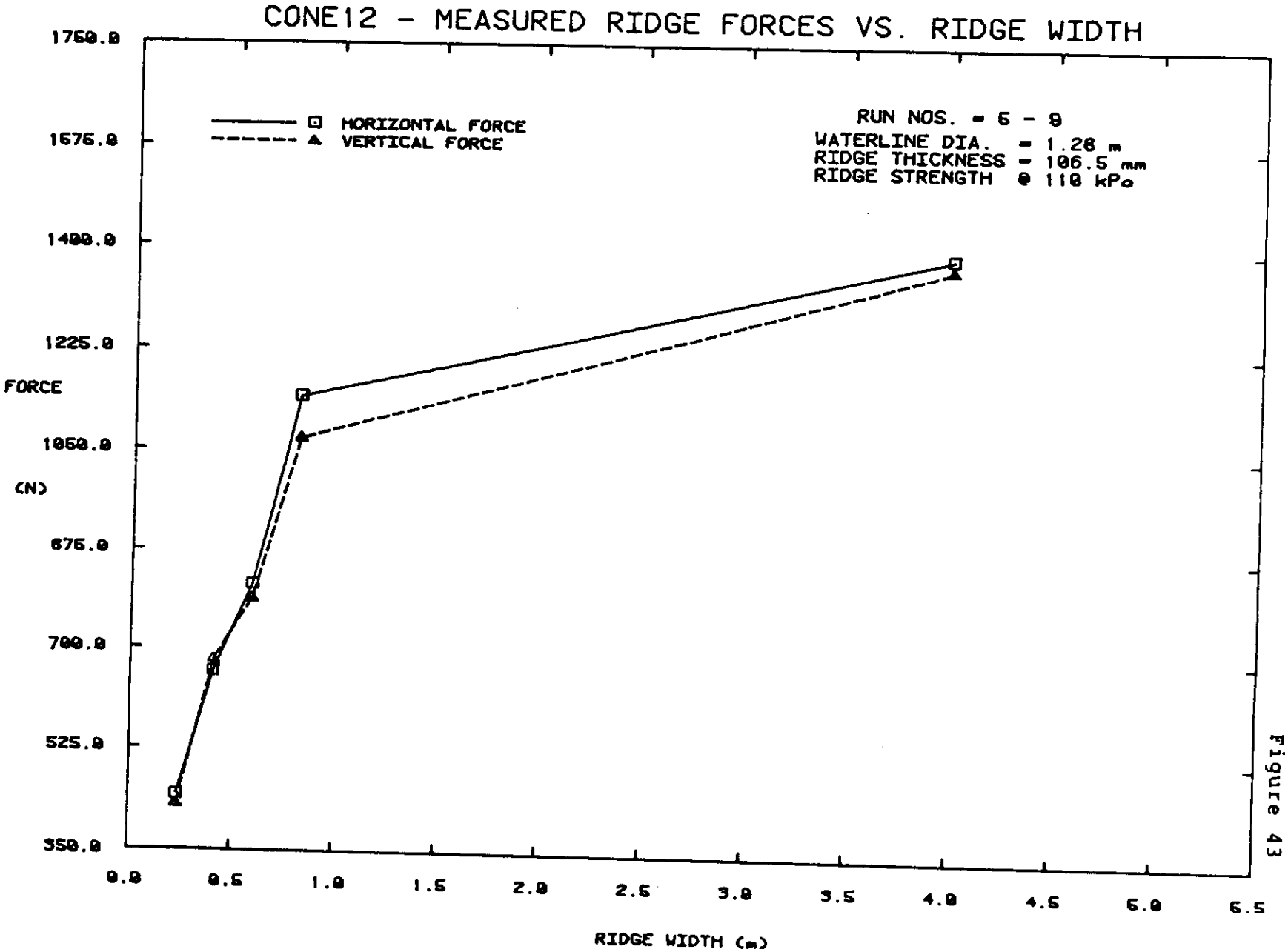
CONE12 - MEASURED RIDGE FORCES VS. RIDGE WIDTH
HORIZONTAL FORCE
VERTICAL FORCE
RUN NOS. = 5 - 9
WATERLINE DIA. = 1.26 m
RIDGE THICKNESS = 106.5 mm
RIDGE STRENGTH @ 110 kPa
1750.0
1575.0
1400.0
1225.0
FORCE
1050.0
(N)
875.0
700.0
525.0
350.0
0.0
0.5
1.0
1.5
2.0
2.5
3.0
3.5
4.0
4.5
5.0
5.5
RIDGE WIDTH (m)

Figure 43

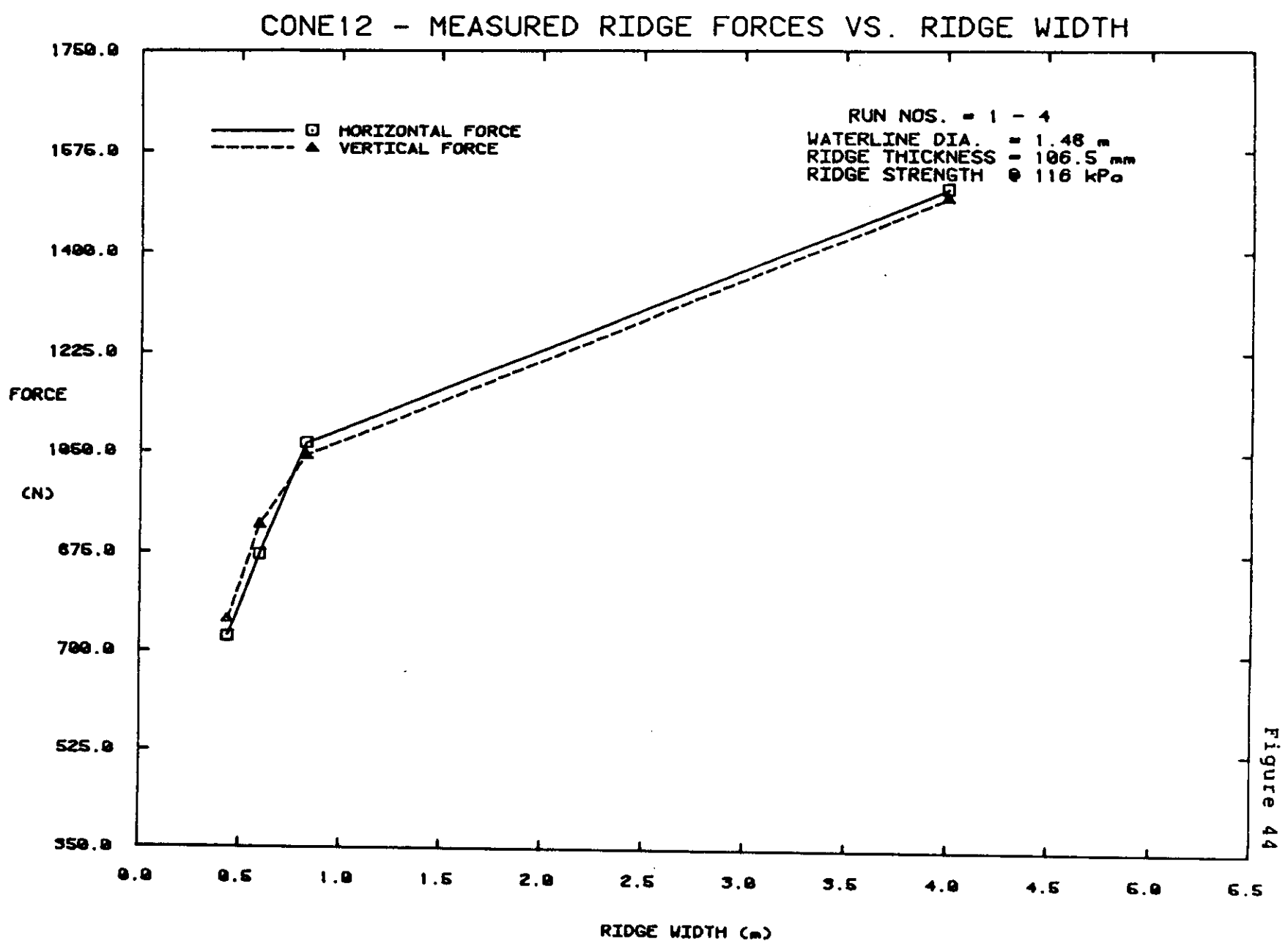
CONE12 - MEASURED RIDGE FORCES VS. RIDGE WIDTH
HORIZONTAL FORCE
VERTICAL FORCE
RUN NOS. = 1 - 4
WATERLINE DIA. = 1.46 m
RIDGE THICKNESS = 106.5 mm
RIDGE STRENGTH @ 116 kPa
1750.0
1575.0
1400.0
1225.0
FORCE
1050.0
(N)
875.0
700.0
525.0
350.0
0.0
0.5
1.0
1.5
2.0
2.5
3.0
3.5
4.0
4.5
5.0
5.5
RIDGE WIDTH (m)

Figure 44

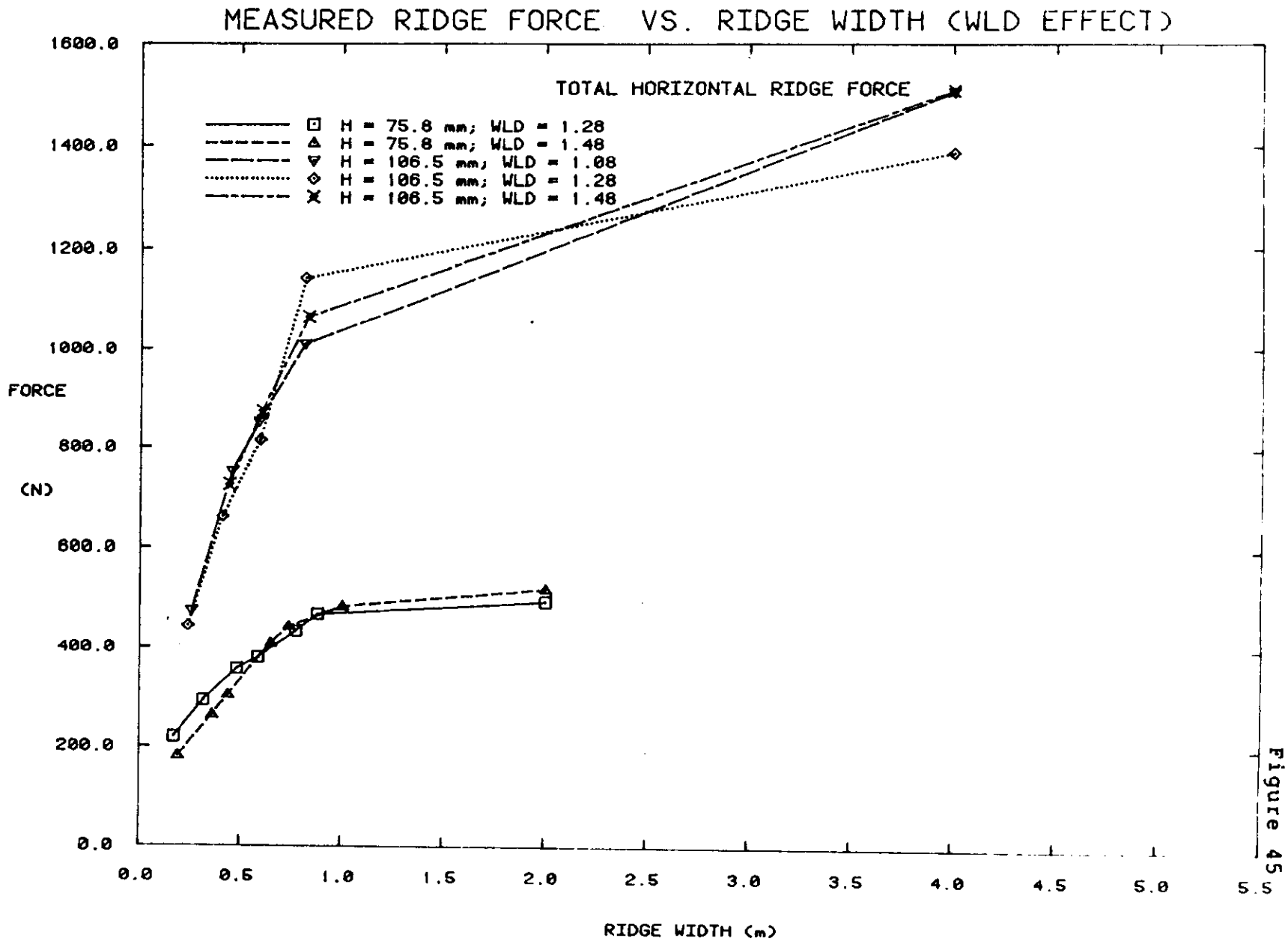
MEASURED RIDGE FORCE VS. RIDGE WIDTH (WLD EFFECT)
TOTAL HORIZONTAL RIDGE FORCE
H = 75.8 mm; WLD = 1.28
H = 75.8 mm; WLD = 1.48
H = 106.5 mm; WLD = 1.08
H = 106.5 mm; WLD = 1.28
H = 106.5 mm; WLD = 1.48
1600.0
1400.0
1200.0
1000.0
800.0
600.0
400.0
200.0
0.0
FORCE
(N)
0.0
0.5
1.0
1.5
2.0
2.5
3.0
3.5
4.0
4.5
5.0
5.5
RIDGE WIDTH (m)

Figure 45

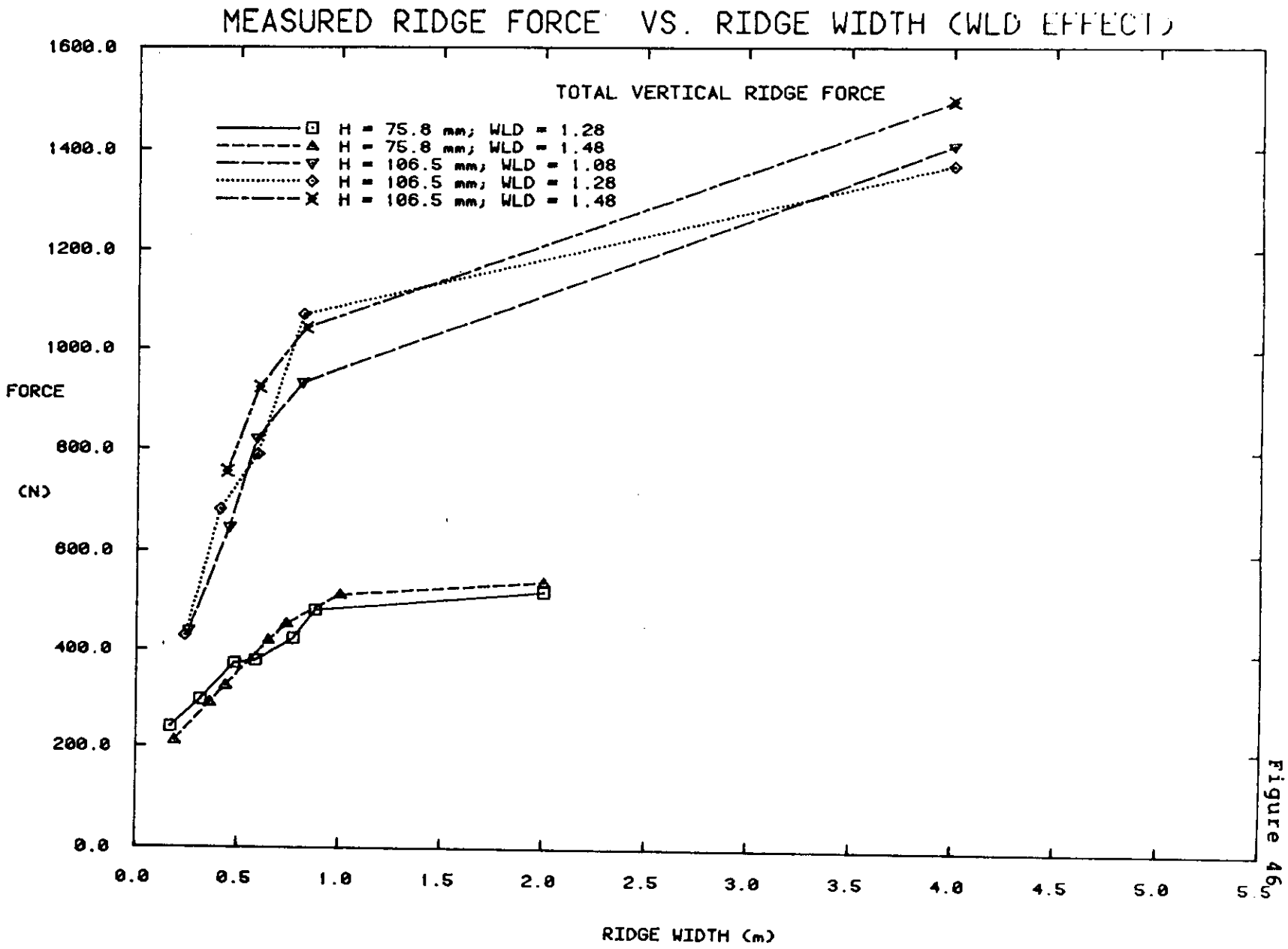
MEASURED RIDGE FORCE VS. RIDGE WIDTH (WLD EFFECT)
TOTAL VERTICAL RIDGE FORCE
H = 75.8 mm; WLD = 1.28
H = 75.8 mm; WLD = 1.48
H = 106.5 mm; WLD = 1.08
H = 106.5 mm; WLD = 1.28
H = 106.5 mm; WLD = 1.48
FORCE
(N)
1600.0
1400.0
1200.0
1000.0
800.0
600.0
400.0
200.0
0.0
0.0
0.5
1.0
1.5
2.0
2.5
3.0
3.5
4.0
4.5
5.0
5.5
RIDGE WIDTH (m)

Figure 46

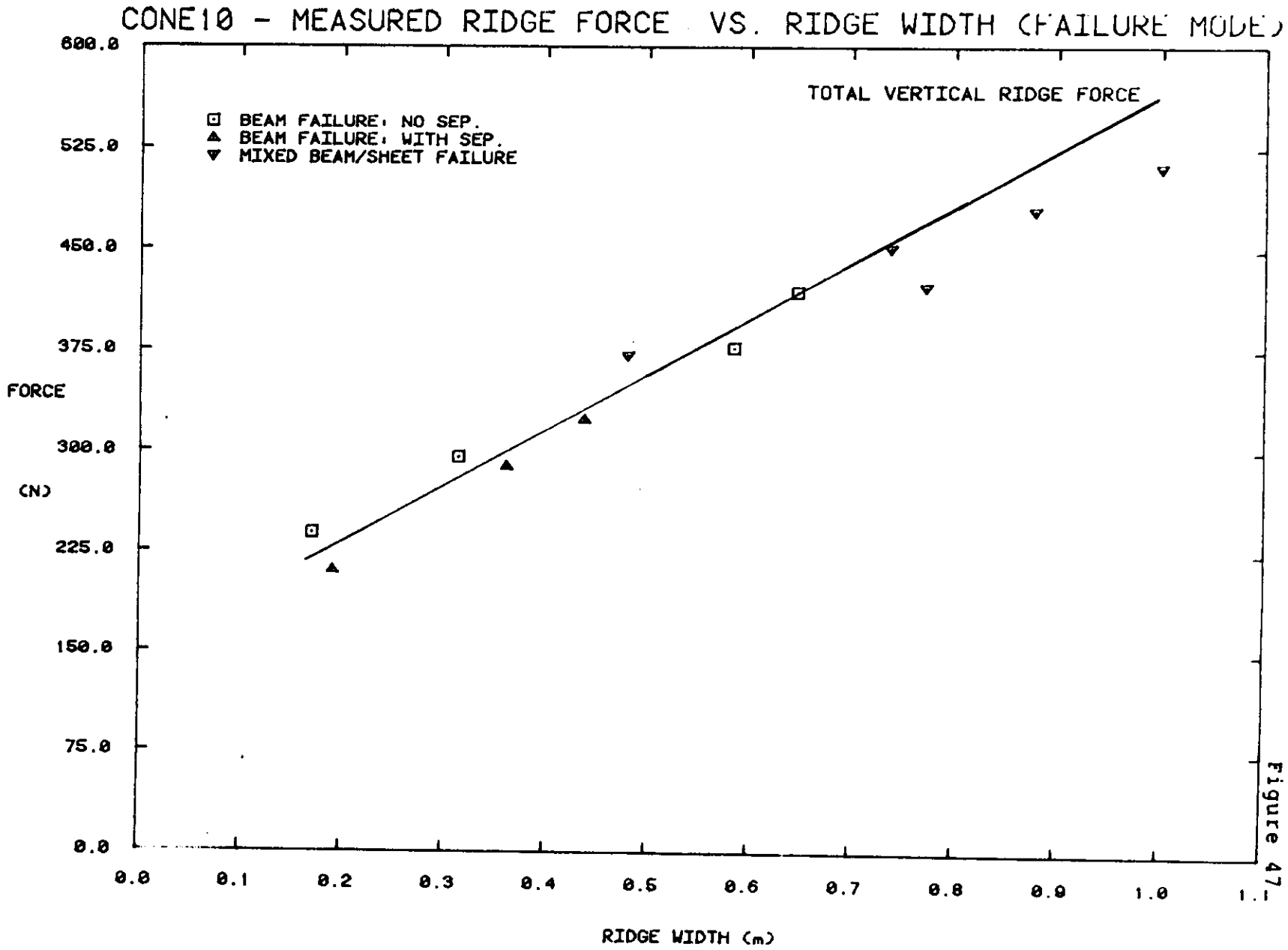
CONE10 - MEASURED RIDGE FORCE VS. RIDGE WIDTH (FAILURE MODE)
TOTAL VERTICAL RIDGE FORCE
BEAM FAILURE: NO SEP.
BEAM FAILURE: WITH SEP.
MIXED BEAM/SHEET FAILURE
600.0
525.0
450.0
375.0
FORCE
300.0
(N)
225.0
150.0
75.0
0.0
0.0
0.1
0.2
0.3
0.4
0.5
0.6
0.7
0.8
0.9
1.0
1.1
RIDGE WIDTH (m)

Figure 47

Figure 48

ALGORITHM FOR CALCULATING HINGE CRACK FORCES

STEP 1 Calculate the adjusted foundation modulus, k^*.

STEP 2 Calculate effective flange, b_{eff}, of the surrounding ice sheet.

STEP 3 Transform the effective flanges of the ice sheet into an equivalent area, nA_s, of the ridge ice to obtained the transformed section. The equivalent flexural strength of ice sheet equals to σ_f/n.

STEP 4 Calculate the distance, y, from the neutral axis and the moment of inertia, I_R, of the transformed cross section at failure assuming the stress configuration as shown in Figure 49b. Governing strength, σ_{gov}, of final failure is determined by the equivalent flexural strength, σ_f/n, of ice sheet or compressive strength, σ_c, of ridge whichever is exceeded first.

STEP 5 Apply simple beam formula,

$$P_V = 6.2 * \frac{\sigma_{gov} * I_R}{y * l_R}$$

$$P_H = p_V \tan(\alpha + \tan^{-1}(\mu))$$

Figure 49

TRANSFORMED SECTION AND
STRESS DISTRIBUTION AT FAILURE

A. TRANSFORM SECTION OF THE RIDGE SHEET COMPOSITE

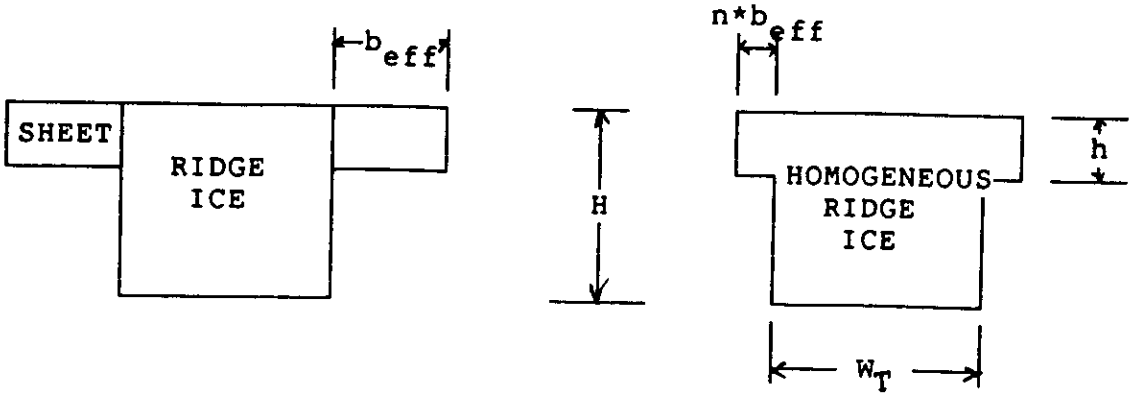

RIDGE SHEET COMPOSITE

TRANSFORMED SECTION
(ASSUMED n = 1/3)

B. STRESS DISTRIBUTION AT FAILURE

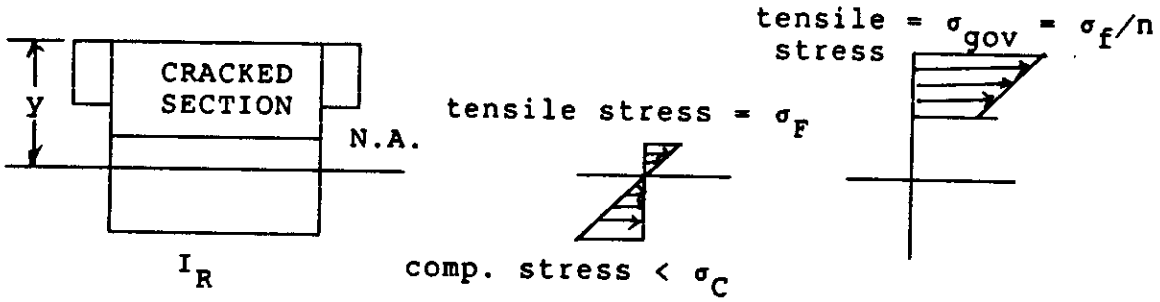

UNCRACKED
BEAM SECTION

ICE FLANGES

CROSS SECTION AT FAILURE

STRESS DISTRIBUTION

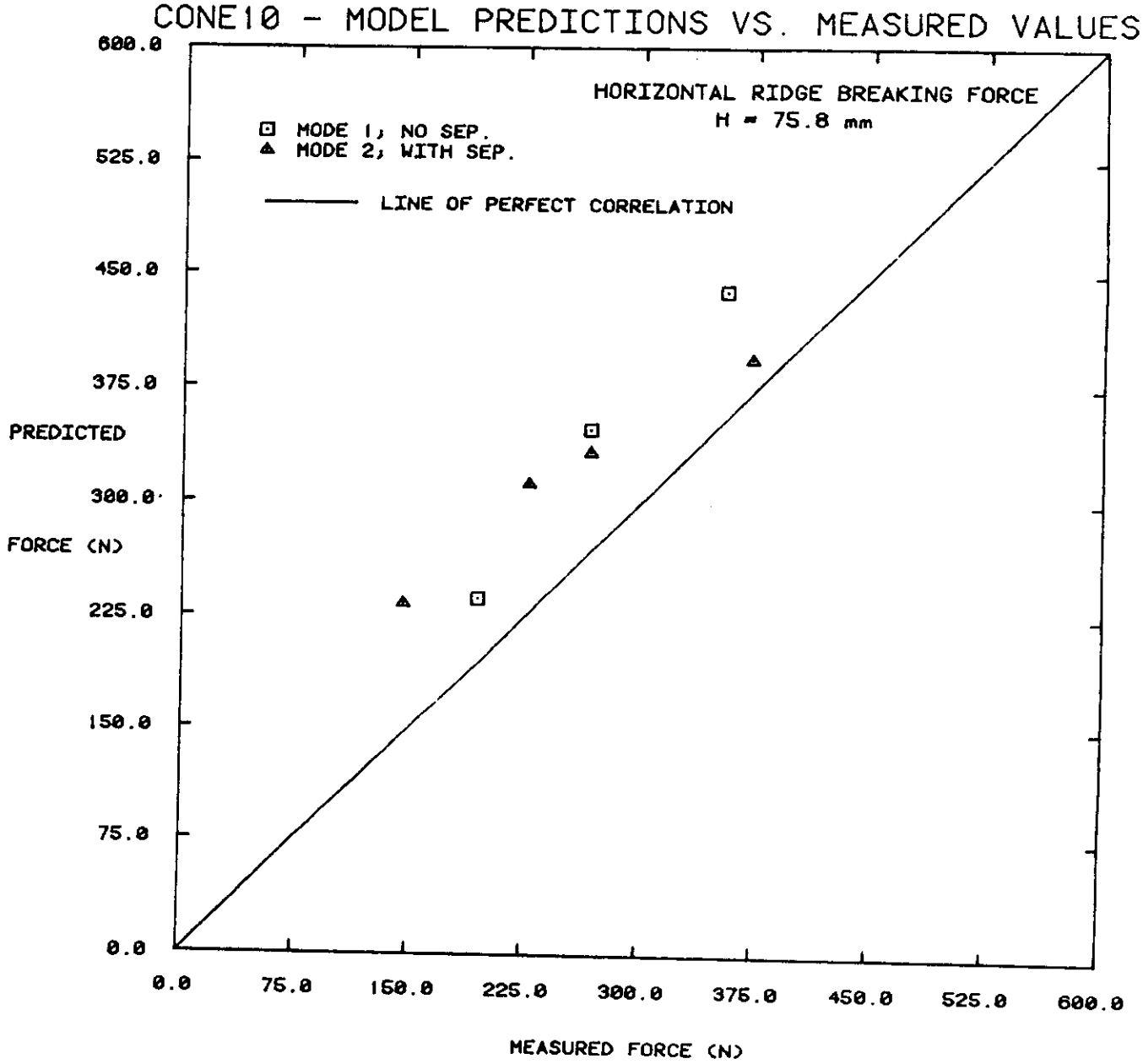
CONE10 - MODEL PREDICTIONS VS. MEASURED VALUES
HORIZONTAL RIDGE BREAKING FORCE
H = 75.8 mm
MODE 1; NO SEP.
MODE 2; WITH SEP.
LINE OF PERFECT CORRELATION
PREDICTED FORCE (N)
MEASURED FORCE (N)
0.0
75.0
150.0
225.0
300.0
375.0
450.0
525.0
600.0

Figure 50

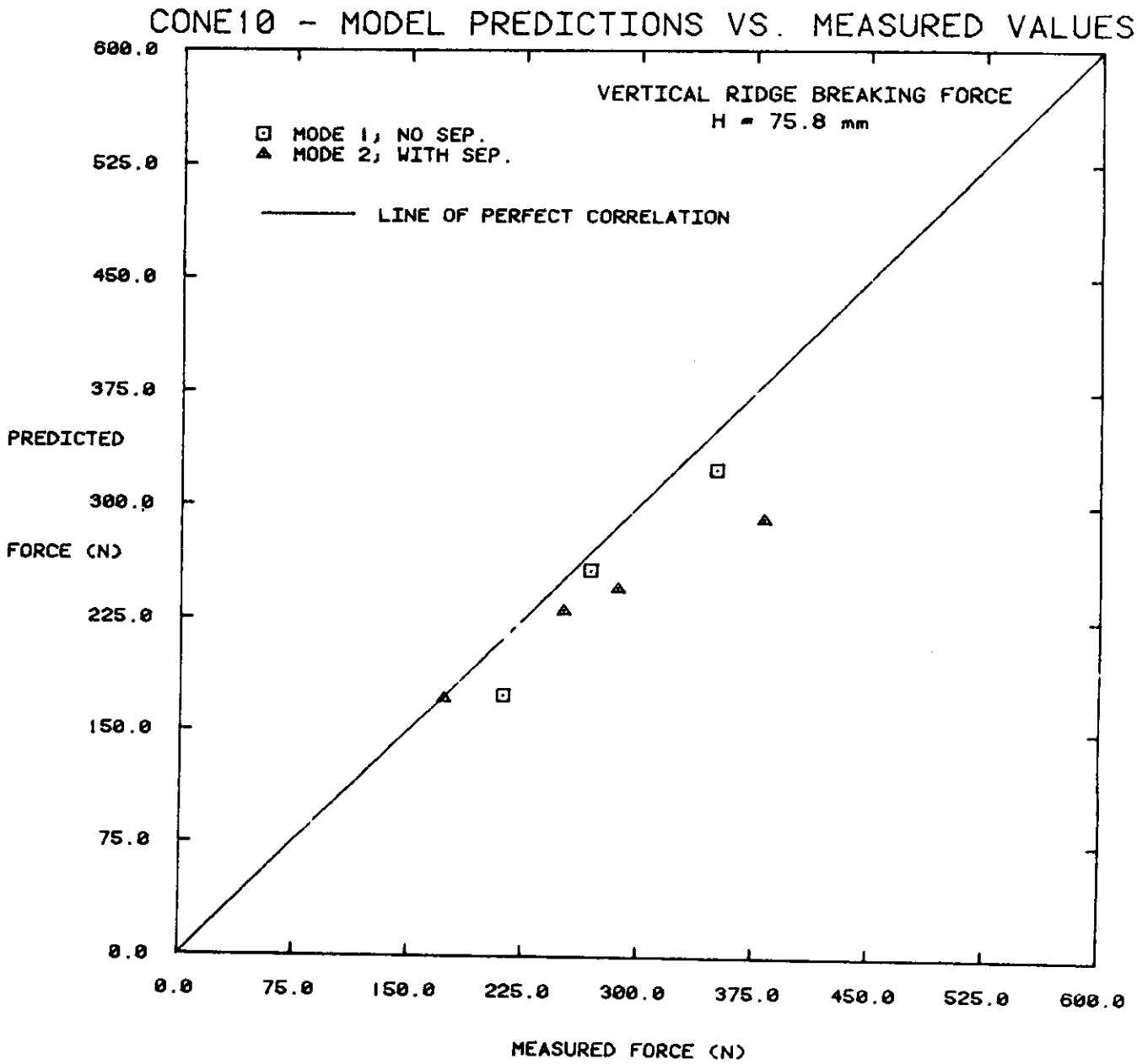
CONE10 - MODEL PREDICTIONS VS. MEASURED VALUES
VERTICAL RIDGE BREAKING FORCE
H = 75.8 mm
MODE 1; NO SEP.
MODE 2; WITH SEP.
LINE OF PERFECT CORRELATION
PREDICTED
FORCE (N)
MEASURED FORCE (N)
0.0
75.0
150.0
225.0
300.0
375.0
450.0
525.0
600.0

Figure 51

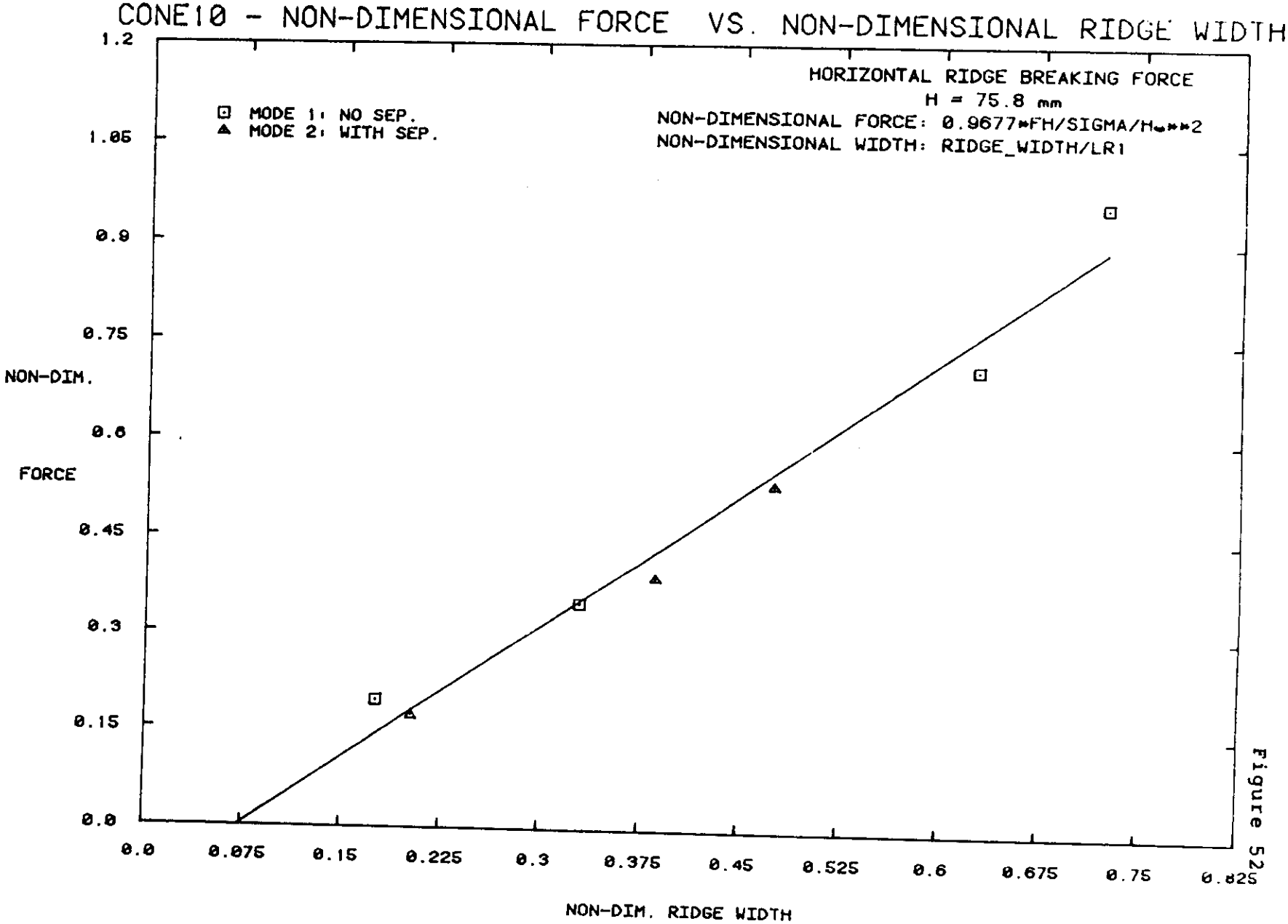
CONE10 - NON-DIMENSIONAL FORCE VS. NON-DIMENSIONAL RIDGE WIDTH
HORIZONTAL RIDGE BREAKING FORCE
H = 75.8 mm
NON-DIMENSIONAL FORCE: 0.9677*FH/SIGMA/H**2
NON-DIMENSIONAL WIDTH: RIDGE_WIDTH/LR1
MODE 1: NO SEP.
MODE 2: WITH SEP.
NON-DIM. FORCE
NON-DIM. RIDGE WIDTH
1.2
1.05
0.9
0.75
0.6
0.45
0.3
0.15
0.0
0.0
0.075
0.15
0.225
0.3
0.375
0.45
0.525
0.6
0.675
0.75
0.825

Figure 52

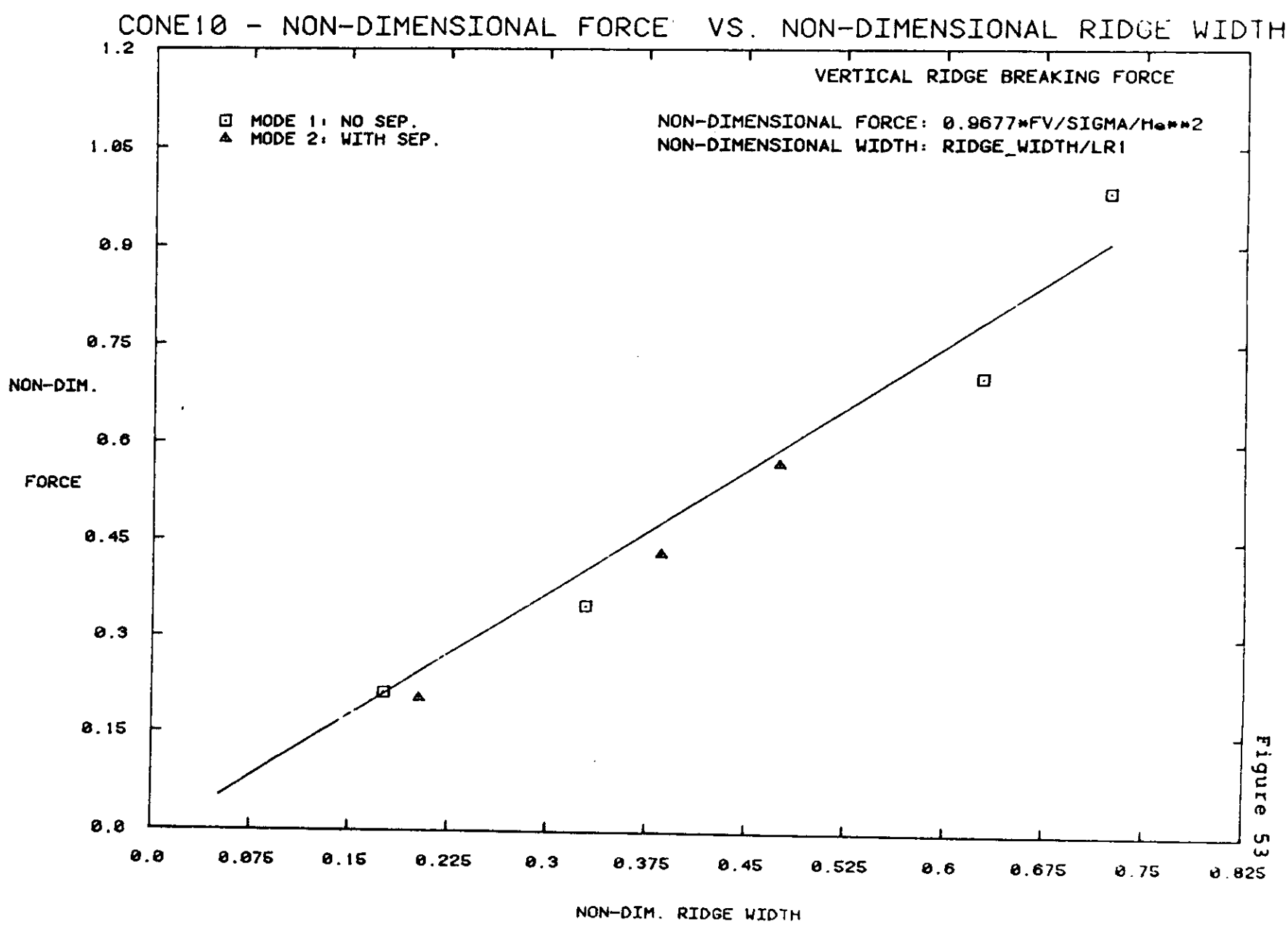
CONE10 - NON-DIMENSIONAL FORCE VS. NON-DIMENSIONAL RIDGE WIDTH
VERTICAL RIDGE BREAKING FORCE
MODE 1: NO SEP.
MODE 2: WITH SEP.
NON-DIMENSIONAL FORCE: 0.9677*FV/SIGMA/H**2
NON-DIMENSIONAL WIDTH: RIDGE_WIDTH/LR1
NON-DIM. FORCE
1.2
1.05
0.9
0.75
0.6
0.45
0.3
0.15
0.0
0.0
0.075
0.15
0.225
0.3
0.375
0.45
0.525
0.6
0.675
0.75
0.825
NON-DIM. RIDGE WIDTH

Figure 53